Utrecht University
Faculty of Geosciences
Department of Earth Sciences

Swagatam Chakraborty – Hydraulic parameter estimation of saturated sand using silica encapsulated, DNA tagged microparticles USES 313

ISSN 2211-4335

313

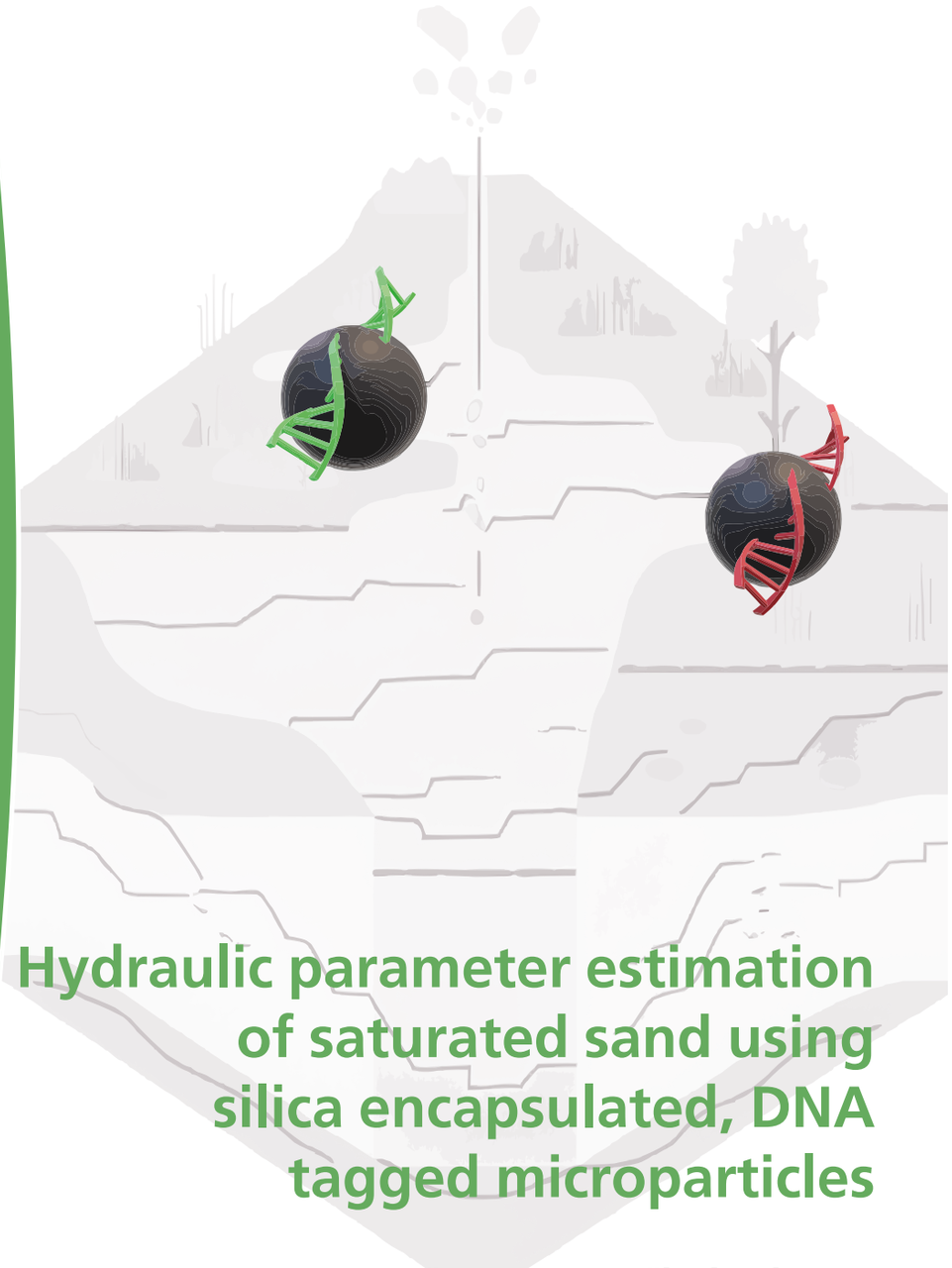

Hydraulic parameter estimation of saturated sand using silica encapsulated, DNA tagged microparticles

Swagatam Chakraborty

UTRECHT STUDIES IN EARTH SCIENCES

Hydraulic parameter estimation of saturated sand using silica encapsulated, DNA tagged microparticles

Laboratory experiments and numerical modeling

Schatting van hydraulische parameters van verzadigd zand met DNA-gemerkte silica deeltjes

Laboratoriumexperimenten en numerieke modellering
(met een samenvatting in het Nederlands)

Proefschrift

ter verkrijging van de graad van doctor aan de
Universiteit Utrecht
op gezag van de
rector magnificus, prof. dr. H.R.B.M. Kummeling,
ingevolge het besluit van het college voor promoties
in het openbaar te verdedigen op maandag 17 Juni 2024

des middags te 12:15 uur

door

Swagatam Chakraborty

geboren op 3 mei 1989
te Kolkata, India

Promotor:

Prof. dr. J.F. Schijven

Copromotor:

Dr. J.W.A. Foppen

Beoordelingscommissie:

Prof. dr. ir. M. Bakker
Prof. dr. ir. C.V. Chrysikopoulos
Prof. dr. W.P. Johnson
Dr. Seetha N
Prof. dr. R.J. Schotting

ISBN 978-90-6266-686-7

Hydraulic parameter estimation of saturated sand using silica encapsulated, DNA-tagged microparticles

-Laboratory experiments and numerical modeling

Schatting van hydraulische parameters van verzadigd zand met DNA-gemerkte silica deeltjes

- Laboratoriumexperimenten en numerieke modellering

Thesis

to fulfil the requirements of the degree of doctor at
the University of Utrecht
by the authority of Rector Magnificus Prof. dr. Henk Kummeling,
pursuant to the decision of the Doctorate Board to defend in public
on 17th Juni 2024 at 12:15

Swagatam chakraborty

Thesis Contents

SUMMARY

Determining hydraulic parameters of aquifers, their associated uncertainties and spatio-temporal variation is important to characterize groundwater flow and mass transport. Of these hydraulic parameters, hydraulic conductivity, effective porosity, and dispersivity are the most crucial ones. Several ex-situ methods such as grain size analysis, and permeameter tests of drilled core samples, and in-situ methods including pumping tests, slug tests, and flowmeter tests, and tracer studies have traditionally been applied for estimating hydraulic conductivity. Effective porosity has been typically estimated by ex-situ and in-situ methods such as mercury intrusion porosimetry, Helium gas pycnometry, magnetic resonance imaging and tracer tests. Compared to the standard drilled core analysis and geophysical methods, groundwater tracer tests have been used for broader applications including in-situ direct hydraulic parameter estimation, transport velocity determination, spatio-temporal variation of hydraulic parameters, and establishing aquifer connectivities. Inorganic salts and fluorescent dyes are the most commonly used groundwater tracers due to their no or low reactivity with sediments, cost efficiency and non-toxicity. In addition to salt and dye tracers, particulate tracers including microspheres, bacteria and bacteriophages have been widely used for characterizing groundwater flow paths, and pathogen migration. Transport behaviour of these microparticle tracers, depending on physico-chemical properties such as size and surface charge, and process variables including ionic strength and particle concentration, can differ from the conservative tracers in terms of transport velocity, mass distribution, and recovery.

This dissertation focuses on the applicability of silica encapsulated DNA tagged microparticles (SiDNA) in determining hydraulic parameters (hydraulic conductivity, effective porosity, longitudinal, and transverse dispersivities) of homogeneous and heterogeneous saturated

medium grain and coarse grain sand. SiDNA particles are ~200 nm spherical silica particles encapsulating double stranded DNA (dsDNA) molecules. The uniqueness of the base pair sequences of the dsDNA, synthesized through combinations of nucleotides, overcomes the general limiation of lack of distinctiveness within a group of solutes (eg. salt) or particulate tracers (e.g. microparticles, bacteria). In laboratory column (1D) and sand tank (3D) experiments, SiDNA with a superparamagnetic core (SiDNAmag) was subjected to retention through first order kinetic attachment, resulting in 1-3 log less mass recovery as comapared to conservative tracers. Chapter 2 of this dissertation demonstrated that SiDNA retention was concentration dependent and decreased with increasing injection particle concentration. The removal efficiency, therefore, decreased with increasing particle injection concentration. Besides SiDNAmag concentration, ionic strength (IS) of injection water influenced the particle attachment and therefore, SiDNA transport. An increase in IS from 1mM to 5mM phosphate buffer injection water increased SiDNA transport with decreased attachment rate, possibly due to competitive adsorption of phosphate onto the collector grains. An increase in IS from 5mM to 20mM, however, increased SiDNA attachment attributing to the compression of electrostatic double layer. In chapter 3, we demonstrated that under experimental conditions free from particle aggregation, the hydraulic parameters (hydraulic conductivity, effective porosity and dispersivities) and associated uncertainties estimated from SiDNA transport experiments were statistically similar to the parameters estimated from salt tracer breakthrough data. Further, the hydraulic parameters and associated uncertainty distributions were not influenced by IS of injection water.

In a homogeneous sand tank, packed with medium grain sand, multipoint SiDNA injection experiments demonstrated that the stochastically (Monte Carlo simulation) determined hydraulic parameters and associated uncertainties estimated from SiDNA breakthrough

curves were statistically similar to the hydraulic parameters estimated from salt tracers. This indicated that the transport velocity and 3D dispersion behaviour of SiDNA were not significantly different than salt tracers, despite significant SiDNA mass loss due to particle attachment on the solid phase. Further, we investigated the applicability of SiDNA in identifying and estimating hydraulic conductivity, effective porosity, dispersivity and associated uncertainties in a heterogeneous sand tank with a lens shaped no conductivity zone and, separately, a same lens shaped high conductivity zone. Multipoint injection and multilevel sampling approach were specifically advantageous in identifying no conductivity lens heterogeneity. The effect of the high conductivity lens was reflected on the bi-peaked breakthrough curves of both the salt and SiDNA. The hydraulic parameters and associated uncertainties stochastically determined from SiDNA breakthrough curves were statistically not significantly different from those determined from salt tracer breakthrough data in both cases (no conductivity and high conductivity). However, longitudinal and transverse dispersivities could not be determined distinctively, possibly due to the small scale of lens heterogeneity and because transverse dispersivities were determined as a ratio of transverse and longitudinal dispersivity.

Overall, this thesis demonstrated that under our experimental conditions, SiDNA was a suitable particle for determining hydraulic parameters (hydraulic conductivity, effective porosity, and dispersivitiy) of saturated, unconsolidated, medium and coarse grained, homogeneous and heterogeneous sand systems. However, we acknowledge that our findings are based on controlled laboratory scale experiments. Therefore, further systematic experiments on SiDNA transport as a function of physical variables such as sand grain size, pH, complex heterogeneity, and chemical factors including major ions (Ca^{2+}, Mg^{2+} etc.), and dissolved organic matter would be a requisite prior to large or field scale applications. In this

research, the primary limitation of SiDNA was the first order kinetic attachment onto the collector grains resulting in 1-3 orders of magnitude of reduced SiDNA recovery as compared to the salt tracer, a potential hindrance in SiDNA application in experiments with longer transport lengths.

SAMENVATTING:

Het bepalen van hydraulische parameters van watervoerende lagen, hun bijbehorende onzekerheden en ruimtelijke-temporele variatie is belangrijk om de grondwaterstroming en massatransport te karakteriseren. Van deze hydraulische parameters zijn hydraulische geleidbaarheid, effectieve porositeit en dispersiviteit de belangrijkste. Verschillende ex-situ methoden zoals korrelgrootteanalyse, permeametertesten van geboorde kernmonsters, en in-situ methoden zoals pompproeven, slugtesten, flowmetertesten en tracerstudies zijn traditioneel toegepast voor het schatten van de hydraulische geleidbaarheid. Effectieve porositeit is meestal geschat door ex-situ en in-situ methoden zoals kwikintrusieporosimetrie, heliumgaspycnometrie, magnetische resonantiebeeldvorming en tracerstudies. In vergelijking met de standaard geboorde kernanalyse en geofysische methoden zijn grondwatertracerstudies gebruikt voor bredere toepassingen, waaronder in-situ directe schatting van hydraulische parameters, bepaling van transportsnelheid, ruimtelijke-temporele variatie van hydraulische parameters en het vaststellen van watervoerende verbindingen. Anorganische zouten en fluorescerende kleurstoffen zijn de meest gebruikte grondwatertracers vanwege hun geen of lage reactiviteit met sedimenten, kostenefficiëntie en niet-toxiciteit. Naast zout- en kleurstoftracers zijn deeltjestracers, waaronder microsferen, bacteriën en bacteriofagen, veel gebruikt voor het karakteriseren van grondwaterstroompaden en pathogeenmigratie. Het transportgedrag van deze micropartikeltracers, afhankelijk van fysisch-chemische eigenschappen zoals grootte en oppervlaktelading, en procesvariabelen zoals ionsterkte en deeltjesconcentratie, kan verschillen van de conservatieve tracers in termen van transportsnelheid, massaverdeling en herstel. Dit proefschrift richt zich op de toepasbaarheid van silicium ingekapselde DNA-getagde micropartikels (SiDNA) bij het bepalen van hydraulische parameters (hydraulische

geleidbaarheid, effectieve porositeit, longitudinale en transversale dispersiviteiten) van een homogeen en heterogeen verzadigd mediumkorrelig en grofkorrelig zand. SiDNA-deeltjes zijn ~200 nm bolvormige siliciumdeeltjes die dubbelstrengs DNA (dsDNA) moleculen inkapselen. De uniciteit van de basenpaarvolgordes van het dsDNA, gesynthetiseerd door combinaties van nucleotiden, overwint de algemene beperking van gebrek aan onderscheidend vermogen binnen een groep opgeloste stoffen (bijv. zout) of deeltjestracers (bijv. micropartikels, bacteriën). In laboratoriumkolom (1D) en zandtank (3D) experimenten werd SiDNA met een superparamagnetische kern (SiDNAmag) onderworpen aan retentie door middel van kinetische hechting van de eerste orde, resulterend in 1-3 log minder massa-herstel in vergelijking met conservatieve tracers. Hoofdstuk 2 van dit proefschrift toonde aan dat SiDNA-retentie concentratieafhankelijk was en afnam met toenemende injectiedeeltjesconcentratie. De verwijderingsefficiëntie nam dus af met toenemende deeltjesinjectieconcentratie. Naast SiDNAmag-concentratie beïnvloedde de ionsterkte (IS) van injectiewater de deeltjeshechting en dus het SiDNA-transport. Een toename van IS van 1 mM tot 5 mM fosfaatbufferinjectiewater verhoogde het SiDNA-transport met een afgenomen hechtingssnelheid, mogelijk als gevolg van competitieve adsorptie van fosfaat op de verzamelaarskorrels. Een toename van IS van 5 mM tot 20 mM verhoogde echter de SiDNA-hechting, toe te schrijven aan de compressie van de elektrostatische dubbellaag. In hoofdstuk 3 hebben we aangetoond dat onder experimentele omstandigheden vrij van deeltjesaggregatie, de hydraulische parameters (hydraulische geleidbaarheid, effectieve porositeit en dispersiviteiten) en bijbehorende onzekerheden geschat uit SiDNA-transportexperimenten statistisch vergelijkbaar waren met de parameters geschat uit zouttracerdoorbraakgegevens. Verder werden de hydraulische parameters en bijbehorende onzekerheidsverdelingen niet beïnvloed door IS van injectiewater.

In een homogene zandtank, gevuld met middelgrote zandkorrels, toonden multipoint SiDNA-injectie-experimenten aan dat de stochastisch (Monte Carlo-simulatie) bepaalde hydraulische parameters en bijbehorende onzekerheden geschat uit SiDNA-doorbraakkrommen statistisch vergelijkbaar waren met de hydraulische parameters geschat uit zouttracers. Dit gaf aan dat de transportsnelheid en het 3D-dispersiegedrag van SiDNA niet significant verschilden van zouttracers, ondanks een aanzienlijk SiDNA-massaverlies als gevolg van deeltjeshechting op de vaste fase. Verder onderzochten we de toepasbaarheid van SiDNA bij het identificeren en schatten van hydraulische geleidbaarheid, effectieve porositeit, dispersiviteit en bijbehorende onzekerheden in een heterogene zandtank met een lensvormige zone zonder geleidbaarheid en, afzonderlijk, eenzelfde lensvormige zone met hoge geleidbaarheid. Multipoint-injectie en multilevel-bemonsteringsaanpak waren specifiek voordelig bij het identificeren van lensheterogeniteit zonder geleidbaarheid. Het effect van de lens met hoge geleidbaarheid werd weerspiegeld in de bi-piekige doorbraakkrommen van zowel het zout als het SiDNA. De hydraulische parameters en bijbehorende onzekerheden stochastisch bepaald uit SiDNA-doorbraakkrommen waren statistisch niet significant verschillend van die bepaald uit zouttracerdoorbraakgegevens in beide gevallen (geen geleidbaarheid en hoge geleidbaarheid). Longitudinale en transversale dispersiviteiten konden echter niet onderscheidend worden bepaald, mogelijk als gevolg van de kleine schaal van lensheterogeniteit en omdat transversale dispersiviteiten werden bepaald als een verhouding van transversale en longitudinale dispersiviteit. Over het algemeen toonde dit proefschrift aan dat onder onze experimentele omstandigheden SiDNA een geschikt deeltje was voor het bepalen van hydraulische parameters (hydraulische geleidbaarheid, effectieve porositeit en dispersiviteit) van verzadigde, ongeconsolideerde, middelgrote en grofkorrelige, homogene en heterogene zandsystemen. We erkennen echter dat onze bevindingen gebaseerd zijn op

gecontroleerde laboratoriumschaalexperimenten. Daarom zouden verdere systematische experimenten over SiDNA-transport als functie van fysische variabelen zoals zandkorrelgrootte, pH, complexe heterogeniteit en chemische factoren, waaronder hoofdionen (Ca2+, Mg2+ etc.), en opgeloste organische stof een vereiste zijn voorafgaand aan grootschalige of veldschaaltoepassingen. In dit onderzoek was de belangrijkste beperking van SiDNA de kinetische hechting van de eerste orde op de verzamelaarskorrels, resulterend in 1-3 ordes van grootte van verminderd SiDNA-herstel in vergelijking met de zouttracer, een mogelijke belemmering voor SiDNA-toepassing in experimenten met langere transportlengtes.

PREFACE

This thesis explores the transport of DNA tagged silica microparticles (SiDNA) through saturated sand, and applicability of the SiDNA in determining hydraulic parameters. The objective of this work was to evaluate the suitability of SiDNA in estimating hydraulic conductivity, effective porosity, and dispersivities and associated uncertainties in saturated, homogeneous and heterogeneous sand. Through this research, I have got the opportunity to learn and explore the subject of microparticles and colloids, colloid transport through saturated porous media and stochastic estimation of hydraulic parameters.

The motivation of taking up this research was my interest to delve deeper into groundwater contamination, aquifer characterization, reactive transport, and groundwater remediation. During this thesis, I not only gained knowledge and experience of the subject, but also learnt how to overcome practical challenges that comes with research.

I would like to express my gratitude to many individuals for their kind support, and encouragement throughout the journey. Foremost, my promoter Prof. Jack Schiven and co-promoter Dr. Jan Willem Foppen for their critical guidance, and persistent support. I would also like to thank Dr. Thom Bogaard, the PI of the project, for his guidance and invaluable support.

I am also indebted to my family and friends for their moral support and understanding, without which this journey would have been tougher.

Swagatam Chakraborty

Delft, April 2024

ACKNOWLEDGMENT

I would like to extend my sincere gratitude to my promoter Prof. Jack Schijven, and co-promoter Dr. Jan Willem Foppen for granting me the opportunity to be a part of this exciting research project as a PhD candidate. Your critical guidance, encouragement and support were invaluable in developing and improving my overall understanding of the subject, and research skills. Alongside guiding me through the research direction, the trust you had put on my abilities, as a student of research, would be immensely significant in my evolution as a researcher and conducting research independently. I would also like to express my gratitude to Dr. Thom Bogaard, the PI of the project 'Watertagging', which, this thesis is a part of, for his kind support and guidance throughout. I would like to acknowledge your time and effort for arranging and organizing the alternate site at the Botanical Garden, TU Delft for conducting experiments during the COVID-19 period, when laboratory access was limited. That was particularly an important lesson on resource management under critical circumstances.

I am truly thankful to my research group colleagues, Dr. Yuchen Tang (Coco), Bahareh Kianfar, and Dr. Ahmed Ahmed Abdelrady for all the technical and personal discussions we had over lunch and coffees. Not only research, but I have learnt a great deal of teamwork and coordination as well, which I believe, will be profoundly useful in my future ventures. I would also like to thank Namata Bright, and Ali Ben Hadi, research associates at the IHE-Delft, Netherlands; for their assitance with the DNA analysis (qPCR) dursing the COVID-19 period. I am highly indebted to Fred Kruis, former laboratory manager at IHE-Delft; and Berend Lolkema, Peter Heerings, Lyzette Robbermont, Zina Al Saffar, Ferdi Battes, and Frank Wiegman, laboratory technicians at IHE-Delft, for their constnat guidance regarding laboratory experiments and analysis. I would also like to thank Armand Middeldorp,

laboratory technician at Technical University of Delft, Netherlands; for his assistance during my experiments conducted at TU-Delft.

I would like to thank Chamath Akalanka, Rayan Elhaj, and Fuad Alqrinawi, the M.Sc. thesis students at IHE-Delft, which whom I had the opportunity to work with and learn from. I would also like to acknowledge Dr. Sulalit Bandyopadhyay (Associate Professor, Department of Chemical Engineering, NUTU, Norway) and his PhD students, Dr. Anuvansh Sharma and Zeeshan Ali for their kind contributions of the DNA tagged microparticles for my research.

I am indebted to Shahnoor (Dr. Shahnoor Hasan) for her support throughout my stay in Delft, the Netherlands. Shahnoor, words are too feeble to thank a friend and guide like you. I would also like to thank Janaka (Dr. Rajapaksha Janaka Bamunawala), Jeewa (Dr. Jeewanthi Sirisena), and Sara (Dr. Sara Masia) for all the discussions, funs and travels we had. Special thanks to Biswa da (Dr. Biswa Chattacharya), Prajna Di, and of course her music team, for the wonderful sessions of music, rehearsals, and performances, and making the journey enjoyable.

Finally, I would like to extent my heartfelt gratitude to my family and friends back home (Kolkata, India) for their continuous support and encouragement. My deepest appreciation to all of you for your persistent support, patience and understanding throughout the journey.

CHAPTER 1: GENERAL INTRODUCTION

Groundwater, accounting for more than 97% non-frozen freshwater resources on earth, has been severely compromised in terms of quality pertaining to natural or anthropogenic contaminations, over extraction and climate change. Natural contaminants are primarily of geogenic origin such as dissolution of natural mineral deposits or rocks (Li et al., 2021; Devic et al., 2014), whereas the anthropogenic pollutants are the offshoots of urbanization, agricultural practices, and industrial operations (Li et al., 2021; Khatri and Tyagi, 2015). Anthropogenic contaminants range from pharmaceutical and personal care products like antibiotics, lipid regulators (Silori et al., 2022; Li et al., 2021), colloids and microparticles (Ren et al., 2021; Żychowski and Bryndal, 2015), to pesticides and fertilizers from agricultural applications (Pradhan et al., 2023). While some of the contaminants are ionic such as nitrate and fluoride (Zhao et al., 2022; Abascal et al., 2022; Kimambo et al., 2019), some are particulate such as bacteria and nanoparticles (Dibyanshu et al., 2022; Grisey et al., 2010; Ferrer et al., 2020). Once the contaminants reach the aquifer through stormwater infiltration (Pitt et al., 2023), landfill leachates (Abiriga et al., 2021), or wastewater leakage (McCance et al., 2018) pathways, the transport and fate of these pollutants depend on the hydraulic properties (hydraulic conductivity, effective porosity, and disersivity) of the aquifers (Guo et al., 2021). Therefore, it is critical to well characterize the hydraulic parameters, associated uncertainties, and spatio-temporal variations within the aquifers. In addition to contaminant transport, and risk analysis, a high-resolution characterization of hydraulic properties of an aquifer is also important for optimizing remediation technologies using chemical or nanoparticles (Hilton et al., 2005; Mobbs et al., 2012; Reginatto et al., 2020)

1.1 Aquifer characterization

Hydraulic conductivity, and effective porosity are the most critical hydraulic parameters to characterize of an unconsolidated or semi-consolidated sedimentary aquifer (Bridge and Hyndman 2004), because these two parameters define the aquifer capacity and average groundwater velocity and mass transport through saturated porous medium. Hydraulic conductivity has been typically determined either through ex-situ methods such as empirical correlation with grain size distribution (Rosas et al., 2013; Boadu, 2000), constant or falling head permeameters (Maliva, 2016), or in-situ methods like pumping and slug tests analysed through Theim solution, Theis solution or hydraulic tomography (Cardiff et al., 2013; Walton, 2019), borehole flowmeter (Genereux and Guardiario, 2001; Jain et al., 2006), electrical resisting profiling (Slater, 2007; Butler , 2007), cone penetration profiling (Voyiadjis and Song, 2003; Chai et al., 2011), vertical electrical sounding (Sattar et al., 2016; Almeida et al., 2021), and tracer tests (Kleipikova et al., 2016; Sutton et al., 2000). Similarly, several ex-situ and in-situ methods such as mercury intrusion porosimetry (Ma., 2014), Helium gas pycnometry (Robin et al., 2016), magnetic resonance sounding (Vouillamoz et al., 2012), and tracer tests (Kim et al., 2005; Fernandez-Garcia et al., 2004; Davis et al., 2000) have been applied for estimating effective porosity. In comparison with the standard physical or geophysical methods, tracer tests have been used for broader applications of direct in-situ measurements of hydraulic and transport parameters of aquifers, groundwater or contaminant flow paths, transport velocities, and investigating specific physical or chemical processes by applying different types of tracers (Divine and McDonnell, 2005). In addition, application of tracers also provides an insight into the fundamental transport process such as longitudinal and transverse dispersion, contributing to the 3-dimensional transport of solute or particulate materials (Sarris et al., 2018).

1.2 Groundwater tracers

Groundwater tracers are either existing or introduced energy (e.g. heat), solute (e.g. salt, dyes) or particulate (e.g. bacteria, spores) variations in the water properties to determine groundwater flow and transport properties, and the hydraulic parameters (Maliva, 2016; Davis et al., 1980). An ideal groundwater tracer is stable, nonreactive, nontoxic, detectable in trace amounts, migrates identically to the water, and according to Davis et al., (1980), does not exist. Tracers are generally categorized based on their origin (i.e. environmental and artificial), and physico-chemical properties (i.e. heat, ion, isotopes, dyes, radioactive, and particles) (Maliva, 2016; Davis et al., 1980). Environmental or passive tracers, such as stable isotopes, microorganisms and major ions, are existing substances in groundwater, either naturally produced or introduced over long period of time, and are used for estimating groundwater residence time, flow and mixing dynamics, and groundwater – surface water interactions (Baskaran et al., 2009; Elliot, 2014; Banks et al., 2021; Stauffer, 1985; Widory et al., 2004). Artificial tracers are ionic, solute (e.g. salts and dyes) or particulate substances introduced in saturated or unsaturated subsurface zones for specific objectives such as groundwater transit time distribution (Lauber and Goldscheider, 2014; Saar, 2010), microorganism transport and removal (Hassanizadeh and Schijven, 2000; Harvey, 1997), determining hydraulic parameter distributions (Molz et al., 1988; Niemann and Rovey, 2000; Worthington, 2022), and aquifer heterogeneity assessment (Larocque et al., 2009; Ptak et al., 2004). Based on the objectives, tracer tests are categorized into qualitative and quantitative tests. Qualitative tests are usually conducted to establish hydrologic connections between surface and groundwater or different aquifer compartments, whereas, quantitative tracer tests are designed to estimate hydraulic parameters, transit or residence time, and physico-chemical attributes (e.g. heterogeneity) of an aquifer (Maliva, 2016).

Salts (e.g. NaCl, KCl, KBr) are the most commonly applied, near ideal, unretarded tracers due to their hydrophilic character (Mastrocicco et al., 2011; Alcala and Custodio, 2008) for both qualitative and quantitative aquifer tracer tests. A number of studies have applied salt tracers to establish groundwater flow dynamics, and hydraulic parameter characterization (e.g. Lile et al., 1997; Doetsch et al., 2012; Davis et al., 2004; Pollock and Cirpka, 2010), or used as reference to demonstrate transport characteristics of bacteria (Becker et al., 2004; Torkzaban et al., 2008), viruses (Chu et al., 2003; Zhuang and Jin, 2003), or other nanoparticles (Bradford et al., 2002; Keller et al., 2004; Shuhua et al., 2023). However, as salt concentrations are commonly measured as total ionic concentration (EC), not considering processes such as cation exchange, surface complexion, or physical mass transport might lead to biased estimation of aquifer hydraulic parameters (Mastrocicco et al., 2011). Like salt tracers, dyes (e.g. Uranine, Rhodamine WT) are non-toxic, cost-efficient groundwater tracing agents and have distinctive wavelength of detection and concentration measurement (Maliva, 2016). A number of studies have used dye tracers to demonstrate surface water – groundwater interaction (Otz et al., 2003; Dujardin et al., 2014), assessment of flow paths and transport (Assari and Mohammadi, 2017; Joun et al., 2023), and collate transport characteristics of nano/microparticles (Goeppert and Goldscheider, 2021; Thomas and Chrysikopoulos, 2007; Kosakowski, 2004). Though often dye tracers had been used as conservative tracer (Goeppert and Goldscheider, 2021; Geyer et al., 2006; Joun et al., 2023), however, low sorption of dyes onto sand or soil grains had been reported (Kasteel et al., 2002; Sabatini, 2000; Sutton et al., 2001), and therefore, should be considered for breakthrough curve modelling and aquifer parameter estimation. Careful field application and sample storage of dye tracers should also be considered because fluorescein dye tracers are also susceptible to photolytic transformation (Maliva, 2016). In addition to salt and dye tracers, natural and engineered

nano/microparticles had also been used for assessing important subsurface bio-physico-chemical characteristics such as aquifer heterogeneity (Harvey and Harms, 2002), biogeochemical processes involved in bacterial transport (Hosono et al., 2014), and intra-aquifer connectivities (Cary et al., 2015). As nano/micro/colloidal particle transport behaviours through saturated porous medium reportedly differ from solute or conservative tracers due to the differences in physico-chemical properties such as size and surface charge (Sirivithayapakorn and Keller, 2004; Bradford et al., 2002), and process variables such as particle concentration and ionic strength (Zevi et al., 2009; Torkzaban et al., 2008; Bradford and Bettahar, 2006), it is important to briefly describe the particle transport processes and modelling approach.

1.3 Colloid transport through saturated aquifer medium

Colloidal particles are particles with a diameter range of ~1 – 1000nm (Everett, 2007; Cosgrove, 2010) or alternatively 10nm - 10µm (DeNovio et al., 2004; Bradford and Torkzaban, 2007), which include natural, such as bacteria, viruses, clay particles or engineered nanomaterials. However, instead of such strict size delineation, literature endorse colloid definition in terms of their dissolution properties and properties influencing transport behaviour (Molnar et al., 2019; Deichmann, 2007), falling between a true solution and bulk material (Hassan et al., 2015).

The fundamental processes controlling the transport of colloids through porous media are advection, dispersion, and colloid retention through attachment onto and detachment from the collector grains (Loveland et al., 2003; Liu et al., 2017; Qi et al., 2014). Colloid attachment had traditionally been explained through Classical Colloid Filtration Theory (CFT). The fundamental product of the CFT is an analytical model predicting the single collector removal efficiency (η) representing the efficiency of a single collector surface to remove colloids from

aqueous phase (Kamai et al., 2015). Under physico-chemical transport conditions unfavourable to colloid attachment, the η is the product of single collector contact efficiency (η_0), and attachment efficiency (α). The first filtration model, given by Yao et al., (1971), considered the diffusion, gravitational sedimentation, and interception to calculate η_0, however, did not consider hydrodynamic interactions (Tufenkji and Elimelech, 2004). The classical CFT was also derived based assumptions such as (a) absence of straining and size exclusion, (b) irreversible attachment, and (c) uniform surface charge on colloids and collectors. Several modifications have been made to improve the prediction colloid deposition by incorporating hydrodynamic interaction and van der Waal forces in Eulerian (Tufenkji and Elimelech, 2004), or Lagrangian (Rajagopalan and Tien, 1976; Nelson and Ginn, 2005) framework.

Overall, transport and fate of colloids in saturated porous medium, with an attention to colloid attachment (or retention or filtration), is generally focused at three different scales, namely, the interface scale, the collector scale and the pore scale. Under saturated condition, the interface scale deals with interfacial energy of a colloid at the solid – water interface and colloid – colloid interface predicting the colloid attachment onto the collector grains and colloidal stability, respectively, through DLVO (electrostatic double layer, van der Waals) and non-DLVO (hydrogen bonding, hydrophobic interactions, steric and Lewis acid-base interactions) forces (Torkzaban et al., 2007; Yuan and Shapiro, 2012; Bradford and Torkzaban, 2008). Whereas the pore scale approach, in addition to interaction forces, also considers size exclusion and straining as important processes for colloid deposition, the collector scale considers colloid capture through surface attachment. Depending on the physico-chemical and process variables, understanding and numerically simulating colloid transport through saturated porous media often requires additional parameters to be considered such as

straining (Bradford et al., 2006; Porubcan and Xu,2011), blocking (Johnson et al., 1996; Vitorge et al., 2013; Treumann et al., 2014), or size exclusion (Sirivithayapakorn and Keller, 2004; Bradford et al., 2003). Straining of colloids is colloid retention in the pore constriction and dependent on the colloid to collector diameter (Bradford et al., 2003). Straining is facilitated through colloid to collector diameter ratio, ranging approximately between 0.001 - 0.008 (Bradford et al., 2003; Shen et al., 2008; Xu et al., 2006) and solution chemistry (Shen et al., 2008) through processes such as aggregation (Qi et al., 2014). Blocking is characterized by progressive filling up of colloid attachment sites resulting in gradual increase in the effluent colloid concentration (Johnson and Elimelech, 1995; Liu et al., 2009), and is dependent on colloid and collector surface physico-chemical properties (Loveland et al., 2003; Johnson et al., 1996). Another colloid size dependent process contributing to colloid transport is size exclusion where colloids are excluded from the smaller pore aperture sizes (Sirivithayapakorn and Keller, 2003), leading to colloid advection velocity enhancement (Harter et al., 2000). Colloid transport could also be influenced by wedging where colloids are retained between two bounding surfaces (Johnson et al., 2007).

1.4 Groundwater flow, and mass transport modeling

Groundwater flow in the saturated zone is generally expressed using Darcy's law as

$$q = \frac{Q}{A} = -K \frac{h_2 - h_1}{l} \quad (1.1)$$

where q is the specific discharge [m/min], A is the cross-sectional area [m^2], Qis the volumetric water flow per unit time [m^3/min], K is the saturated hydraulic conductivity [m/min], and ($h_2 – h_1$)/l is the hydraulic head gradient [-].

Conservative mass transport through saturated porous media is defined through advection and dispersion responsible for bulk mass movement and spread of the mass plume,

respectively. The general conservative mass transport in saturated porous media is expressed as (Yang et al., 2019)

$$\frac{\partial c}{\partial t} = D\frac{\partial^2 c}{\partial x^2} - v\frac{\partial c}{\partial x} \quad (1.2)$$

where c is the dissolved solute concentration in water as a function of space and time, i.e. x and t, respectively. D is the hydrodynamic dispersion coefficient [m^2/min], and v is the pore water velocity [m/min]. The term on the left denotes the change in mass concentration with time, whereas the first term on the right-hand side denotes dispersion and second term represents the advective transport. While the advection – dispersion equation (eq 1.2) represents 1D conservative mass transport, modified versions are required to simulate 3D, conservative and reactive mass transport processes. In 3D mass transport equation, D is modified to D_{ij} representing the longitudinal, horizontal transverse and horizontal vertical dispersivities as is expressed as (Zheng and Wang, 1999)

$$\frac{\partial c}{\partial t} = D_x\frac{\partial^2 c}{\partial x^2} + D_y\frac{\partial^2 c}{\partial y} + D_z\frac{\partial^2 c}{\partial z^2} - v\frac{\partial c}{\partial x} \quad (1.3)$$

D_x, D_y, and D_z are the respective hydrodynamic dispersion coefficient as a function of space in three-dimension (i.e. x, y, and z), c is the dissolved (for salt and dyes) or suspended (for SiDNA) tracer concentration as a function of space and time (i.e. x, y, z, and t, respectively). To interpret colloid mass transfer from aqueous to solid phase, the first order kinetic attachment – detachment terms (Zheng and Wang, 1999) are incorporated in eq 1.3 and is presented in chapter 2 for 1D mass transport, and chapters 3, 4, and 5 for 3D mass transport.

Groundwater numerical models are a simplified representation of real systems with the capability to explain empirical observations through a set of state variables, and flow and mass transport equations. Groundwater numerical models are either deterministic or stochastic. In deterministic groundwater mass transport models, the hydraulic and mass

transport parameters are uniquely determined (Renard et al., 2013), or with limited parameter uncertainty (Pool et al., 2015). However, unless the boundary conditions and parameters governing the mass transport equation are known, the deterministic solutions are less reliable because the real-world aquifers are intrinsically heterogeneous (Renard et al., 2013) and non-unique. Stochastic groundwater mass transport modelling does not consider that the aquifer hydraulic parameters, such as hydraulic conductivity and effective porosity, are unique values, rather a distribution of values and combination of parameter value sets resulting in equifinality (Yidana et al., 2016; Beven and Binley, 1992). Application of statistical Bayesian framework using Monte Carlo approach is one of the common methods to perform stochastic modeling for estimating hydraulic parameter values and associated uncertainties (Radle et al., 2022; Hassan et al., 2009). The overall workflow of the Monte Carlo approach for estimating hydraulic parameters and associated uncertainties involves, (a) generating multiple parameter realization sets, (b) solving the groundwater flow and mass transport for each parameter realization sets, and (c) statistically inferring predictive outputs (Refsgaard et al., 2012), which in case of mass transport, is concentration as a function of time. Monte Carlo modeling approach in combination with tracer transport experiments have been widely implemented for flow path analysis (Assari and Mohammadi, 2017; Fernandez-Garcia et al., 2010), hydraulic and mass transport parameter uncertainty estimation (Yoon et al., 2013; Wheater et al., 2000; Fu and Gomez-Hernandez, 2009; Saley et al., 2016), and contamination risk analysis (Acar et al., 2013; Alberti et al., 2018).

There are a number of groundwater and reactive transport modelling programs capable of simulating 1D and 3D transport simulations such as HPx, OpenGeoSys, PFLOTRAN, HYDROGEOCHEM, MT3D and PHT3D (Steefel et al., 2015). While few programs are process specific, such as PHREEQC for geochemical modeling, few are coupled to enhance the

versatility in process simulation, e.g. HPx is a reactive transport code coupled between HYDRUS and PHREEQC, or PHT3D coupled with MT3DMS. The program applicability can vary based on the modeling objectives, and required physico-chemical processes, because the codes differ in capabilities, e.g. PHT3D and PHREEQC do not simulate unsaturated flow in contrast to OpenGeoSys or HYDROGEOCHEM. There are also time and computation efficient programming language packages, e.g. Flopy (Bakker et al., 2016), for stochastically simulating and post-processing groundwater flow and mass transport.

1.5 DNA tagged microparticles in hydrogeology

As discussed in the section 1.2, a wide variety of inorganic or organic solutes (e.g. salt, dyes) or particulate (bacteria, clay, bacteriophage, nanoparticles) tracers have been applied to characterize aquifer hydraulic parameters, aquifer connectivities, contaminant transport and risk analysis. Each tracing candidate suffers from certain limitations. For instance, for salt tracers, a limitation is the possible bias in estimation of aquifer parameters using electric conductivity as a proxy of total ions disregarding cation exchange between aqueous and solid phase (Mastrocicco et al., 2011), low sorption of often-used conservative dyes tracer (Kasteel et al., 2002; Sabatini, 2000), limited in-situ survival or viability knowledge of bacterial tracers, and change in attachment dynamics due to engineered surface modifications (Taylor et al., 2004; Harvey and Harms, 2002), or high sedimentation rates of larger particles such as yeast or protozoa (Harvey and Harms, 2002). However, the general and an important limitation of the conventional solute and particulate tracers is lack of distinctiveness within the same group of tracers hindering their application in characterizing physico-chemical variability, the most salient feature of subsurface. Therefore, efficient characterization of the flow and mass transport complexity in subsurface require tracer candidates that are uniquely identifiable with low detection limit, rendering them free from natural background concentration

interference and low particle detection limit. Synthetic deoxyribonucleic acid (DNA) molecules comply with these requirements (Liao et al., 2018; Foppen, 2023). Four nucleotides, namely adenine, guanine, cytosine and thymine, combined in different arrangements impart the distinctiveness in the DNA sequence. The DNA specificity and avoidance of background concentration interference are achieved through subjecting the designed DNA sequences to a public domain software, BLAST, for sequence similarity match (Liao et al., 2018). In hydrological applications, the artificially synthesized DNA molecules are often encapsulated in protective layers such as clay, silica, polylactic-co-glycolic acids (PLGA) or polylactic acids (PLA) to stabilize the DNA molecules against physico-chemical stressors such as nuclease enzyme, radiation, temperature, pH, and ionic strength (Chandrasekaran and Haloversen, 2020; Garnett et al., 2009; Mikutis et al., 2018; Pang et al., 2020, Liao et al., 2020, Paunescu et al., 2013).

In the last 20 years, a number of studies have demonstrated the applicability of DNA particles, in naked or in encapsulated microparticle form, in surface water (Foppen et al., 2011; McCluskey et al., 2021; Pang et al., 2020), in saturated, unsaturated, and variably saturated porous media studies (Mikutis et al., 2018; Sabir et al., 1999; Pang et al., 2017; Aquilanti et al., 2013, Wang et al., 2022), and in glacial flow pathways (Dahlke et al., 2015). As the use of naked or free DNA and transport in surface water is out of the scope of this thesis, only the applications of encapsulated DNA tagged particles in saturated subsurface as yet are described further.

Pang et al., (2020) investigated transportability of alginate-chitosan encapsulated DNA particles (diameter of 312 ± 132 nm) in alluvial sand aquifer. Though encapsulated particles were detectable at a transport distance of 37m, the retentions were higher than free DNA and therefore comparably less applicable in subsurface. Mikutis et al., (2018) applied silica

encapsulated DNA particles (diameter 159 nm) to determine the hydraulic conductivity of an unconsolidated aquifer, where the particles exhibited size exclusion and velocity enhancement as compared to sulforhodamine B dye tracer. As such phenomena are dependent on particle size (Sirivithayapakorn and Keller, 2004; Auset and Keller, 2004), therefore, for 2D or 3D subsurface characterization it is important to use DNA particles with unique sequences, but identical size (Mikutis et al., 2018). In a sandy aquifer, Kong et al., (2018) applied silica coated DNA particles (diameter 141 – 159 nm) to determine 2D hydraulic conductivity field through tomographic inversion. Though the particles yielded higher mass recovery rates and lower dispersion as compared to dye tracers, tomographically inverted hydraulic conductivity fields from estimated from DNA particles and dye tracers were similar. Kittila et al., (2019), in a crystalline rock aquifer, observed higher transport velocity of silica encapsulated DNA particles (diameter 166 nm) with lower mass recovery as compared to uranine and sulphorhodamine dye tracers. Georgakakos et al., (2019) investigated the applicability of biodegradable plastic-coated DNA particles through silt loam soil to track potential contamination pathway from septic system.

1.6 Research questions

The broader research question addressed in this work was:

Can DNA tagged microparticles be used for determining hydraulic parameters (e.g. hydraulic conductivity, effective porosity, dispersivity) of a homogeneous and heterogeneous sand medium?

The secondary questions were (a) how physico-chemical variables (e.g. particle concentration, ionic strength) influence the DNA-particle transport in comparison with conservative salt tracer and, (b) how the DNA particle transport behaviour difference or similarity with salt tracers influence hydraulic conductivity, effective porosity and dispersivity estimations in a

homogeneous and a heterogeneous system? Overall, this dissertation explored the application of DNA tagged microparticles in estimating hydraulic parameters, e.g. hydraulic parameters of unconsolidated homogeneous and heterogeneous sand media.

1.7 Research objectives and thesis outline

The general objective of this study was to contribute to the application of silica encapsulated DNA tagged particles in the quantitative characterization of hydraulic parameters and associated uncertainties of a homogeneous and heterogeneous systems. The specific objectives were

a) To investigate the transport characteristics of silica encapsulated double stranded DNA tagged particles (SiDNA) in homogeneous sand columns as a function of SiDNA concentration.
b) To evaluate the effect on injection water ionic strength on the SiDNA transport, hydraulic parameters and associated uncertainties estimation of an unconsolidated saturated sand media.
c) To investigate the applicability of the SiDNA in determining hydraulic conductivity, effective porosity, longitudinal and transverse dispersivities of saturated sand medium
d) To statistically compare the hydraulic parameters and their associated uncertainties estimated from SiDNA transport with conservative salt tracers (i.e. NaCl and Fluorescein).

Chapter 2 describes the quantitative effect of 7 orders of magnitude injection concentration variation of silica encapsulated DNA tagged silica core microparticles (SiDNASi) on transport and retention such as SiDNA attachment rate and removal efficiency through saturated sand columns.

Chapter 3 describes the applicability of silica encapsulated, superparamagnetic DNA particles (SiDNAmag) in determining aquifer hydraulic conductivity, effective porosity, and dispersivities for injection water with different ionic strengths (1mM, 5mM, and 20mM phosphate buffer). In contrast to 1D column experiments conducted in chapter 2, experimentation, analysis, and numerical modelling conducted in this chapter involved multi-point injection and sampling in a three-dimensional sand tank. The injection concentrations of SiDNAmags at different injection points were consistent with each other.

Chapter 4 focuses on determining 3D dispersion of colloids, i.e. longitudinal dispersivity, transverse horizontal and transverse vertical dispersivities. Thereto, in a saturated, homogeneous sand tank two uniquely sequenced SiDNAmag were injected and sampled through multi-point and multi-plexed sampling points. Dispersivity distributions were determined using a Monte Carlo modelling approach and output was compared with dispersivity distributions obtained from conservative salt tracer breakthrough curves for the same sand tank.

While the applicability of SiDNAmag in a homogeneous medium grained sand system was established in the previous chapters, in chapter 5 the use of SiDNAmag in identifying ‘no conductivity’ and ‘high conductivity’ heterogeneous zones through multi-point injection and sampling is dealt with. In addition, through stochastic modelling, this chapter determines the hydraulic parameters and associated uncertainties of each of the heterogeneous domains containing medium and coarse grain sand.

Finally, in chapter 6, a summary and overall conclusion of the study are presented. In addition, the limitations of the use of silica encapsulated DNA tagged microparticles in medium and coarse grain sand, and recommendations for further research are summarized.

CHAPTER 2: EFFECT OF CONCENTRATION OF SILICA ENCAPSULATED DS-DNA COLLOIDAL MICROPARTICLES ON THEIR TRANSPORT THROUGH SATURATED POROUS MEDIA

Chakraborty, S., Foppen, J. W., & Schijven, J. F. (2022). Effect of concentration of silica encapsulated ds-DNA colloidal microparticles on their transport through saturated porous media. *Colloids and Surfaces A: Physicochemical and Engineering Aspects*, *651*, 129625. **https://doi.org/10.1016/j.colsurfa.2022.129625**

Abstract:

We investigated the transport and retention kinetics of silica encapsulated – silica core double stranded DNA particles (SiDNASi) through 15 cm saturated quartz sand columns as a function of wide range of colloidal injection concentrations (C_0 = 8.7x10^2 - 6.6x10^8 particles ml^{-1}). The breakthrough curves (BTCs) exhibited an overall 2-log increase of maximum relative effluent concentration with increasing C_0. Inverse curve fitting, using HYDRUS1D, demonstrated that a 1-site first order kinetic attachment (k_{att}) and detachment (k_{det}) model sufficed to explain the C_0-dependent SiDNASi retention behaviour. With increasing C_0, k_{att} log-linearly decreased, which could be expressed as an overall decrease in the single-collector removal efficiency (η). The decrease in η is possibly due to increasing electrostatic repulsion between aqueous phase- solid phase colloids, formation of shadow zones downstream of deposited colloids and removal of weakly attached colloids from the solid phase (quartz sand) attributing to increasing aqueous phase-solid phase intercolloidal collisions as a function of increasing SiDNASi concentration. Our results implied, firstly, that the aqueous phase colloid concentration should be carefully considered in determining colloidal retention behaviour in saturated porous media. Secondly, the colloidal transport and retention dynamics in column studies should not be compared without the consideration of the colloid influent concentration. Thirdly, our results implied that the applicability of SiDNASi as a conservative subsurface tracer was restricted, because transport distance and retention was colloid concentration dependent.

[Keywords: silica encapsulated – silica core dsDNA particles, injection concentration, saturated porous media, attachment rate, single collector removal efficiency]

2.1. Introduction

An understanding of the physicochemical processes governing the transport and retention of colloidal particles through saturated porous media is imperative due to their importance in carrying subsurface contaminants such as radionuclides, organic compounds, tracer elements (Amme, et al., 2004; Lu & Mason, 2001), in-situ contaminated site remediation (Sangani, Owens, & Fotovat, 2019), use as hydrological tracers (Mikutis et al., 2018; Zhang et al., 2021) or being contaminant themselves (Honeyman, 1999).

Physical and chemical factors, such as collector size, injection solution chemistry, colloidal size, flow velocity, have been widely documented to significantly influence subsurface transport of inorganic (e.g. fullerene, graphene oxide, latex, titanium dioxide, silica) or (bio)colloids (e.g. bacteria, viruses) (figure 1.1). The colloidal input concentration ranges used in these studies, however, vary over 10 orders of magnitude (figure 1.1) with little or no inter-study overlapping. This complicates comparing the outcomes and their applicability of the colloidal transport behaviour over a large spectrum of colloidal concentrations. In comparison with the physicochemical parameters mentioned, regardless of multiple researches indicating the significance of colloidal injection concentration on colloidal deposition and retention behaviour, a systematic investigation to this end is still limited. A careful consideration of colloidal injection concentration and its influence on the colloidal transport behaviour, therefore, is imperative. Additionally, implications of colloidal concentration dependent transport and retention kinetics could be even more significant when colloid facilitated contaminant or microorganism transport is considered (Gentile & de Cortalezzi, 2016; Yang, Tong, & Kim, 2013), specifically when contaminant transport have been observed to be hindered or facilitated depending on colloidal concentration (Qin et al., 2020).

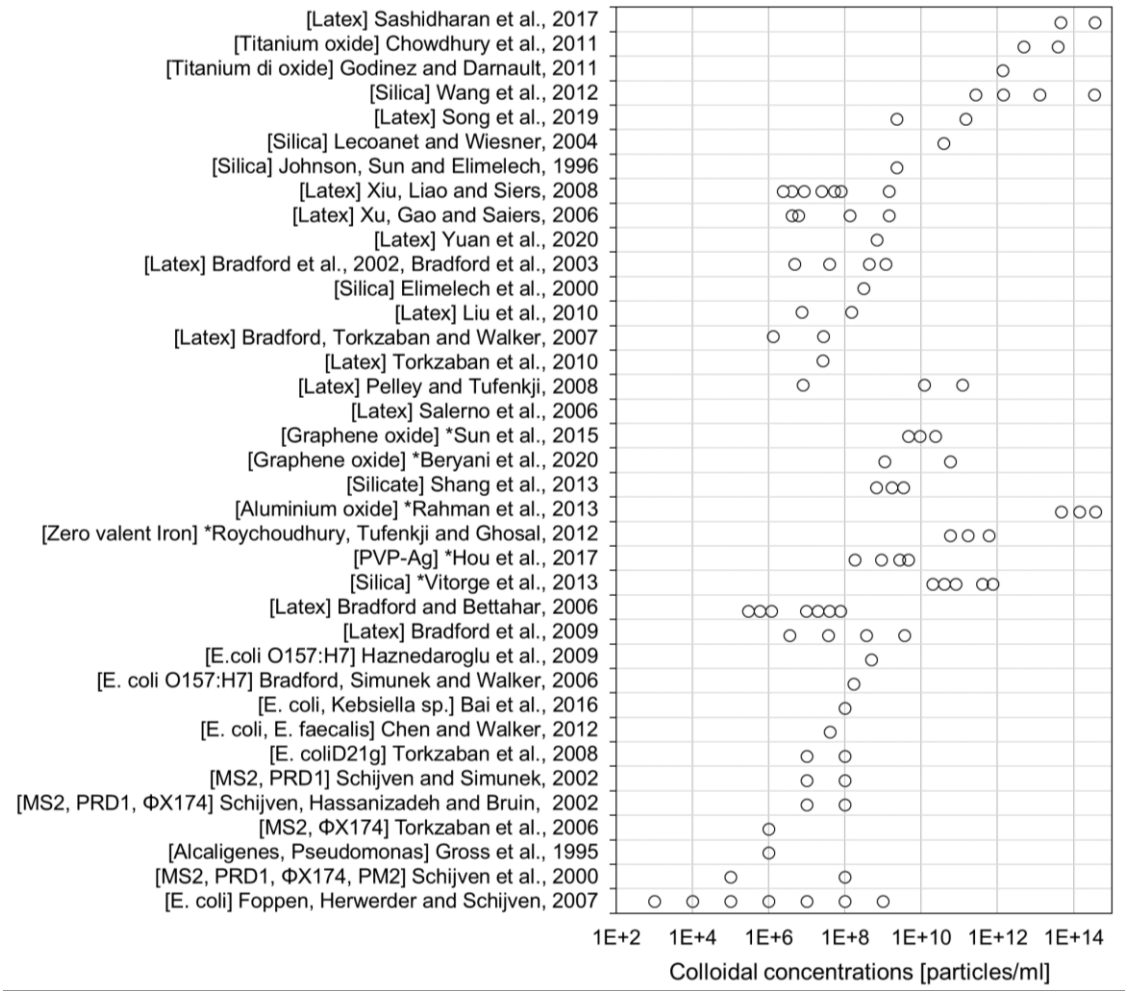

Figure 2.1.: Injection particle concentrations (particles/ml) used for different colloid transport experiment studies under saturated flow conditions. The approximated 'particles/ml' concentration for the asterisked (*) references were calculated by dividing the estimated particle weight (from particle diameter and particle density) by injected W/V concentration information provided by the authors (Sashidharan et al., 2017; Bai et al., 2016; Beryani et al., 2020; Chowdhury et al., 2011, Godinez and Darnault, 2011; Wang et al., 2012, Song et al., 2019; Lecoanet and Wiesner, 2004; Johnson et al., 1996; Xiu et al., 2008; Xu et al., 2006, Yuan et al., 2020; Bradford et al., 2002; 2003; 2006; 2007; 2009; Elimelech et al., 2000; Liu et al., 2010; Torkzaban et al., 2006; 2008; 2010; Pelley and Tufenkji, 2008; Salerno et al., 2006; Sun et al., 2015; Shang et al., 2013; Rahman et al., 2013; Roychoudhury et al., 2012; Hou et al., 2017; Vitorge et al., 2013; Bradford and Bettahar, 2006; Haznedaroglu et al., 2009; Chen and

Walker, 2012; Schijven and Simunek, 2002; Schijven et al., 2000; 2002; Gross et al., 1995; Foppen et al., 2007).

In light of that, a few studies (Vitorge et al., 2013; Wang et al., 2012, Bradford et al., 2006, 2009) have investigated concentration dependent colloidal transport and retention behaviour under unfavourable deposition condition (in the presence of an energy barrier to deposition). Retention of colloids is generally explained as single collector removal efficiency (η), the product of concentration independent single collector contact efficiency (η_0) and single collector attachment efficiency (α), dealing with intercolloidal and colloid-collector grain interactions and subsequent attachment probability (Tufenkji & Elimelech, 2004). α and η_0 are individually influenced by chemical conditions of the experimental system, transport solution chemistry and collector surface properties (Elimelech, 1992; Hahn & O'Melia, 2004). However, while a few researchers considered a concentration independent η_0 and reported α to be concentration dependent due to increased probability of aggregate formation with increasing colloidal concentration resulting in higher deposition (Roychowdhury, Tufenkji and Ghosal, 2012; Rahman et al., 2013), Phenrat et al., (2010) modified the equation for predicting η_0 considering that aggregation alters the effective particle size, an important variable for predicting η_0. A trend of a declining attachment coefficient (k_{att}) and a declining attachment efficiency (α) leading to decreased retention with increasing colloidal input concentrations (C_0) was observed by Wang et al., (2012). Lower mass retention with increasing input colloidal concentration was reported by Bradford and Bettahar (2006) as well. Vitorge et al., (2013), while investigating transport of colloids within a concentration range of $7.7 \times 10^8 – 2.9 \times 10^{12}$ particles/ml for four different colloidal sizes (110, 260, 450 and 660 nm) identified a critical injection concentration, below which k_{att} increased with injection concentration denoting the onset of blocking. Contrasting colloidal transport behaviour, where deposition and

attachment increased with colloidal injection concentration due to formation of particle aggregates leading to pore plugging or straining, have also been reported (Esfahani et al., 2014; Chowdhury et al., 2011; Phenrat et al., 2010). However, such aggregation is only possible when the energy barrier between colloidal particles is diminished.

The widely observed and accepted explanation of enhanced colloidal mobility at higher injection concentrations, colloidal deposition on or removal from solid matrix have also been attributed to inter-colloidal collisions resulting in aggregation or re-entrainment of weakly deposited colloids in the aqueous phase. Bradford et al., (2009) hypothesized intercolloidal collision to be an important mechanism for removal or "knocking off" of solid phase particle. The authors considered η_0 to be concentration independent and the relative reduction in aqueous-to-solid phase colloidal mass transfer with increasing C_0 was due to enhanced inter-colloidal collision at higher concentrations, leading to increased detachment of colloids, weakly attached (i.e. at secondary energy minima) to the collector grains. Linear increase in inter-colloidal collision frequency (F_c) with increase in colloidal number concentration (n) is expressed as (Crowe et al., 1998):

$$F_C = n\pi D^2 v_r \tag{2.1}$$

Where D is the diameter of the particles and v_r is velocity of one particle relative to other particles.

Increasing the injection concentration of nanobubbles (gas containing bubbles used for water treatment, soil remediation of organic chemicals etc.) for enhancing nanobubbles-deposited latex colloidal collision probability and therefore removal of attached latex colloids on porous media has been suggested by Sugimoto et al., (2021).

Aqueous phase colloid-solid phase colloid collisions had been suggested to be a probable mechanism for reversal of nanoscale arsenic thiosulphate aggregation and detachment from porous media (Zhang et al., 2021). A similar mechanism was proposed by Sun et al., (2015) to remove zinc oxide (ZnO) nanoparticles from soil particles deposited at weak secondary energy minima with an energy barrier of only -1.2k_BT at pH 8.5. However, extended release of deposited ZnO nanoparticles under acidic pH condition was attributed to dissolution of the particles due to increasing ZnO solubility with decreasing pH (Han et al., 2016). The effluent concentration of ZnO nanoparticles showed an increase with increasing injection concentrations, with no obvious trend of attachment and detachment coefficients, from 82 to 430 mg/L in soil system. Depending on the depth of existing energy barrier between the particles, colloids were reported to aggregate due to higher collision frequency with increasing injection concentration as well, resulting in higher deposition (Ersenkal et al., 2011).

Collectively, though the aforementioned investigations provide an overview of the parameters (k_{att}, k_{det}, α, η_0) and processes (e.g. blocking, aggregation, knocking off) responsible for colloidal retention and transport as a function of C_0, however, we identified an investigation limitation of bridging the colloid concentration effect over a wide a range of C_0 on the deposition and retention of colloidal particles, because most of the concentration ranges investigated lies within only 2-3 order of magnitudes with little or no inter-study overlap.

The choice of the colloidal particles for this study was directed by the advantage of SiDNASi being environmentally nontoxic, uniquely sequenced, low detection limit and no background noise in natural environment (Kong et al., 2018; Mikutis et al., 2018, 2019). Silica encapsulation is advantageous for its capability of acting as a physical barrier between

delicate DNA molecules and chemical (e.g. metal ions) and physical (e.g. pH, temperature and ionizing radiation) environmental stresses, high chemical and thermal stability, nontoxicity, ability to be synthesized and dissolute at room temperature and chemical compatibility with nucleic acid analysis (Mora et al., 2015; Paunescu et al., 2013; Puddu et al., 2014). Use of these particles is also gaining increasing attention as a potential hydrological tag for investigating subsurface (Aquilanti et al., 2016; Mikutis et al., 2018; Pang et al., 2017; Sabir et al., 1999), surface (Foppen et al., 2011, 2013; Liao et al., 2018, Tang et al., 2021) and glacial (Dahlke et al., 2015) hydrological systems. The concentration range was selected based on its relevance in natural subsurface systems.

The objective of this study was to investigate the quantitative effect of a broad spectrum (7 orders of magnitude) of silica encapsulated deoxyribonucleic acid particles (SiDNAp) injection concentrations on colloidal transport and retention parameters through saturated sand columns. We hypothesized that if removal of colloids weakly associated with collector grains would depend on colloidal injection concentration (C_0), then in systems free of clogging, site saturation, with constant water quality, and where particle collector interactions were predominantly determined by the presence of a secondary energy well, the single collector removal efficiency (η) would remain constant as a function of C_0.

2.2. Materials and methods:

2.2.1. Silica encapsulated DNA colloidal particles (SiDNASi)

4mg/ml (~4×10^{10} particles/ml) *SiDNASi* dispersions (Silica encapsulated 80 bp dsDNA) were obtained from ETH, Zurich, prepared at Functional Materials Laboratory at the Institute of Chemical and Bioengineering, ETH, Zurich, Switzerland, produced using the protocol detailed in Mikutis et al. (2018). The particle number concentration was calculated by dividing the W/V concentration (4mg/ml) of stock suspension by approximated particle weight (obtained from

W/V particle concentration and particle number concentration information at the manufacturing lab). A calibration curve was prepared (qPCR) from the stock suspension to determine the DNA concentration and SiDNASi/ml concentrations used for injection experiments. Zeta potential (ζ) and hydrodynamic diameter ($\emptyset_h$) (Malvern Panalytical Zetasizer Nano-Zs ZEN 3600, the Netherlands) were measured with a concentration of ≈$4x10^7$ – $4x10^8$ particles/ml dispersed in 5mM phosphate buffer using dynamic light scattering (DLS) method (173^0 backscattering). 5mM phosphate buffer prepared using $0.77gL^{-1}$ of $Na_2HPO_4•7H_20$ (0.0029M) (EMSURE®, Merck KgaA, Germany) and $0.29gL^{-1}$ of $NaH_2PO_4•H_20$ (0.0021M) (J.T.Baker, Spain) dissolved in demineralized water. The pH was adjusted to 7.0-7.1 using 100mM NaOH (J.T. Baker, Poland).

2.2.2. Column preparation

To remove surface associated metal oxides (e.g. K^+, Ca^{2+}, Mg^{2+}, Fe^{3+}) and chemical nonidealities (Godinez & Darnault, 2011; Liu et al., 2010; Xu et al., 2008), 355-425µm diameter grain size quartz sand (Sibelco, Soignes, Belgium), with a median diameter of 400µm, was acid washed by soaking in 4N 65% nitric acid (HNO_3) for 2 hours. The acid-soaked sand was further washed with demineralized water till an electric conductivity of <2µS/cm was achieved. The wet sand was then dried at 105^0C in drying oven (TERMAKS, series TS8000, Germany).

The acid washed sand was packed in duplicate Polyvinyl chloride columns (15cm long and ID 2.1cm; Milder B.V., Rotterdam, the Netherlands) in 1-cm increments under constant vibration in order to avoid air entrapment and layering. The sand volume was treated with carbon-di-oxide ($CO_{2(g)}$) in a closed lid container to eliminate air pockets in the saturated column because $CO_{2(g)}$ has a higher solubility in water than air. Injection suspension was injected at

the bottom of each column using a peristaltic pump for suspension injection (WATSON MARLOW 101U/R and BT100-2J) and samples were collected using an automatic fraction collector (OMNICOLL Fraction Collector, Lambda Laboratory Instruments) from the top of the columns (figure 2.1). Prior to each experiment, the columns were equilibrated with at least 10-12 pore volumes of 5mM phosphate buffer. The porosity (ε) of the sand packed columns were measured gravimetrically using:

$$\varepsilon = \frac{W_{SS} - W_{DS}}{v_c} \tag{2.2}$$

Where W_{DS} is dry sand weight [gram], W_{SS} is saturated sand weight [gram], v_c is the total volume of the column [cm^3]. Under completely saturated conditions, the difference between W_{DS} and W_{SS} was considered for determining total void volume (Flint & Flint, 2002).

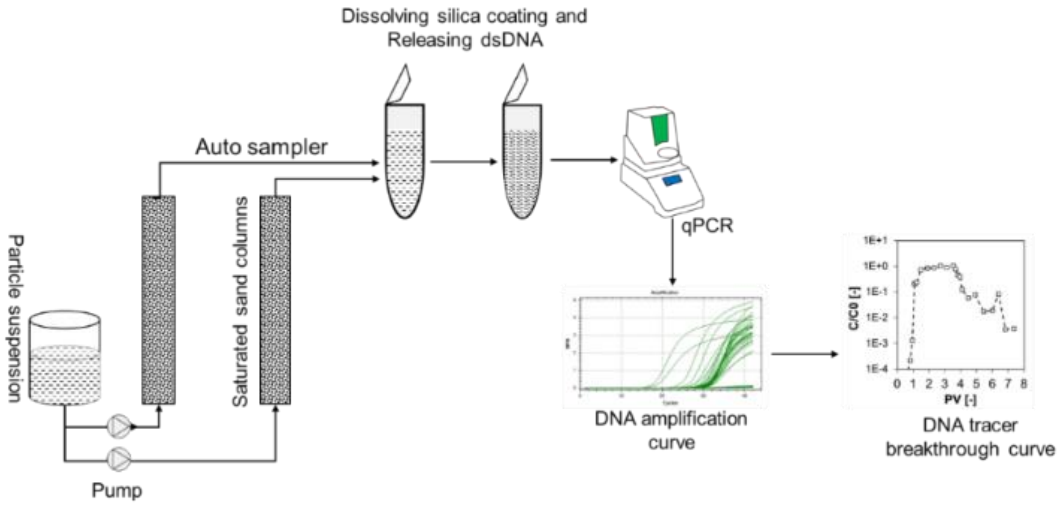

Figure 2.2.: Schematic set up of the column experiments. Sand packed (Ø 355-425µm) PVC columns (l=15cm; ID=2.1cm) in duplicate were fed with SiDNASi suspension of different injection concentrations using a peristaltic pump (bottom-top direction).

2.2.2.1. Column injection experiments

Following the equilibration of the columns with 5mM phosphate buffer, 66-70ml (ca. 3 pore volumes) of seven SiDNASi injection concentrations ranging from 8.72x10^2 to 6.6x10^8

particles/ml (table 1) were injected at a flow rate of 0.3ml/min. Then, 4-5 PVs of particle free solution was injected with subsequent injection of demineralized water (low IS solution) in order to obtain an insight into the type of colloidal-collector kinetic interaction and reversibility of colloid retention process. An overview of the experimental episodes has been summarized below (table 1). The pH of the column influent and effluent were monitored to be stable between 7 – 7.2. Prior to particle injection, conservative salt tracer transport tests were conducted with 3 pore volumes (PVs) of NaCl to check the column packing as well as obtaining ε and D. Particle injection suspensions were well mixed using a magnetic stirrer throughout the injection period and 3-5 samples were collected to determine the stability of injection concentration throughout the injection duration. Samples were collected every 5 minutes in 15-ml polypropylene tubes. NaCl injection experiment samples were analysed using an electric conductivity sensor (WTW-Portable conductivity meter ProfiLine Cond 3310, Germany) and SiDNAp samples were quantified using quantitative polymerase chain reaction (qPCR) as described in the next section.

Table 2.1: Column injection experiment concentrations and episodes

Particles/ml	**Porosity [-]**	**Dispersivity (Std err.) [cm]**	**Episode 1**	**Episode 2**	**Episode 3**	**Episode 4**
6.6×10^{8} **4.7×10^{7}** **3.2×10^{6}** **4.2×10^{5}** **4.8×10^{4}** **3.7×10^{3}** **8.7×10^{2}**	≈0.40	6.24×10^{-2} (1.9×10^{-3})	Equilibrate with phosphate buffer (5mM) for 10-12 PVs	2.5-3 PV particle suspension	4-5 PVs of particle free suspension	5-6 PVs of lower ionic strength solution (demineralized water)

2.2.3. Sample analysis

20µL sample was mixed with 1µL of buffered Oxide Etch (BOE) for dissolving silica and releasing DNA in suspension, followed by addition of 100µL of TRIS-HCl to stabilize pH. 5µL of this suspension was mixed with 1µL of sequence specific, 17 base pair long reverse and forward primers (40-45% GC content) obtained from Biolegio (Biolegio B.V, Nijmegen, the Netherlands) and 13 µl of KAPA SYBR FAST qPCR enzyme master mix (KAPA SYBR® FAST, KK4601 07959389001, South Africa). BOE comprises equal proportions of Ammonium hydrogen Difluoride (NH_4FHF) (Mikutis et al., 2018) (Sigma Life Sciences, the Netherlands) and Ammonium Fluoride (NH_4F) (J.T.Baker®, Holland). Diethyl-pyrocarbonate (DEPC)-treated and sterile filtered water was used for sample preparation. All mixing was done using a QIAgility high-precision automated PCR set up (QIAgility System HEPA/UV, Cat No. /ID: 9001532).

The DNA amplification protocol in MiniOpticonTM detector Real-Time PCR system (Bio-Rad laboratories, USA and Singapore) started with one-time sample treatment at 95^0 C for 280 seconds followed by 41 cycles of 90^0 C for 14 seconds, 58^0 C for 27 seconds and 72^0 C for 25 seconds. The outputs, obtained as quantification cycle (Cq) values, were converted to particle concentrations using a standard dilution curve. A positive control and no template controls (NTCs) were included in sample series analysis for quality control. All positive controls were similar and the negative controls were sufficiently high (Ct>30 amplification cycles) to warrant for the detection specificity of the DNA sequences at low concentrations and contamination free analysis.

2.2.4. Breakthrough curve analysis and 1D modeling

One-dimensional advective transport, longitudinal dispersivity, first-order kinetic attachment and detachment are the processes considered to be major for our experimental conditions. In this study, upon comparing the goodness of fit for the curve fitting and Akaike Information

criteria for one-site and two-site attachment/detachment model, one-site attachment/detachment model (equation 3) was used for experimental curve fitting and parameter optimization. The overall transport equation (Simunek et al., 1998) used was as follows:

$$\frac{\partial \theta c}{\partial t} + \theta k_{att} \Psi c - k_{det} \rho s = \frac{\partial}{\partial x}\left(\theta D \frac{\partial c}{\partial x}\right) - \frac{\partial qc}{\partial x} \quad (2.3)$$

Where *c* is the colloid concentration in liquid phase [particles/ml], *t* is transport time [min], k_{att}, k_{det} are the first order kinetic attachment and detachment rate coefficient, respectively [min^{-1}], $\Psi = (1-s/s_{max})$ is the dynamic blocking function [-] applied for the highest injection concentration, *s* is kinetically attached particle on solid phase [number of particles/g of sand], s_{max} is the maximum solid phase concentration [number of particles/g of sand], ϑ is the volumetric water content [-], *q* is the Darcy flux [cm/min], *D* is the longitudinal dispersion coefficient [cm^2/min], and *x* is the spatial coordinate along the transport length [cm].

To consider the effect of blocking on attachment rate we used the product of blocking function and first order kinetic attachment rate coefficient, denoted by $k_{att}\Psi$, instead of using only first order kinetic attachment coefficient (k_{att}), where *s* tends to s_{max} (Li et al., 2008). The *D* and the estimations of $k_{att}\Psi$, k_{det}, *s*, and s_{max} were obtained by fitting experimental breakthrough curve with a one-site kinetic attachment-detachment, non-equilibrium particle transport model using an open source, widely used software package HYDRUS1D (v.4.17.014). Briefly, in HYDRUS 1D, a Galerkin-type linear finite element method was used to spatially discretize with finite difference methods for estimating the temporal derivatives. A Crank–Nicholson finite difference scheme was used for solving the advection–dispersion equation. Initially an objective function was defined (Šimůnek et al., 1998), and further minimized using the Levenberg-Marquardt non-linear minimization method, a weighted least-squares

approach based on Marquardt's maximum neighborhood method (Marquardt, 1963). HYDRUS1D was chosen for parameter optimization and estimation because the model was open source, well documented and widely used.

D and ε were optimized by fitting salt tracer breakthrough curve to the solute transport code. Then ε was then compared with the gravimetric method.

The single collector contact efficiency ($\eta_{0,CFT}$), for calculating the single collector sticking efficiency (α), was determined by Tufenkji-Elimelech (TE) correlation equation (Tufenkji and Elimelech, 2004) considering a Hamaker constant of $5x10^{20}$ J. The k_{att} and $\eta_{0,CFT,}$ obtained from equation 3 and TE correlation equation, respectively, were further used to compute α, using equation 4 (Tufenkji and Elimelech, 2004). However, in order to evaluate the effect of blocking function for the highest colloidal injection concentration, $k_{att}\Psi$ was used instead of k_{att}:

$$\alpha = \frac{4k_{att}a_c}{3(1-\varepsilon)v_p\eta_{0,CFT}} \quad (2.4)$$

Where a_c is the collector sand grain radius [cm], v_p is the pore water velocity [cm/min].

In addition to kinetic attachment and detachment, as concluded by many researchers, colloidal mobility can also be influenced by filling up of maximum available attachment sites on the collector grains, by reaching a jamming limit (Adamczyk et al.,2013; Johnson & Elimelech,1995). In order to check whether attaining such limit is critical for any changes in k_{att} observed, the *s* and s_{max} obtained from the inverse fitting of experimental breakthrough curves were used to determine the fractional filling of favourable attachment sites or possibility of blocking. In order to determine whether a jamming limit had been reached for the injected concentrations, fractional collector surface coverage (ϑ) was determined as a

ratio of collector surface covered by the maximum solid phase attached particles per gram of sand (s_{cov}) and maximum possible coverage of sand grains per gram of sand ($s_{max.cov}$). To calculate s_{cov}, the maximum particle number deposited s, was selected by comparing deposited particle number at different time steps throughout the experiment. This maximum was typically found to be at the immediate end of a loading phase. $s_{max.cov}$ was estimated by multiplying the total surface area of spherical collector grain per gram of sand and maximum surface coverage (ϑ_∞) possible for sphere-on-sphere deposition, given by Adamczyk et al. (2013):

$$\theta_\infty = 0.547\left(1+\frac{a_c}{a_p}\right)^2 \quad (2.5)$$

2.2.5. DLVO interactions

DLVO interaction energy profiles based on the equation given by Loveland et al., (1996) between colloid-colloid and colloid-collector grains were calculated in order to determine the strength of the interactions in terms of depth of secondary minima ($\Phi_{sec.min}$) and primary energy maxima ($\Phi_{pri.max}$) and therefore possibility of colloidal aggregation or deposition on collector grains (see S1 for the equation and figure S1 for the DLVO profile).

2.3. Results:

2.3.1. SiDNASi characterization

The hydrodynamic diameter and zeta potential (ζ) were found to be 280-300nm and -47.2±7.6 mV at pH 7-7.1 and 23^0C, respectively. The ζ was well above the accepted value (≥30mV for electrostatic and ≥20mV for steric stabilization) for which the inter-particle repulsion is large enough to overcome the van der Waal forces, therefore remaining well dispersed in the aqueous phase rendering the colloidal suspension stable (Alves Júnior & Baldo, 2014; Bhattacharjee, 2016; Patel & Agrawal, 2011). Because the ζ measurement was restricted to a

concentration of ≈4Ex10^7 to 4Ex10^8 due to instrument limitation, evaluating the particle concentration dependent change in $Ø_h$ and ζ due to phosphate buffer was not feasible. However, such changes were not expected because the phosphate ions were in well excess (3x10^{21} ions/ml) as compared to the particle number concentration (phosphate ions: particles of ≈7x10^{12}).

2.3.2. NaCl breakthrough

The effective porosity (ε) determined gravimetrically (≈0.39-0.40) and from iteration based HYDRUS1D code (0.42) were in good agreement with each other. The longitudinal dispersivity (D) was estimated to be ≈6.24x10^{-2} ± 1.9x10^{-3} cm for the duplicate columns. Symmetrical salt tracer breakthrough curves indicated the absence of dual porosity and sink pockets inside the columns. These values were further used for curve fitting of SiDNASi breakthrough curves considering that the dispersion behaviour for the conservative tracer and the colloidal particles are comparable because the peclet number of the experimental conditions were high ($Pe >1$) indicating an advection dominated transport. The coefficient of determination (R^2) between observed and fitted salt breakthrough curves was 0.99±0.002.

2.3.3. Particle breakthrough curve from saturated sand columns

Breakthrough curve behaviour – The maximum effluent colloidal particle concentrations (C_{max}/C_0) (figure 3.1) differed within one order of magnitude between experiments and increased with increasing particle injection concentration(C_0), apparently due to less retention of particles at a higher injection concentration. There was no delayed or early breakthrough observed for any of the concentrations relative to the conservative NaCl tracer. This agreed with the assessment that there was no preferential flow domain or retardation of the SiDNASi. The plateau phase for the SiDNASi breakthrough curves were attained between 1.2-

1.5 pore volumes of injection and remained till 3-4 pore volume of injection following similar trend of salt injection solution, however, the declining limb showed significant tailing as compared to a sharp decline for NaCl injection solution. Prior to demineralized water (low IS solution) injection, similar to maximum effluent colloidal particle concentration, mass recovery also showed pronounced differences among concentrations. Mass recoveries were estimated to be 10, 33, 65, 67, 62, 74, and 83% with increasing injection concentration, respectively. The complete set of breakthrough curves in figure 3.1 showed that injection of lower ionic strength water removed most of the retained particles, supported by the total mass recoveries of nearly 100%. Regression analysis between the observed and model estimated data demonstrated >85% agreement for all concentrations, but $8.7x10^{2}$ particles/ml (table 2). Low injection concentration as well as high colloidal retention led to effluent particle concentration near to detection limit, in turn, higher measurement errors.

2.3.4.First order kinetic attachment (k_{att}) and detachment rate (k_{det})

At first, we tried both one-site and two-site attachment/detachment. However, a comparison between one-site and two-site revealed the two-site model was not better than the one-site in terms of goodness of curve fitting and Akaike Information Criteria (data not shown). Therefore, we chose to further use optimized parameters from the one-site model. The k_{att} ranged between $4.4x10^{-2}$ and $1.7x10^{-3}$ min^{-1} (figure 2.4, table 2), log-linearly decreasing within one order of magnitude with increasing injection particle concentration. The kinetic attachment rate for the highest SiDNASi injection concentration, is considered to be a product of attachment rate and blocking function because $\Psi<0.1$. In contrast, the k_{det} increased with increasing injection concentration from $7.4x10^{-4}$ to $9.8x10^{-3}min^{-1}$ (table 2.2), combinedly indicating higher relative retention with lower injection particle concentration. The estimation

errors at 95% confidence interval ranging within one order of magnitude of the estimated values indicate high and comparable accuracies of the estimated values among different injection concentrations.

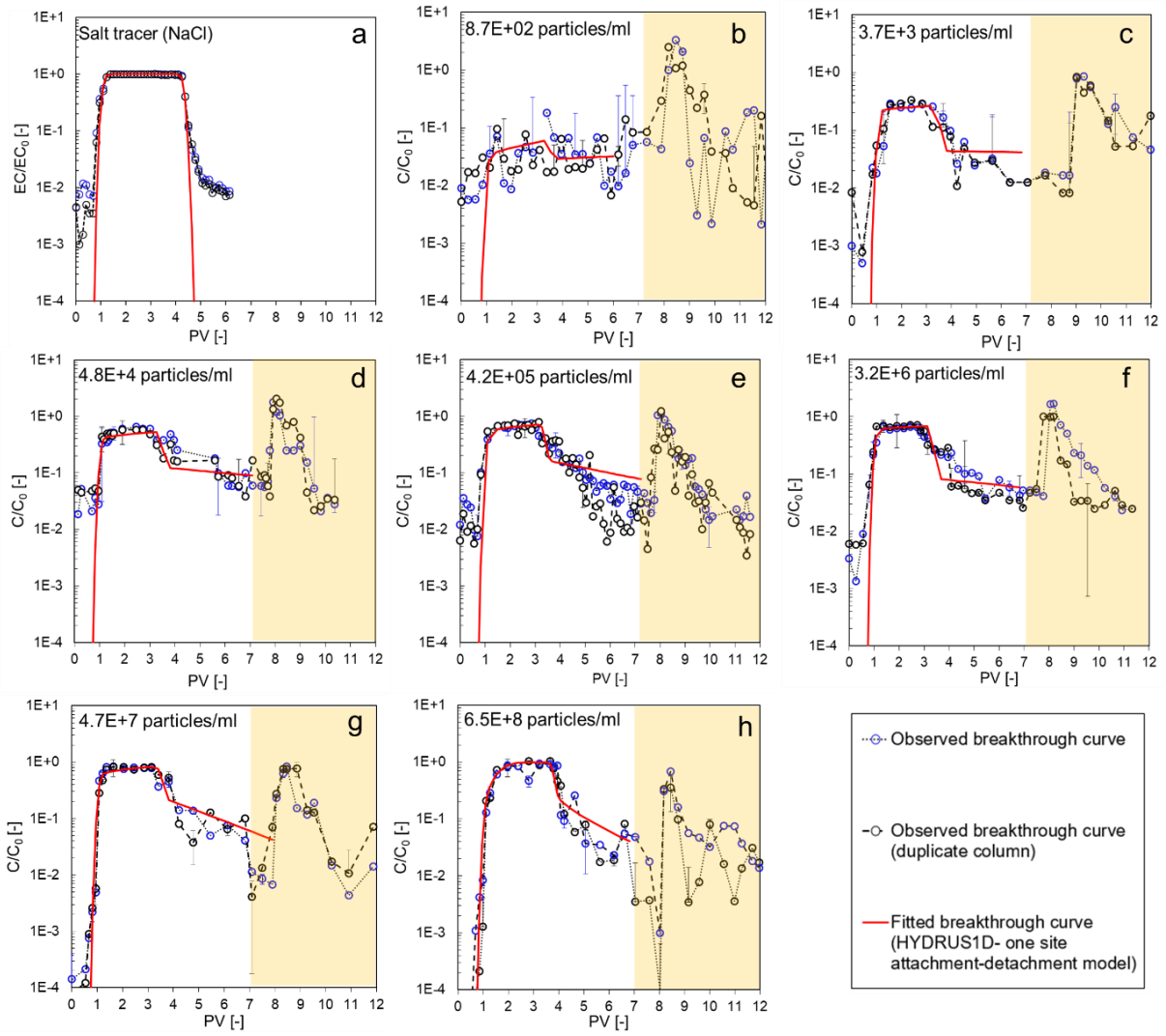

Figure 2.3.: Relative SiDNASi particle concentrations observed in column effluent in duplicate. Figures a and b-h represent the breakthrough curves for conservative tracer (NaCl) and different SiDNASi injection concentrations ranging from $8.7x10^2$ to $6.5x10^8$ particles/ml with one site kinetic attachment-detachment model fitted breakthrough curve (solid red line), respectively. The white blocks denote the injection of SiDNASi particle suspension followed by background solution injection (episode 2 and 3) and the yellow blocks denote the demineralized injection episode (episode 4)Table 2.2: SiDNASi injection concentration

dependent effective attachment ($k_{att}\Psi$) and detachment rate (k_{det}) coefficients [min^{-1}] obtained from one site attachment-detachment model curve fitting, s_{max} and s [Particles/g of sand] denotes maximum solid phase and maximum number of attached SiDNASi particles at the end of loading phase, respectively. Calculation of $\eta_{0,exp}$ considers $\alpha_{max.exp}$= $9.42x10^{-2}$ [-]

C_0 [Particles/ ml]	HYDRUS1D **k_{att} (Std error) [min^{-1}]**	**K_{det} (Std error) [min^{-1}]**	**R^2 [-]**	**s_{max} (Std error) [particles/g of sand]**	**s [particles/g of sand]**
$6.6x10^8$	‡$1.7x10^{-3}$ ($3.6x10^{-4}$)	$9.8x10^{-3}$ ($3.4x10^{-3}$)	0.92	$6.5x10^7$ ($1.1x10^7$)	$5.9x10^7$
$4.7x10^7$	$6.2x10^{-3}$ ($8.5x10^{-4}$)	$6.9x10^{-3}$ ($1.9x10^{-3}$)	0.90	$3.9x10^{12}$ ($4.8x10^{-17}$)	$4.7x10^6$
$3.2x10^6$	$6.5x10^{-3}$ ($3.5x10^{-4}$)	$1.8x10^{-3}$ ($5.6x10^{-4}$)	0.88	$4.3x10^{12}$ ($4.9x10^{-17}$)	$4.2x10^5$
$4.2x10^5$	$7.5x10^{-3}$ ($4.8x10^{-4}$)	$3.8x10^{-3}$ ($5.2x10^{-4}$)	0.87	$3.1x10^{12}$ ($3.3x10^{-17}$)	$5.6x10^4$
$4.8x10^4$	$1.1x10^{-2}$ ($6.1x10^{-4}$)	$2.1x10^{-3}$ ($2.7x10^{-4}$)	0.80	$7.3x10^{10}$ ($5.5x10^{-17}$)	$2.9x10^4$
$3.7x10^3$	$1.8x10^{-2}$ ($1.3x10^{-3}$)	$7.4x10^{-4}$ ($1.9x10^{-4}$)	0.83	$4.8x10^{12}$ ($6.8x10^{-17}$)	$1.3x10^3$
$8.7x10^2$	$4.4x10^{-2}$ ($2.9x10^{-3}$)	$1.3x10^{-3}$ ($3.4x10^{-4}$)	0.17	$3.9x10^{11}$ ($1.4x10^{-16}$)	$6.5x10^2$

‡ First order kinetic attachment rate for the highest SiDNASi injection concentration is $k_{att}\Psi$ (attachment rate * blocking function)

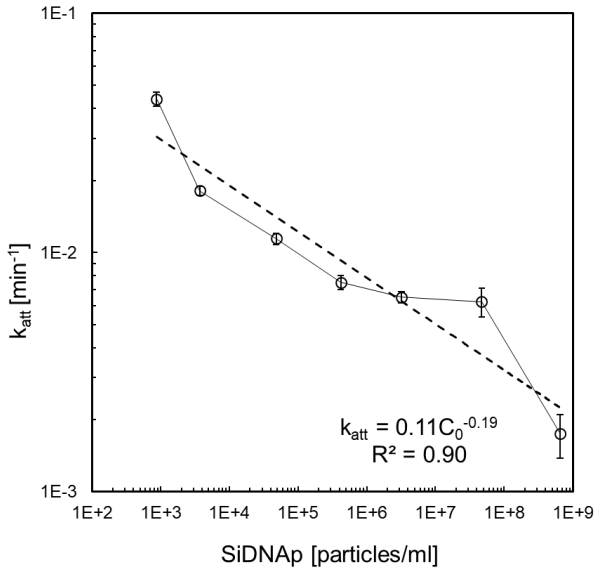

Figure 2.4.: Log-linear correlation of first order kinetic attachment rate (k_{att}) [min^{-1}] with SiDNASi injection concentration. The kinetic attachment rate corresponding to the highest SiDNASi injection concentration is $k_{att}\Psi$ (attachment rate * blocking function

2.3.5. Blocking function (Ψ) and fractional surface coverage (ϑ)

The maximum surface coverage (s_{max}) was found to be $6.5x10^7$ particles/g of sand, (table 2.2). The surface coverages (s) ranged from $6.5x10^2$ to $5.9x10^7$, increased with increasing SiDNASi injection concentration. The blocking function (Ψ) estimated from s and s_{max}, being $s<<s_{max}$ and therefore $\Psi \rightarrow 1$, indicated that time-dependent retention of SiDNASi particles due to filing up of favourable particle retention sites did not play a significant role in the particle retention. However, for the highest injection concentration ($6.6Ex10^8$ particles/ml), s was $0.91s_{max}$, indicating maximum colloidal retention sites to be filled up slightly over 90% of the total available retention sites. In view of SiDNASi size (a_c=$2.8x10^{-5}$cm) and collector (a_p=$4x10^{-2}$cm) radius, the maximum fraction of surface coverage (ϑ_∞) of the spherical collector grain by SiDNASi particle possible was $5.47x10^{-2}$. The fractional surface coverage (ϑ), as a ratio of collector surface coverage by SiDNASi particles (s_{cov}) and maximum possible collector grain surface coverage ($s_{max.cov}$), ranged between $1.7x10^{-8}$ to $6.2x10^{-2}$, with increasing injection

concentration. Even though ϑ log-linearly increased with increasing injection SiDNASi concentration, the values were low (ϑ<<1) enough to be insignificant.

2.3.6. Sticking (α), single collector contact (η_0) and removal efficiency (η)

The sticking efficiency (α) determined using TE correlation equation was found to be ranging between 2.16×10^{-1} and 8.58×10^{-3}, and decreased with increasing injection concentration. The single collector contact efficiency (η_0) was 4.52×10^{-2} [-], using the TE correlation equation.

2.3.7. DLVO calculation

The depth of secondary energy minima ($\Phi_{sec.min}$) for inter-colloidal interaction (figure S1) was -0.86k_BT. The energy barrier ($\Phi_{pri.max}$) for irreversible deposition for both the scenarios was at least one order of magnitude higher than 300k_BT, indicating that deposition in the primary minima was unlikely and deposition in the secondary minima energy well is the primary mechanism of colloidal retention.

2.4. Discussion

With an increasing colloidal injection concentration of SiDNASi under saturated conditions, the maximum effluent concentration (C_{max}/C_0) increased, which was in agreement with Wang et al. (2012), Bradford and Bettahar (2006), Bradford et al. (2009) and Vitorge et al. (2013). The first order kinetic attachment rate (k_{att}) decreased log linearly with increasing injection concentration, which was consistent with Wang et al., (2012), though the underlying mechanism had been attributed to blocking by the authors. Under current experiment conditions and analysing SiDNASi breakthrough curves, blocking was not found to be the primary mechanism controlling the differences in transport behaviour as a function of injection concentration. However, for the highest injection concentration blocking function was estimated to be <0.1, indicating the attachment rate could be influenced by gradual filling

up of the available colloidal retention sites. The correlation equation between k_{att} and C_0 indicated that at a given SiDNASi injection concentration, attachment rate was inversely dependent on the fifth root of injection concentration. This correlation was true if $0 < C_0 <$ blocking concentration, as in this work, because blocking is expected to further enhance the transport possibly resulting in a different trend in attachment rate. On the other hand, the detachment rate coefficient (k_{det}) declined with increasing injection concentration leading to reduced retention at higher injection concentrations.

The concentration dependence of first order k_{att} , k_{det} and overall colloidal retention under consistent physico-chemical experiment conditions could have been arisen either due to changes in α or the η_0. The α estimated applying the attachment rate coefficient obtained from the curve fitting method in equation 4 indicated an inverse relation with the SiDNASi injection concentration, considering that η_0 is constant. However, because α was dependent on the injection solution chemistry and collector surface properties, it is constant under current experimental conditions. Therefore, alternatively we considered α to be constant and propose that the concentration dependent variation of colloidal retention is possibly due to the effect of injection concentration on the single collector collision efficiency (η_0). Considering a value of 9.42×10^{-2} [-] for α_{max}, corresponding to the injection concentration 3.7×10^3 particle/ml, both the $\eta_{0\ and}$ η showed a log linear inverse dependence on the injection SiDNASi particle injection concentration, decreasing with increasing injection concentration. The constant value of α represented maximum attachment efficiency observed in our experimental condition assuming the intercolloidal interaction was relatively negligible (e.g. pH ~7.0, IS 5mM, Temperature 23^0 C). Injection concentration 3.7×10^3 was preferred over 8.7×10^2 particles/ml, because the lowest concentration did not show a well-formed breakthrough curve, effluent concentrations were near detection limit with a low coefficient

of determination (R^2=*0.17*) for curve fitting, indicating low confidence of the parameters estimated.

According to TE correlation equation, η_0 is colloidal injection concentration independent considering that the injection concentration does not significantly alter the colloid size due to aggregation, porosity or approach fluid velocity (Tufenkji and Elimelech, 2004). Because different underlying attachment and detachment mechanisms could not be distinguished through the numerical model, we propose to attribute the effect of increasing SiDNASi injection concentration as overall log linear reduction in η. η log linearly reduced from 9.7×10^{-3} to 3.9×10^{-4} with increasing SiDNASi injection concentration. However, a systematic porous scale observation needs to be conducted to determine the underlying mechanism of such concentration dependent changes in colloidal removal efficiency.

Because the physicochemical conditions for all the column experiments were consistent, site saturation as well as pore clogging or straining were not relevant (particle to collector grain ratio ranges from 7.05×10^{-4} to 8.45×10^{-4} in our experiments, which is more than one order of magnitude than the threshold value (Porubcan & Xu, 2011)), we attributed the colloidal deposition were either weak and at the shallow secondary energy minima or at nanoscale surface charge heterogeneities. Increasing k_{det} and enhanced mobility of SiDNASi with increasing colloidal concentration could be attributed to electrostatic double layer repulson between the aqueous phase and deposited colloidal particles (Johnson, Sun and Elimelech, 1996; Adamczyk et al., 1992, Kuhnen et al., 2000) and by developing a shadow zone downgradient of the deposited particles restricting the probability of subsequent colloidal deposition (Ko and Elimelech, 2000; Sashidharan et al., 2014). Release of weakly attached colloidal particles (deposited in secondary energy minimum or nanoscale surface asperities)

could also be attributed to the enhancement of electrostatic colloid-collector repulsion or charge reversal of surface charge heterogeneities due to adsorption of phosphate onto both collector grains and colloid particles (Chen et al., 2015; Wang et al., 2019; Wang et al., 2020; Xu et al., 2018). Another possible explanation of the concentration dependent changes in k_{att} and the η could be colloidal re-entrainment due to aqueous phase-solid phase inter-colloidal collision. Intercolloidal collision, being a linear function of particle number density, as in $F_C=n\pi D^2 v_r$ (Crowe et al., 1998), increased with increasing SiDNASi injection concentration (Sheng-Hua et al., 2005; Sun et al., 2019; Tourbin & Frances, 2009). Increase in the aqueous phase-solid phase colloidal collision frequency with increasing injection concentration resulted in higher percentage of weakly attached SiDNASi removal from collector grains at higher concentration than in subsequent lower concentrations, a mechanism hypothesized by Bradford et al., (2009) for polystyrene latex microparticles. Increase in 'knocking off' and therefore removal of particles from the collector grain was also observed in the increasing effluent mass recovery with increasing injection concentration. The concept of increased colloid-colloid collision leading to removal of weakly deposited colloids had also been mentioned for zinc oxide nanoparticles (Sun et al., 2015) under alkaline pH condition from soil particles or removal of latex colloids (Sugimoto et al., 2021). Though inter-colloidal collisions have been reported to cause colloidal aggregation and therefore higher deposition (Ersenkal et al., 2011; Roychowdhury et al., 2010). However, at higher concentration ($\approx 10^6$ - 10^7 SiDNASi/ml) of the particles used in this study, did not exhibit time dependent change in hydrodynamic diameter in 5mM phosphate buffer within the injection interval, either in quiescent or mixing condition (Tang et al., 2021) suggesting that aggregation did not occur. However, a detailed pore scale investigation would be required to distinguish between

different attachment and detachment mechanism contributing the mobility of SiDNASi and the effect of injection concentration on the processes.

Under current experiment conditions, the attachment-detachment model demonstrated that the attachment theory suits well to explain the observed breakthrough curves. However, in general, the numerical model is limited regarding the distinction between attachment and retention due to straining. Specifically, when colloid to collector grain mean diameter ratio exceed $1.7x10^{-3}$ (Bradford et al., 2002), and straining is dominant for colloidal retention (Ryan and Elimelech, 1996), the attachment theory would not be able to explain the colloidal transport.

In addition, the correlation between $k_{att,}$ k_{det} and C_0 might be specific to the up-flow direction as adopted in this work because injection flow direction had been reported to significantly influence colloidal deposition. The down-flow direction had been reported to have reduced particle deposition for kaolinite and montmorillonite (Chrysikopoulos and Syngouna, 2014). Basha and Culligan, (2010) observed similar phenomena attributing the particle retention to straining and collector surface asperities during downward flow direction. Surface roughness had comparatively limited influence on particle deposition in up-flow orientation.

2.5. Conclusion

- The current work illustrates a systematic investigation of the influence of injection concentration of silica encapsulated silica core DNA colloidal microparticle (SiDNASi) on their migration characteristics and interaction with one dimensional saturate porous media, under unfavourable deposition conditions.
- The mass recovery, prior to the injection of low ionic strength water (DI water), increased with increasing in injection concentration. However, no correlation between

the increase in recovery with subsequent increasing injection concentration were found.

- Colloidal attachment onto collector grain could be explained well using a one-dimension model considering first order kinetic attachment and detachment. Attachment and detachment rate coefficients respectively decreased and increased with increasing injection SiDNASi concentration.
- The k_{att} reduced with increasing SiDNASi injection concentration, indicating an overall decrease in single collector removal efficiency. The increased SiDNASi mobility with increasing injection concentration could be due to electrostatic repulsion between aqueous phase and deposited colloids, enhanced colloid-collector electrostatic repulsion due to phosphate adsorption and/or increase in aqueous phase-solid phase colloidal collision leading to removal of deposited particles.
- The connotations of these findings are two-fold. Firstly, the significance of understanding the colloidal retention trend and probable processes as a function of injection SiDNASi concentration and secondly, considering the effect of wide ranged colloidal concentration while comparing studies with non-overlapping injection concentrations.
- The primary limitation of this approach could be that the numerical relationship between single collector removal efficiency and injection concentration might be experimental system specific and might alter depending on physicochemical parameters such as flow velocity, ionic strength, flow orientation etc. Therefore, possibility of proposing a generalized numerical correlation is limited.

2.6. Acknowledgement:

This research had been financially supported by The Dutch Research Council (NWO), TTW grant 14514. We would like to extent our gratitude towards Institute of Chemical and Bioengineering, ETH, Zurich, Switzerland for the kind contribution with the SiDNASi particles.

Supplementary information:

S1: The total DLVO interaction energy profile [k_BT] were calculated as a sum of van der Waal force ($\phi^{tot}_{(x)}$), electrostatic double layer repulsion ($\phi^{dl}_{(x)}$) and Born potential ($\phi^{Born}_{(x)}$) using equation S1, as given by Loveland et al., (1996)

$$\varphi^{tot}(X) = \frac{A_{s-w-q} r_c}{6X}\left[1+\left(\frac{14X}{\lambda}\right)\right]^{-1} + \pi\varepsilon\varepsilon_0 r_c\left[2\psi_c\psi_s \ln\left(\frac{1+e^{-KX}}{1-e^{-KX}}\right) + (\psi_c^2+\psi_s^2)\ln(1-e^{-2KX})\right] + \frac{A_{s-w-q}\sigma^6}{7560}\left[\frac{8r_c+X}{(2r_c+X)^7} + \frac{6r_c-X}{(X)^7}\right] \quad \text{(eq S1)}$$

Where X is the colloid-collector distance [nm], r_c is the colloid radius [m], λ is the characteristic wavelength [m], ε is the dielectric constant of water (78.58 [-]), ψ_c and ψ_s are the surface potential of colloid and sand [mV], K is the inverse debye length [m-1], $A_{(s\text{-}w\text{-}q)}$ is the Hamaker constant of 6.3E-21J for SiDNAmag-collector interaction (silica-water-quartz system) (Bergstrom, 1997). A di-electric constant of water and permittivity of free space were considered to be and 8.84E-12 [C Vm-1], respectively. The commonly used value of 5Å was used for the born collision parameter (σ).

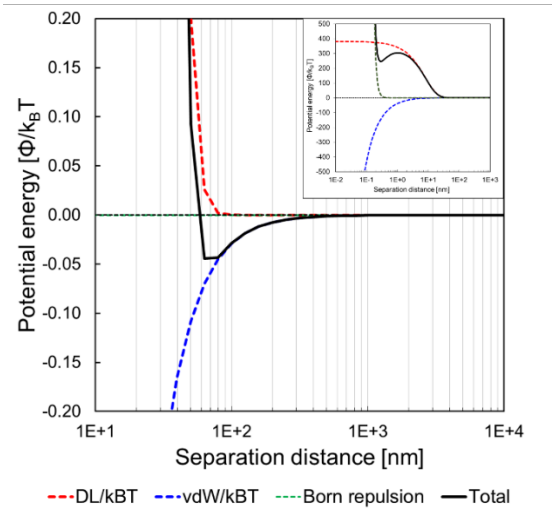

Figure S1: DLVO energy profile of colloid-collector interaction with shallow secondary energy minima and overall DLVO profile (inset)

CHAPTER 3: DISPERSION OF SILICA-ENCAPSULATED DNA MAGNETIC PARTICLES IN A HOMOGENEOUS SAND TANK

Chakraborty, S., Elhaj, R., Foppen, J. W., & Schijven, J. Dispersion of silica-encapsulated dna magnetic particles in a homogeneous sand tank. (Under review).

Abstract:

In this study, we focused on the 3D dispersion of colloids. To our knowledge, we were the first to do so. Thereto, we injected silica encapsulated DNA tagged superparamagnetic particles (SiDNAmag)in a homogeneous coarse grain sand tank. At four downstream locations, SiDNAmag concentrations were determined as a function of time. Longitudinal and transverse dispersivity values and associated uncertainties of SiDNAmag were determined using Monte Carlo modelling approach. The dispersivity uncertainty ranges were then statistically compared with the salt tracer (NaCl, and fluorescein) dispersivities. Our results indicated that time to rise, time of peak concentration and shape of the breakthrough curves of SiDNAmag were similar to those of the salt tracer breakthrough curves. Despite the size difference between the salt tracer molecules and SiDNAmag, size exclusion did not occur, probably due to the large pore throat diameter to SiDNAmag diameter ratio. The median longitudinal dispersivity (α_L) of salt tracer and SiDNAmag were 4.9 and 5.8 x 10^{-4} m, respectively. The median ratio of horizontal and vertical transverse dispersivities to α_L, (α_{TH} /α_L and α_{TV} /α_L, respectively), for salt tracer and SiDNAmag ranged between 0.52 to 0.56. Through the statistical tests, we concluded that the longitudinal and traverse dispersivities of SiDNAmag were not statistically significantly different from salt tracer in 3 dimensions and could be used to characterize the hydraulic properties of the medium we used. Our work contributes to a better understanding of 3D dispersivity of SiDNAmag in saturated porous media.

Keywords: longitudinal dispersivity, transverse dispersivity, colloids, sand tank

3.1 Introduction

Estimation of longitudinal (α_L), horizontal transverse (α_{TH}), and vertical transverse dispersivities (α_{TV}) of colloids in sand is important to predict transport of colloids through sand (Chrysikopoulos and Katzourakis, 2015), and colloid associated contaminant transport (Won, et al., 2019; McCarthy, 2018).

In understanding colloid transport through saturated sand, a usual approach is to consider the α_L of salt tracer and colloids to be identical (Tosco et al., 2012; Schijven et al., 2013; Wang et al., 2012). Where few saturated sand column studies have observed similar arrival and time to peak for colloids as compared to conservative tracers (Solovitch et al., 2010; Tosco et al., 2012; Wang et al., 2012), others have reported otherwise. In a number of saturated sand column studies, with a collector grain to colloid diameter ratio ranging between 100 – 110000 [-] at average linear velocities ranging between 0.1 – 1.95 cm/min (table 3.1), an earlier arrival, earlier time to peak and higher longitudinal dispersivity of colloids as compared to salt tracers, were attributed to velocity enhancement due to size exclusion of colloids and effective porosity reduction (Mikutis et al., 2018; Higgo et al., 1993; Keller et al., 2004; Bennacer et al., 2013; Chrysikopoulos and Katzourakis, 2015; Grolimund et al., 1998; Chrysikopoulos and Syngouna, 2014). In micromodels, Sirivithayapakorn and Keller, (2003), and James and Chrysikopoulos, (2003), reported a reduction in the longitudinal dispersion coefficient and dispersivity with increasing colloid size as compared to conservative tracers. The dispersivity reduction with increasing colloid size was due to smaller colloids and the colloids migrating near the collector grain walls tended to remain near the collector grain wall without migrating to the higher velocity streamlines due to negligible diffusion, therefore, following a more tortuous path (James and Chrysikopoulos, 2003).

Table 3.1: Literature overview of experimental conditions and effect on longitudinal dispersivity, size exclusion and velocity of colloids

Colloids	Study type	d_c (nm)	d_a (μm)	~d_p/d_c*	~d_t/d_c*	V_{cons} (cm/min)	Effect on colloid transport		Reference
							α_L (cm)	Size exclusion and velocity	
Silica DNA	Column	159	200 - 630	918 - 2890	424 - 1600	0.75	Increased	Enhanced	Mikutis et al., (2018)
Silica Colloid	Field	107	600	4000	2200	-	-	Similar peak time	Ryan et al., (1999)
Silica colloid	Column	30	0.5 - 1000	12 - 24000	7 - 13000	0.17	-	Enhanced	Higgo et al., (1993)
Polystyrene beads	Column	50, 3000	350	5000, 150	2800, 50	0.1, 1	Decreased	Enhanced	Keller et al., (2004)
Polystyrene microspheres	Column	30 - 5500	2000	50000 - 265	27000 - 148	0.5 - 2	Increased with increasing size	Enhanced	Chrysikopoulos and Katzourakis, (2015)
Kaolinite, Pseudomonas putida	Column	Kaolinite <2000, P. putida = 2400(900)	2000	Kaolinite = 600, P. putida = 700	Kaolinite = 340, P. putida = 400	0.98 – 1.95	Increased	Kaolinite retarded, P. putida enhanced	Vasiliadou and Chrysikopoulos, (2011)
E. coli	Column	2000 (600)	425 - 600	155 - 220	90 - 120	0.72	Decreased	No enhancement/ retardation	Syngouna and Chrysikopoulos, (2012)

* Approximated from $d_p = 0.73d_a$ and $dt = 0.56d_p$ (correlation applicable to simple cubic packing) (Ren and Santamarina, 2018)

In addition to size exclusion and velocity enhancement, colloid retention by straining or attachment onto the collector grains could affect the longitudinal dispersivity of colloids (Vasiliadou and Chrysikopoulos, 2011; Syngouna and Chrysikopoulos, 2011) and overshadow the effect of size exclusion and velocity enhancement by colloid retardation (Pang et al., 2021; Keller et al., 2004; Grolimund et al., 1998).The minimum pore throat to colloid diameter ratio was < 1.5 for size exclusion to occur (Sirivithayapakorn and Keller, 2003). In a pore network model, Meng and Yang, (2019) reported that for small diameter (100nm as compared to 500nm) particles the effect of size exclusion was negligible and did not affect the longitudinal dispersivity estimation. The contrasting outcomes suggested that dispersion was not only dependent on the porous medium properties but also on the physical properties of colloids (e.g. size) and interaction with the collector grains. Because there were no trends identified as the effect of collector grain diameter, colloid diameter, average flow velocity, pore throat to colloid diameter ratio (table 1), on longitudinal dispersivity, therefore, a colloid (SiDNAmag) and collector grain size specific estimation of α_L, and evaluation of occurrence of size exclusion and velocity enhancement is required.

Horizontal transverse (α_{TH}) and vertical transverse (α_{TV}) dispersivities, in addition to α_L, are also important mechanisms for mass transfer through the porous medium and overall concentration distribution of a plume (Bijelic and Blunt, 2007). α_{TV} and α_{TH} are prevalently considered to be an order of magnitude lower than α_L, which may not be true under all flow and solute transport conditions and therefore, should be determined as an independent parameter (Zech et al., 2019). The consideration of α_{TV} and α_{TH} being 1 order or magnitude lower than α_L, was valid only for advection dominated transport (Bijelic and Blunt, 2007). The knowledge gap that still remained unaddressed is the estimation of α_{TV} and α_{TH} as independent parameters, specifically for colloid transport, in a 3D system.

DNA particles, either naked or encapsulated in polylactic acid, alginate, or silica, had been used for investigating subsurface flow properties, contaminant transport, and aquifer characterization in last two decades (Foppen et al., 2023; Mikutis et al., 2018; Pang et al., 2020; Zhang et al., 2021; Chakraborty et al., 2022). Unlike the salt or dye tracers, uniqueness in the DNA sequences imparts the advantage of DNA particles in concurrent injection experiments without background concentration interference (Pang et al., 2020; Chakraborty et al., 2023). The encapsulation provides stability to the DNA molecules against physico – chemical stressors such as pH, radiation, or enzymatic activities (Pang et al., 2020; Sharma et al., 2012). The additional advantages of DNA particles were high specificity of detection, and low detection limit in polymerase chain reaction (Dahlke et al., 2015; Foppen et al., 2011).

In order to address this knowledge gap, our objective was to assess the α_L, α_{TV}/α_L, and α_{TH}/α_L, of colloid, in the form of SiDNAmag, in a 3D, saturated, homogeneous and unconsolidated sand medium and evaluate the parameter uncertainty relative to the conservative salt tracer transport. Because our sand to SiDNAmag diameter is at least 1-2 order of magnitude larger than threshold of displaying size exclusion or pore clogging (Sirivithayapakorn and Keller, 2003), and small sized colloids migrate similar to conservative salt tracer (Wang et al., 2013), we hypothesize that under our experimental conditions, α_L, α_{TV}/α_L, and α_{TH}/α_L values and associated uncertainties estimated from SiDNAmag transport would not be statistically significantly different to that of conservative tracers.

3.2 Materials and methods:

3.2.1 SiDNAmag and injection suspension preparation

SiDNAmags are spherical colloidal particles with an iron oxide core and silica covering, impregnated with double stranded DNA (dsDNA) molecules (Sharma et al., 2021). The

advantage of dsDNA is the low detection limit, high specificity in quantitative polymerase chain (qPCR), no background concentration interference and are unique in nucleotide sequences providing the advantage of multipoint groundwater flow tracing (Mikutis et al., 2018; Pang et al., 2020). The superparamagnetic property of the iron oxide core imparts the advantage of rapid magnetic separation, therefore, there are no sample volume and up-concentration limitations (Sharma et al., 2021).

At first, we diluted 50µL of stock suspensions of 0.75mg/ml (~10^{10} particles/ml) of two uniquely sequenced SiDNAmags (SiDNAmag$_1$ and SiDNAmag$_2$) (Particle Engineering Research Centre, NTNU, Norway) to 5ml (~10^8 particles/ml) of demineralized water. We treated the 5ml SiDNAmag suspensions with 1µL of bleach to remove any free DNA. After dividing the 5ml suspensions into 1ml aliquots, we washed the SiDNAmags with demineralized water twice by magnetic separation of the SiDNAmags to remove any traces of bleach. We further prepared the injection suspensions by diluting the 5ml SiDNAmag suspension into 495ml (~10^6 particles/ml) of tap water (EC 550 µS/cm; pH 7.0; hardness 145.36mg/L). The diameter of SiDNAmag$_1$ and SiDNAmag$_2$ were 206.4±85.6 nm and 183.9±58.1 nm with a unimodal size distribution and zeta (ζ) potentials of -11mV and -14mV in demineralized water, respectively. We measured the hydrodynamic diameter (D_{hyd}) and the electrophoretic mobility of the SiDNAmags (at a concentration of ~10^7 particles/ml) in tap water using Smoluchowski's equation (Malvern Panalytical Zetasizer Nano-Zs ZEN 3600, the Netherlands). The D_{hyd} were measured using 173° dynamic light backscattering.

3.2.2. Sand tank experiments, and sample analysis

We wet packed a 1.3 m long (1.3 m x 0.7 m x 0.4 m) PVC tank with coarse grain quartz sand (500 – 700 µm) to represent an unconsolidated, homogeneous aquifer system. The tank

dimension was determined through pre-modelling exercise using flow and solute transport module (MT3D) considering suitable transport length, effect of injection volume of flow, and interaction of injection water with tank boundaries. We ensured the homogeneity of the tank by settling the sand through repetitive saturation and desaturation with tap water. Prior to the experiments, we conducted several small scale (10 – 20 cm) salt transport experiments to validate the homogeneity of the system. The ζ potential of the sand was measured by grinding the sand and suspending the sand dust in tap water at a concentration of 0.01 g/ml. The sand grain size distribution was measured by dry sieve analysis (Fritsch vibrating sieve, Dijkstra vereenigde, the Netherlands). The d_{60}, d_{50} and d_{10} of the sand were 665, 630, and 370 µm (coefficient on uniformity = d_{60}/d_{10} = 1.8), respectively. The bulk density of the sand was 1623 kg/m^3. We estimated the pore diameter (d_p) and pore throat diameter (d_t) from sand grain characteristics using (Ren and Santamarina, 2018)

$$d_p = 8\frac{\sqrt[\beta]{\frac{k}{k_0}}\rho_w G_s D_{50}}{3(C_u+7)\rho_m} \quad (3.1a)$$

$$d_t = 0.56 d_p \quad (3.1b)$$

Where β is the sensitivity of hydraulic conductivity to void ratio, K is the hydraulic conductivity (m/min), k_0 is the reference hydraulic conductivity at reference void ratio (e_0 = 1), ρ_w is the density of sand (g/m^3), G_s is the specific gravity of the sand, D_{50} is the media grain diameter (m), Cu is the coefficient of uniformity and ρ_m is the mass density of the sand (g/m^3) (refer to Ren and Santamarina, (2018) for more details). The estimated mean pore diameter to SiDNAmag diameter ratio was ~1.24 x 10^3 ± 3.34 x 10^1. The median pore throat diameter to SiDNAmag diameter ratio was ~6.97 x 10^2 ± 1.87 x 10^1.

We installed two injection wells and one multilevel sampling well at a longitudinal distance of 0.3 m (Inj_1), 0.6 m (Inj_2), and 1.1 m (W_1, W_2, W_3) from the inflow chamber, respectively on single flowline. The screens of the injection wells were installed at a depth of 13 -16 cm from the bottom of the tank. The screens of the multilevel sampling well were installed at depths of 7 – 10 cm, 13 – 16cm, and 19 – 22cm from the bottom of the tank. Another sampling well (W_4) was placed 3cm – 4cm away from the multilevel sampling well, transverse horizontally perpendicular to the flow line (figure 3.1).

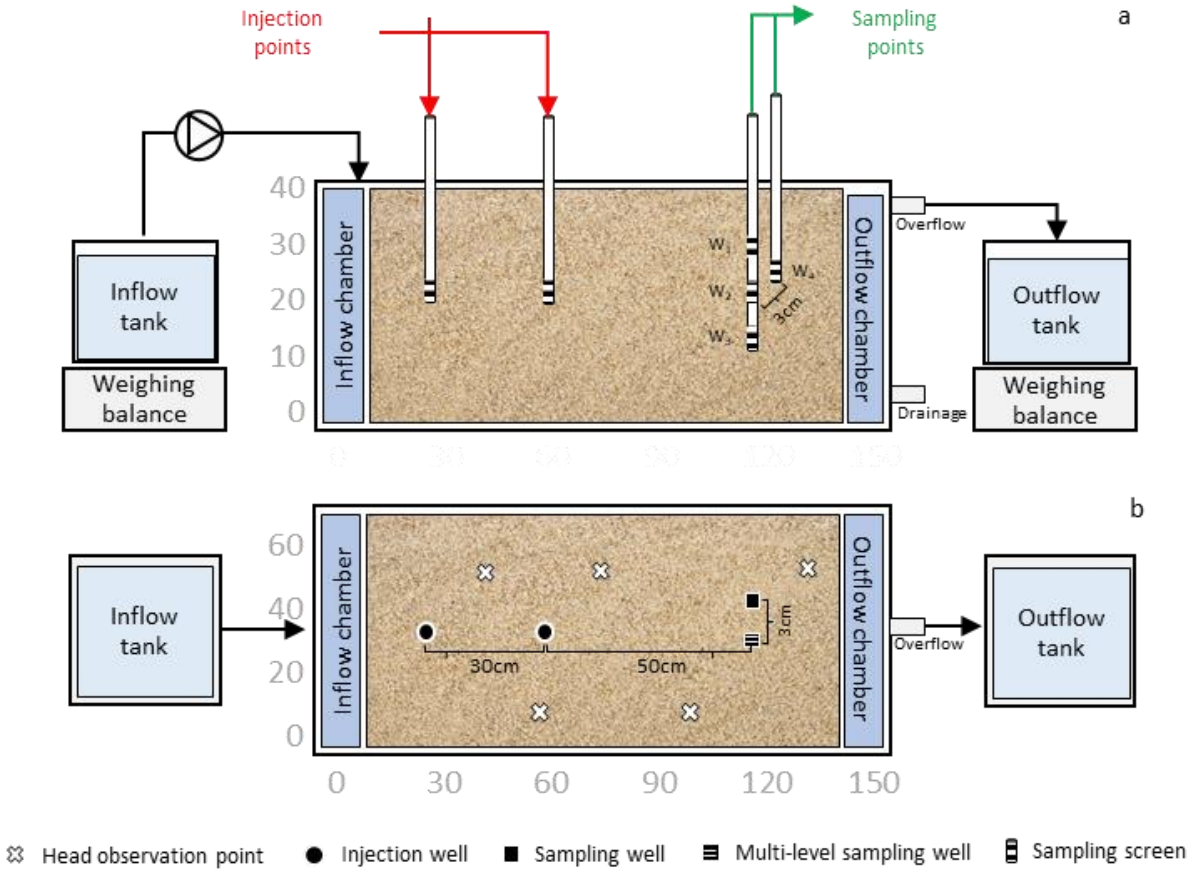

Figure 3.1: Schematic experimental setup

At first, we conditioned the sand with flowing tap water for 14-15 hours. During the experiments, tap water was constantly pumped (Masterflex 7528-30, Vernon Hills, USA) into the inflow chamber at a rate of 511 ± 7.1 mL/min. Inflow (511 ± 7.1 mL/min) and outflow (505

± 7.3 mL/min) rates (water balance discrepancy <5%) were monitored gravimetrically (SBSPF100A1, Steinberg Systems, Germany) in order to maintain a steady inflow. We monitored the hydraulic heads manually at 8 different locations inside the sand tank and by water level data loggers at the inflow (~0.36 ± 0.002 m) and outflow (~0.31 ± 0.001 m) chambers (figure 1) (TD-Diver, Van Essen Instruments B. V., the Netherlands). Further, we injected (Dirac pulse) 100 mL of 0.017g/L fluorescein-disodium salt (Acros Organics B.V.B.A., Thermofisher Scientific, the Netherlands) and 500 mL of 1.8g/L of NaCl (J.T. Baker, the Netherlands) solution in Inj_1 and Inj_2, sequentially in order to avoid any influence of fluorescein-disodium salt on the electric conductivity, and therefore interference with the NaCl breakthrough curves. Because of the uniqueness of the DNA sequences in the SiDNAmags, we injected the different particles at the same time. The fluorescein and NaCl concentrations were analysed by measuring the absorbance at 489nm using UV-visible spectrometer (Lambda 365, PerkinElmer, USA) and electric conductivity (Cond3310, WTW, Wiilheim, Germany), respectively. SiDNAmag concentrations were quantified by measuring DNA concentrations using quantitative polymerase chain reaction (qPCR) (Biorad, USA), as described by Chakraborty et al., (2022). The salt tracer breakthrough datapoints (figure 3.2), were background concentration subtracted as

$$\frac{EC}{EC_0} = \frac{EC - EC_{BG}}{EC_0 - EC_{BG}} \tag{3.2}$$

where EC, EC_0, and EC_{BG} [µS/cm], were observed, injected and background electric conductivity. We presented the salt and SiDNAmag breakthrough curves with only the datapoints above the background concentration and No template control (NTC), respectively.

3.2.3 Breakthrough curve analysis and 3D modelling

We compared the characteristics of the experimental breakthrough curves (BTC) between the salt tracers and SiDNAmags in terms of maximum effluent relative concentration (C_{max}/C_0) and time of C_{max}/C_0 for all sampling locations. Then we estimated the distributions of the α_L, α_{TV}/α_L, and α_{TH}/α_L of the salt tracers and the SiDNAmags, by subjecting the BTCs to convective-diffusive transport modelling adopting a Monte Carlo approach.

3.2.4 Monte Carlo simulation and parameter uncertainty analysis

We estimated the α_L, α_{TV}/α_L, and α_{TH}/α_L distributions using a 3D block-centred finite difference groundwater flow model Modflow-2005 (Harbaugh et al., 2017) in combination with the mass transport module, MT3DMS (Zheng and Wang, 1999). We solved the groundwater flow (equation not shown) in conjunction with solute transport (eq 3.3) equation using an iteration based generalized conjugate solver in a python package, FloPy (Bakker et al., 2022). For the simulations, we used only the observed datapoints above background concentration (for NaCl and fluorescein) and above no template control (for SiDNAmags). Thereto, we could negate the influence of the datapoints below the background concentrations on the objective function. We considered first order kinetic attachment and detachment processes were the differences between the salt tracer and the SiDNAmag transport through the saturated sand (Chakraborty et al., 2022). The mass (salt and SiDNAmag) transport equation (Zheng and Wang, 1999) was

$$n_e \frac{\partial C}{\partial t} + k_{att} n_e C - k_{det} \rho_b S = \frac{\partial}{\partial x_i}\left(n_e D_{ij} \frac{\partial C}{\partial x_j}\right) - \frac{\partial}{\partial x_i}(n_e v_i C) \quad (3.3)$$

Where n_e is the effective porosity of the sand [-], C is the concentration of the salt tracer or SiDNAmag in the water, D_{ij} is the hydrodynamic dispersion coefficient tensor [m^2/min], k_{att} and k_{det} are the first order kinetic attachment and detachment rates of the colloids [1/min], v_i is the linear pore water velocity [m/min], S is the SiDNAmag concentration at the solid surface

of the sand [kg/kg], ρ_b is the bulk density of the sand [kg/m^3] and t is the time [min]. In the mass transport module for SiDNAmag transport, k_{att} is expressed as β/n_e [1/min] and k_{det} is expressed as $\beta/\rho_b k_d$ [1/min], where β is the mass transfer rate from water to sand [1/min] and k_d is the distribution coefficient [m^3/kg] (Babakhani, 2019). We did not consider straining to be important because the colloid to sand grain diameter ratio was well below the threshold of 0.004 (Johnson et al., 2010) or 0.003 (Bradford and Bettahar, 2006). Though fluorescein dye is conventionally used as non-reactive conservative tracer, a number of studies had demonstrated a weak sorption capacity of fluorescein onto soils (Torrentó et al., 2017; Gerke et al., 2008). Therefore, we included the attachment and detachment terms for fluorescein as well.

We discretized the 0.36 m high sand tank spatially in 12 horizontal and variably confined-unconfined layers of equal thickness considering a specified constant head boundary condition. We temporally discretized transient mass transport simulations with a Dirichlet boundary condition in three stress periods (50, 1, 300 minutes) for stabilizing the hydraulic head distribution, solute or SiDNAmag injection and sampling period, respectively. We estimated the input ranges of hydraulic conductivity (k) from the Darcy flux and observed hydraulic gradients in observation wells. We also solved groundwater flow equation, using MODFLOW-2005 in FloPy, with 10000 random-uniformly distributed K and n_e value sets to simulate the observed hydraulic heads. Based on the maximum objective function (coefficient of determination, R^2), we considered the best 1% of the K and n_e value sets as the input ranges. The input ranges of K and n_e were 0.07 – 0.1 [m/min] and 0.2 – 0.4 [-], respectively. The input ranges for α_L, α_{TV}/α_L, and α_{TH}/α_L were 10^{-6} – 10^{-1} [m], 0.01 – 1, and 0.01 – 1, respectively for both the salt tracer and the SiDNAmag. For SiDNAmag transport simulations,

we used input ranges of 0.001 – 0.1 [1/min] and 0.001 – 0.1 [m^3/kg], for β and K_d, respectively.

The mass transport equation was then solved for 10,000 uniformly distributed random parameter sets of α_L, α_{TH} /α_L, and α_{TV} /α_L. The goodness of fit of the parameter sets were evaluated based on root mean squared error (RMSE), both for individual sampling locations and combined for all sampling locations and transport distances (C-RMSE) (Ward et al., 2016). Based on the least C-RMSE, we considered the best 1% parameter sets as the parameter sets to construct the distributions of α_L, α_{TH} /α_L, and α_{TV} /α_L. We assessed the normality of the distributions using Kolmogorov – Smirnov test and Quantile – Quantile plot (QQ plot). Due to non-normality of few of the distributions, we evaluated the statistical significance of differences for each parameter, for conservative tracers and SiDNAmag using distribution non-specific Mann Whitney U test. The fitted breakthrough curves (figure 3.2) were based on the best parameter sets obtained for each parameter.

3.3. Results

3.3.1 SiDNAmag and sand characterization

The ζ potential of the two SiDNAmags (at a concentration of ~10^7 particles/ml) were -22.9±0.05 and -22.06±4.3 mV in the tap water, respectively. The D_{hyd} for the SiDNAmags were 586±30.7 and 688±69.5 nm, respectively. Under quiescent condition, D_{hyd} of the SiDNAmags, did not alter significantly throughout the experiment interval (table 3.2), indicating SiDNAmag aggregation was unlikely to occur during the experiments. The ζ potential of the quartz sand was -26.3±7.9 mV, suggesting an unfavourable SiDNAmag – sand grain attachment condition.

Table 3.2: Salt and SiDNAmag breakthrough curves characteristics and estimated parameter distributions for hydraulic conductivity, effective porosity, longitudinal dispersivity, vertical and horizontal transverse dispersivities. The parameter ranges are presented as median (5^{th} – 95^{th} percentile)

	Transport distance [m]		Tracer characteristics					BTC characteristics		Parameter distributions						
			ζ - potential [mV]	D_{hyd} [nm] 0min	60min	120min	240min	C_{max}/C_0 [-]	t_{peak} [min]	K [m/min]	n_e [-]	α_L [m]	α_{TH}/α_L [-]	α_{TV}/α_L [-]	K_{att} [1/min]	K_{det} [1/min]
Salt tracer	0.5	W_1	-	-				2.5×10^{-1}	75	0.078 (0.074 - 0.081)	0.31 (0.29 - 0.35)	4.9×10^{-4} (6.7×10^{-5} - 9.1×10^{-4})	0.55 (0.12 - 0.92)	0.56 (0.1 - 0.94)	-	-
		W_2						5.7×10^{-1}	75							
		W_3						5.0×10^{-1}	70							
		W_4						4.2×10^{-1}	80							
	0.8	W_1						1.1×10^{-1}	120						8.5×10^{-4} –1.9×10^{-3}	5×10^{-7} – 1.1×10^{-6}
		W_2						4.4×10^{-1}	115							
		W_3						3.9×10^{-1}	115							
		W_4						1.9×10^{-1}	125							
SiDNAmag	0.5	W_1	22.9±0.05	586±31	547±41	525±81	599±99	9.5×10^{-4}	70	0.082 (0.079 - 0.085)	0.31 (0.27 0.35)	5.8×10^{-4} (5.6×10^{-5} - 9.5×10^{-4})	0.52 (0.09 - 0.94)	0.56 (0.09 - 0.92)	0.063 (0.05 – 0.1)	3.2×10^{-4} (1.5×10^{-4} - 1.6×10^{-3})
		W_2						2.9×10^{-2}	70							
		W_3						5.3×10^{-3}	70							
		W_4						7.7×10^{-3}	75							
	0.8	W_1	22.06±4.3	688±69	625±52	613±89	688±79	5.1×10^{-4}	125							
		W_2						1.1×10^{-2}	120							
		W_3						5.3×10^{-4}	120							
		W_4						1.0×10^{-4}	125							

3.3.2 Conservative and SiDNAmag breakthrough curves

The t_{peaks} of the salt tracer for 0.5m transport distance ranged between 70 -80 minutes, similar to 70 – 75 minutes for SiDNAmag. At 0.8 m transport distance the t_{peaks} of the salt tracer ranged between 115 – 125 minutes, which was similar to the t_{peaks} of 120 -125 minutes for the SiDNAmag (table 3.2). For both the salt tracer and SiDNAmag, we observed maximum effluent concentration at W_2, as compared to W_1, W_2 and W_4, due to sampling at the same depth (0.13 - 0.16 m from the bottom of the tank) and flow line as the injection depth. A C_{max}/C_0 of <1 for salt tracer was due to α_L, α_{TH}, α_{TV}. We observed a 1 – 3 log reduction in C_{max}/C_0 of SiDNAmag as compared to the salt tracer, and SiDNAmag to salt mass recovery ratio of 0.003 – 0.032, due to first order kinetic attachment in combination with α_L, α_{TH}, α_{TV}, and SiDNAmag plume mixing with background water (figure 3.2).

Except for the sampling location W_1 for 0.5m transport distance, all breakthrough curves had breakthrough curve tailing. The tailings were possibly due to the detachment of the SiDNAmags from sand grains. However, we did not include the complete tail datapoints in the modeling and parameter estimation process because the SiDNAmag concentrations were near no template control (NTC) and similar to the scattered datapoints prior to the breakthrough. We treated the tail datapoints as sample analysis uncertainty. For fluorescein, at a transport distance of 0.8m, we observed breakthrough tailing, possibly due to the weak sorption behaviour of fluorescein.

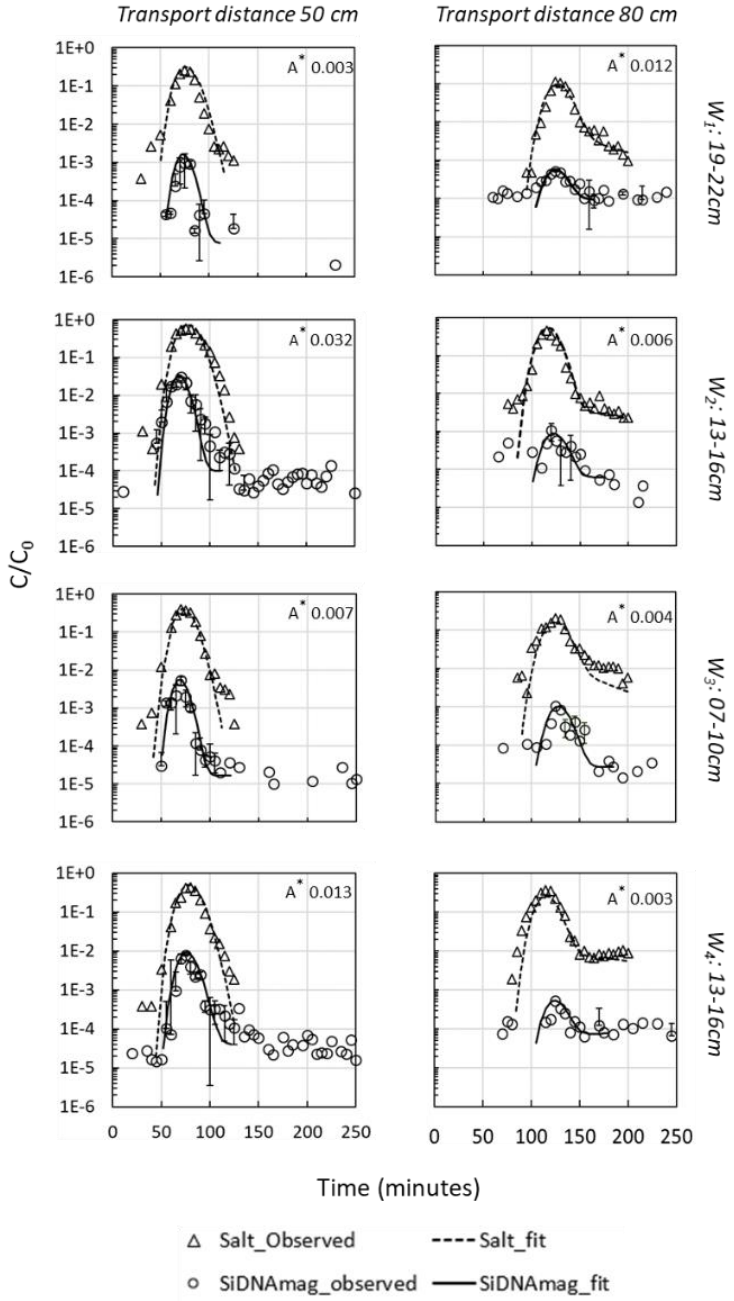

Figure 3.2: Breakthrough curves of conservative (NaCl, fluorescein) and SiDNAmag for 50cm (left column) and 80cm (right column) transport distance at W_1, W_2, W_3 and W_4 sampling locations

3.3.3 Parameter estimation

The RMSE of the individual sampling locations for 50cm transport distance ranged between 0.034 – 0.074 and 0.006 – 0.085 for the salt and SiDNAmag, respectively. For 80cm transport distance, the RMSE of the individual sampling locations ranged between 0.029 – 0.105 and

7.93×10^{-5} – 2.22×10^{-4} for salt and SiDNAmag, respectively. C-RMSE for both the transport distances and all sampling locations ranged between 0.023 – 0.025 and 1.86×10^{-3} - 1.97×10^{-3} for the salt tracer and the SiDNAmag. Based on the best 1% parameter sets estimated from objective function of RMSE for all sampling points combined, the median K values for the salt and the SiDNAmag were 0.078 and 0.082 [m/min], respectively. The K value uncertainty (5^{th} – 95^{th} percentile) for the salt tracer and the SiDNAmag were 0.074 – 0.081, and 0.079 – 0.085 [m/min], respectively. Parameter distributions of n_e for all the sampling locations combined ranged between 0.29 – 0.35, and 0.27 – 0.35 [-], for the salt and SiDNAmag, respectively. The median α_L, for the salt and the SiDNAmag estimated from sampling locations combined were 4.9×10^{-4} and 5.8×10^{-4} m, with a 5^{th} – 95^{th} percentile ranges of 6.7×10^{-5} – 9.1×10^{-4}, and 5.6×10^{-5} – 9.5×10^{-4} [m], respectively. The median α_{TH}/α_L, and the α_{TV}/α_L for both the salt and the SiDNAmag estimated from all sampling points combined ranged between 0.52 – 0.56 [-] with a 5^{th} – 95^{th} percentile of 0.09 – 0.94 [-]. The 5^{th} – 95^{th} percentile ranges for each parameter for combined simulations are summarized in table 3.2. A QQ plot and Kolmogorov – Smirnov test analysis (data not shown) indicated non-normality of the parameter distributions of the α_L, α_{TH}/α_L, and α_{TV}/α_L.

The distributions of all the three parameters estimated either from individual sampling location or from all locations combined for SiDNAmag were not statistically significantly different from the parameter distributions estimated from salt tracer breakthrough curves, when compared using distribution non-specific Mann Whitney U test. The parameter distributions of k, n_e, α_L, α_{TV}/α_L, and α_{TH}/α_L, estimated from the salt and SiDNAmag breakthrough curves, and simulations combined for all transport distances and sampling locations has been shown as box plots with 5^{th} – 95^{th} percentile ranges in figure 3.3. For both the salt and the SiDNAmag, the parameter values and uncertainty ranges estimated from

individual sampling locations were statistically similar to the all sampling locations combined. Therefore, we presented only the ranges estimated from all sampling locations combined.

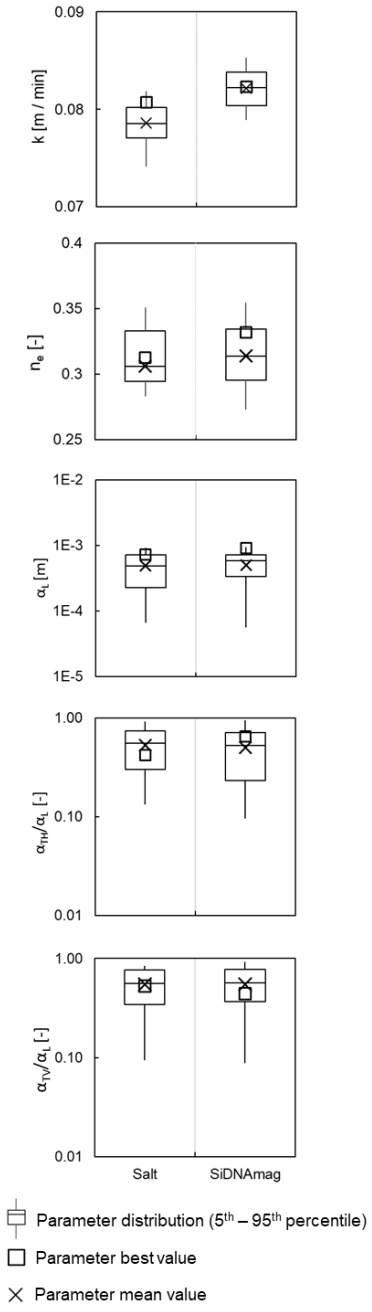

Figure 3.3. Parameter distribution of α_L [m] (a), α_{TH}/α_L [-] (b) and α_{TV}/α_L [-] (c), for conservative tracers (NaCl and Fluorescein) and SiDNAmag particles. (Box = quartiles; horizontal line = median; whiskers = 5^{th} – 95^{th} percentile; X = mean of the distribution

The 1 – 3 log reduction in the C_{max}/C_0 of SiDNAmag, as compared to the conservative salt tracer was due to first order kinetic attachment of SiDNAmag onto the collector grains. The

k_{att} for simulations combined for all the sampling locations and distances was 0.063 [1/min] with a 5^{th} – 95^{th} percentile ranges of 0.055 – 0.11 [1/min]. The k_{det} of the combined simulations was 3.26 x 10^{-4} [1/min] with a 5^{th} – 95^{th} percentile range of 1.48 x 10^{-4} to 1.58 x 10^{-3} [1/min]. The k_{det} were approximately 3 orders of magnitude lesser than that of k_{att}. The tailing of the fluorescein breakthrough curves could be explained through a low first order kinetic sorption ranging between 8.5 x 10^{-4} - 1.9 x 10^{-4} [1/min], indicating the weak sorption behaviour of fluorescein.

3.4 Discussion

The statistically similar α_L, α_{TH} /α_L, and α_{TV} /α_L parameter distributions for both the salt tracer and the SiDNAmag indicated that SiDNAmags had similar 3D dispersive behaviour as the salt tracer. The 1 – 3 log difference in maximum effluent concentration between the salt tracer and the SiDNAmags implied that a significant fraction of injected SiDNAmags could reach the sand grain surfaces, which are the low velocity regions in the parabolic Poiseuille's velocity profile in pores and pore throats. Further, as observed by Auset and Kellet, (2004) in micromodel for smaller colloids (2µm), the SiDNAmags tended to remain in the low velocity streamlines and migrated along the sand grain surfaces. Therefore, SiDNAmags were not restricted to high velocity streamlines. Hence, as observed by Auset and Keller, (2004) and Guo et al., (2016) for smaller particles in microscale, in our experiments the SiDNAmags probably travelled through as tortuous path as the salt tracer, resulting in similar 3D dispersive behaviour. In addition to low diffusion, the sand – SiDNAmag repulsion (charge exclusion) probably was not significant enough to force the SiDNAmags to move from grain surface (low velocity streamlines) towards the high velocity streamlines (Puls and Powell, 1992).

The SiDNAmags did not exhibit an earlier breakthrough or velocity enhancement at any of the sampling locations. This could be due to two orders of magnitude higher pore throat size as

compared to the SiDNAmag diameter. This ratio was higher than the threshold of d_t/d_c of 1.5, the ratio below which colloids cannot enter the pore (Sirivithayapakorn and Keller, 2003). However, our results were not similar to Mikutis et al., (2018), even with similar colloid size (159nm) and sand grain size (200 - 630µm) used in both the studies. Unlike Mikutis et al., (2018), we did not observe increased colloid velocity and increased longitudinal dispersivity. The difference could be due to lower Darcy (0.002 m/min) and average linear velocity (0.006 m/min) applied in our sand tank (Chrysikopoulos and Katzourakis, 2015).

At the lowest average linear velocity (0.005m/min), which was similar to our study (~0.006m/min), Chrysikopoulos and Katzourakis, (2015) did not observe velocity enhancement for any of the colloid sizes. Also, the longitudinal dispersivity of SiDNAmag was higher than the conservative tracer, which could be due to the larger glass beads (2000µm) than the mean sand grain diameter we used (630µm). This is because smaller grain size produces less heterogeneity in the pore size distribution and more irregularity in grain shape increases continuity between medium and large pores (He et al., 2021). Heterogeneity in pore size distribution, in turn, influences the longitudinal dispersivity of colloids. The heterogeneity of sand grain diameter (0.5 - 1000 µm, whereas median diameter similar to this study) could be the cause why our results differ from the size exclusion observed in saturated sand columns by Higgo et al., (1993) as well. It was not possible to reconcile the results of this study with the observations of varying extent of size exclusion, velocity enhancement and longitudinal dispersivity alteration for colloids reported by Higgo et al., (1993); Grolimund et al., (1998); Keller et al., (2004); James and Chrysikopoulos, (2003) due to the differences in all the experimental conditions, such as, flow rate, average linear velocity, colloid size and porous media grain size.

In our study, the ratio of median transverse dispersivities for both the salt tracer and the SiDNAmag was higher than the oftentimes accepted value of 0.1 (Bijeljic and Blunt, 2007). This

was possibly due to a low peclet number and a low flow velocity. Bijeljic and Blunt (2007) reported the α_{TV}/α_L and α_{TH}/α_L for solutes can be as high as ≈1 at low peclet number (0.5 – 1). To further characterize the mechanism of 3D dispersion of SiDNAmags and compare with the salt tracer, a pore scale modelling is required (Auset and Keller, 2004; Baumann et al., 2010). However, pore scale observation was not within the scope of this study.

3.5 Conclusion

- From the salt tracer and colloid (SiDNAmag) particle transport experiments, under our experimental conditions, we found that the longitudinal dispersivity, horizontal transverse and vertical transverse dispersivities of SiDNAmags were similar to the salt tracers. Therefore, we can accept our null hypothesis.
- The parameter distributions of longitudinal dispersivity, horizontal and vertical transverse dispersivities estimated from the individual sampling locations were not statistically significantly different as compared to the distributions estimated from the simulations combined for all sampling distance and locations.
- The SiDNAmags did not show size exclusion or velocity enhancement under current experimental conditions. Due to that, the longitudinal and transverse dispersivities for SiDNAmags were similar to the salt tracer.
- The implication of this study lies in, as applied in our experiments, when the collector grain diameter is few orders of magnitude higher than the colloid diameter, the colloids have similar three dimensional dispersive behaviour and can be applied to predict the transport of solute tracer plumes in 3D.

3.6 Acknowledgement:

This research had been funded by the Dutch Research Council (NWO), TTW grant 14514. We would like to thank Dr. Sulalit Bandyopadhyay, Department of Chemical Engineering, Faculty

of Natural Sciences, NTNU, Norway for the kind contribution with SiDNAmag particles. We would like extend our gratitude to thank Dr. Thom Bogaard, Department of Civil Engineering and Geosciences, TU-Delft, the Netherlands, for his contribution and support with experimental setup preparation and modelling. We would like to thank Hortus Botanicus, TU-Delft, the Netherlands; and IHE-Delft, the Netherlands for the laboratory work support. We would also like to thank Mr. Fuad Alqrinawi for his technical contribution in developing the code for Monte Carlo simulation.

CHAPTER 4: EFFECT OF INJECTION WATER IONIC STRENGTH ON ESTIMATING HYDRAULIC PARAMETERS IN A 3D SAND TANK USING SILICA ENCAPSULATED MAGNETIC DNA PARTICLES

Chakraborty, S., Elhaj, R., Foppen, J. W., & Schijven, J. (2023). Effect of injection water ionic strength on estimating hydraulic parameters in a 3D sand tank using silica encapsulated magnetic DNA particles. *Advances in Water Resources*, *179*, 104507. **https://doi.org/10.1016/j.advwatres.2023.104507**

Abstract

We investigated the applicability of Silica encapsulated, superparamagnetic DNA particles (SiDNAmag) in determining aquifer hydraulic parameters at different ionic strengths (1mM, 5mM, and 20mM phosphate buffer) of injection suspension. Thereto, in a homogeneous, unconsolidated sand tank (1.3m x 0.7m X 0.4m), we injected two uniquely sequenced SiDNAmag at two injection points. At 0.5m and 0.8m downstream from the injection points, we measured the concentration of SiDNAmags at three vertically distributed and two horizontally distributed sampling locations. We estimated the hydraulic parameter distributions from the SiDNAmag breakthrough curves through a Monte – Carlo approach and compared the parameter distributions with salt tracer breakthrough curves. Our results indicated that at all the ionic strengths, the times of peak concentrations, and the shapes of the breakthrough curves were similar to the salt tracer. However, as compared to the salt, the maximum effluent concentrations were reduced by 1 – 3 log units for SiDNAmags due to first order kinetic attachment. The attachment rate reduced from 1mM to 5mM phosphate buffer possibly due to competitive adsorption of phosphate onto the favourable attachment sites. SiDNAmag attachment rate further increased in 20mM buffer suspension, possibly due to the compression of electric double layer and reduction in energy barrier for attachment. The median hydraulic conductivity (k), effective porosity (n_e), and longitudinal dispersivity (α_L), estimated from the SiDNAmag dispersed in 1mM, 5mM, and 20mM and the salt tracer ranged between 0.072 – 0.08 (m/min), 0.34 – 0.36 (-), and 1 x 10^{-4} – 9.7 x 10^{-4} (m), respectively. The vertical transverse dispersivity (α_{TV} /α_L) and horizontal transverse dispersivity (α_{TH} /α_L) for both the salt and the sidnamag ranged between 0.06 – 0.93 [-]. Our results indicated that the parameter distributions of k, n_e, and α_L, determined from SiDNAmag BTCs, corresponding to 5^{th} – 95^{th} percentile, were not statistically different from the salt tracer. Our work contributes

to the applicability of colloidal SiDNAmags for determining hydraulic parameters at different ionic strength conditions.

Keywords: colloids, hydraulic conductivity, effective porosity, longitudinal dispersivity, sand tank

4.1 Introduction

Encapsulated DNA particles have recently attracted significant attention in tracer experiments for investigating subsurface flow, contaminant transport and porous media hydraulic properties characterization (Mikutis et al., 2018, Pang et al., 2020; Zhang et al., 2021; Kong et al., 2018; Kianfar et al., 2022; Chakraborty et al., 2022). In contrast to the conventional tracers (e.g. salt and fluorescent dyes), DNA particles have unique sequences, therefore, can ideally be produced in unlimited number of distinct particles and be used in multipoint injection experiments for aquifer characterization and contaminant transport tracking (Pang et al., 2020). In addition, DNA particles have low detection limit, high detection specificity in quantitative polymerase chain reaction (qPCR), no background noise interference due to uniqueness in nucleotide sequences (Liao et al., 2018). Encapsulated DNA particles have higher stability against environmental physico-chemical stressors (pH, UV radiation, enzymatic and microbial activity) (Sharma et al., 2012, Mikutis et al., 2018) as well.

Under unfavourable condition to colloid - collector attachment, colloidal attachment increased with increasing ionic strength (IS) for polystyrene spheres (Nocito-Gobel and Tobiason, 1996; Wu et al., 2020; Tufenkji and Elimelech, 2005; Tiraferri et al., 2011; Xu et al., 2021; Li et al., 2017) due to compression of electric double layer. Such compression led to weakened electrostatic repulsion between the colloid and collector grains and increased depth of secondary energy minimum (Xu et al., 2021; Wu et al., 2020; Bolster et al., 2001; Kermani et al., 2021). A fraction of heterogeneous collector surface contributing to colloid immobilization can induce a primary or a secondary energy minima interaction as well. Primary minima interaction and re-entrainment, while generally considered to be IS independent (Torkzaban and Bradford, 2016), may be influenced when the area of Zone Of electrostatic Influence (ZOI) is greater than the area of surface heterogeneity (Bradford et al., 2012) and colloids are deposited on rough patches (Torkzaban and Bradford, 2016). In

contrast, Wang et al., (2011), observed an approximate 10-fold reduction in attachment efficiency of *E. coli* when IS increased from 10 to 100mM. A decrease in *E. coli* zeta potential and subsequent increase in the repulsive energy barrier (DLVO) at higher IS hindered bacterial deposition. In addition to the ionic strength, phosphate ions reduced colloid attachment efficiency (α) and attachment rate (k_{att}), therefore, enhanced colloidal mobility (Chen et al., 2021; Liu et al., 2017; Chen et al., 2015; Wang et al., 2019; Zhang et al., 2018; Lin et al., 2021; Li and Schuster, 2014; Wang et al., 2011; Wang et al., 2019). The reduction in α and k_{att}, were attributed to the adsorption of phosphate onto the colloids and competitively on favourable deposition sites on collector grains leading to increased repulsive energy barrier and electrostatic repulsion.

One important implication of IS dependent colloidal release/deposition had been reported to alter the hydraulic conductivity (k) of porous media (Soma and Papadopoulos, 1995; Xinqiang et al., 2019; Won et al., 2018; Dikinya et al., 2008; Samari-Kermani et al., 2021; Torkzaban et al., 2015; Ochi and Vernoux, 1999; Ye et al., 2019). Xinqiang et al. (2019) attributed the reduction in K to "superficial" clogging due to higher colloid attachment at higher ISs (30 and 150mM). Similarly, in column experiments with core samples, Torkzaban et al., (2015), attributed the reduction in the hydraulic conductivity to the hydrodynamic bridging of colloids at the pore constrictions. When the colloid to collector diameter ratio ranged between 0.01 to 0.25, at ionic strengths of 1mM – 100mM, Won et al., (2018) attributed reduction in K to straining due to higher detachment at lower ionic strength. Won and Burns, (2017) attributed the reduction of the K at lower ionic strength (1mM $CaCl_2$) to straining due to aggregation or clustering of clay particles. Similarly, higher colloid release from collector grains, a function of lowered IS (1mM), was reported to decrease 'k' due to pore clogging (Dikinya et al., 2008). In contrast, in 60cm saturated sand (d_{50} = 375 µm) column experiments, at ionic strengths ranging between 0 to 13.68mM, Mesticou et al., (2013), did not observe any reduction in the

sand hydraulic conductivity. However, with longer experiment duration, the authors conclude that the pore clogging and therefore, permeability reduction would have occurred caused by the suspended colloids at the column inlet. In addition to permeability changes due to IS, colloid attachment onto the collector grains could affect the dispersivity estimation of colloids (Vasiliadou and Chrysikopoulos, 2011; Syngouna and Chrysikopoulos, 2011). Studies on the quantitative effect of IS on the effective porosity and dispersivity estimation are still limited. Because there is no general trend of permeability, effective porosity or dispersivity modification as a function of IS, and the modifications are influenced by critical colloid-collector ratio and critical deposition concentration (Bradford et al., 2002), a colloid and collector grain specific evaluation is required.

Stochastic methods are required for identifying simulation errors in hydraulic parameter estimations in deterministic models (Yan and Ji-Chun, 2005) and to represent parameter uncertainties (Ptak et al., 2004). Monte Carlo algorithm is a robust tool for uncertainty assessment of aquifer hydraulic parameters (Hoffmann et al., 2019; Fu and Gomez-Hernandez, 2009), spatial variability of hydraulic parameters (Herrick et al., 2002; Yan and Chun, 2005; Lapcevic et al., 1999; Chen et al., 2012), and to evaluate tracer specific parameter sensitivity (Hoffmann et al., 2019). Saley et al., (2016) successfully adopted Monte Carlo approach for representing hydraulic conductivity distribution using heat tracer. Herrick et al., (2002) determined the correlation between hydraulic gradient, hydraulic conductivity and pore water velocity using Monte Carlo approach.

A number of studies have previously investigated groundwater flow, solute and contaminant transport, characterized hydraulic parameters of 3D laboratory models of saturated sand medium (Ojuri and Ola, 2010, Fadugba et al., 2018; Danquigny et al., 2004; Illman et al., 2011), or Karst aquifer systems (Mohammadi et al., 2021). A limited number of studies so far have

used encapsulated DNA particles for aquifer hydraulic properties characterization (Mikutis et al., 2018; Kong et al., 2018). To our knowledge, we are the first to evaluate the use of SiDNAmag for estimating permeability, effective porosity, and longitudinal dispersivity (k, n_e and α_L, respectively) using a Monte Carlo approach under environmentally relevant and varying injection water quality parameters in a 3D system. The additional advantage of SiDNAmag over non-magnetic DNA particles is that in large scale experiments, the superparamagnetic property of SiDNAmags' imparts the advantage of rapid magnetic separation, therefore, no sample volume and up-concentration limitations (Sharma et al., 2021). The objectives of this study were to investigate the effect of IS perturbation of pore water by injection water on (1) transport of SiDNAmag microparticles in saturated porous media and, (2) probability distribution estimation of aquifer k, n_e and α_L parameters. We hypothesize that if the IS of SiDNAmag injection suspensions are varied between 1mM, 5mM and 20mM of phosphate buffer, then the differences between the estimated probability distributions of k, n_e and α_L at different injection ISs would be statistically insignificant. Therefore, the aquifer parameter estimation would remain uninfluenced by varying extent of SiDNAmag deposition and release rates.

4.2 Materials and method

4.2.1 Silica-encapsulated ds-DNA superparamagnetic particles (SiDNAmag)

We obtained stock suspensions of (0.75mg/ml ~10^{10} particles-ml^{-1}) of two uniquely sequenced SiDNAmags ($SiDNAmag_1$ and $SiDNAmag_2$) (Particle Engineering Research Centre, NTNU, Norway) in demineralized water. The diameter of $SiDNAmag_1$ and $SiDNAmag_2$ were 206.4±85.6 nm and 183.9±58.1 nm and zeta (ζ) potentials were -11 and -14mV in demineralized water, respectively.

4.2.2 SiDNAmag and sand

We suspended 50µL of the SiDNAmag stock suspensions in 5ml of demineralized water. Then, we treated the 5ml SiDNAmag suspension with 1µL of bleach to remove any free DNA present in the suspension. This was followed by washing the suspension twice by magnetic separation (BioRad, the Netherlands) of SiDNAmags to remove the bleach from the suspension. Finally, we prepared the injection suspension by resuspending the magnetically separated SiDNAmags in 1, 5, and 20mM phosphate buffer solutions to a final concentration of ~ 10^6 particles/ml. The stability of the suspended particles in different injection waters were evaluated by means of ζ-potential using Smoluchowski's equation (dielectric constant $_{water}$ = 78.54) (Malvern Panalytical Zetasizer Nano-Zs ZEN 3600, the Netherlands), at a concentration of ~10^7 particles/ml. We checked the possibility of SiDNAmag aggregation within the experiment time interval by measuring hydrodynamic diameter (D_{hyd}) (Malvern Panalytical Zetasizer Nano-Zs ZEN 3600, the Netherlands), as a function of time (0, 60, 120 and 240 minutes), of particles suspended in tap water, 1, 5 and 20 mM phosphate buffer, in quiescent condition (Tang et al., 2021). We checked the ζ-potential of the quartz sand by dispersing 0.1g of manually ground sand in 10ml of tap water, 1mM, 5mM and 20mM phosphate buffer.

4.2.2 Sand tank preparation and injection experiments

We homogeneously wet packed the 1.3 m (1.3m x 0.7m x 0.4m) long sand tank with quartz sand fraction of 500-700 µm diameter (Sibelco, Belgium). The dimension of the sand tank was determined through pre-modelling of hypothetical solute transport experiments in groundwater flow model, MODFLOW (Harbaugh, 2005), and solute transport module MT3DMS (Zheng and Wang, 1999). The dimension of 1.3m x 0.7m x 0.4m was sufficient for performing multipoint and multilevel injection experiments with distinct breakthrough curves as outputs, and, for, parameter estimation.

The sand was wet packed with gradual height increment in order to minimize air entrapment and consolidation (Ojuri and Ola, 2010). Further, to achieve saturation, we flushed the sand tank for 10 – 12 hours with tap water prior to the experiments. In order to inspect the uniform packing throughout the sand tank, we conducted multiple small scale (20 – 30cm) salt tracer tests (data not shown) using the observation wells and compared the peak arrival time. In order to maintain constant hydraulic heads during the experiments, we pumped tap water at a rate of 511 ± 7.1 mL/min into the inflow chamber. We monitored the inflow and the outflow (~505 ± 7.3 mL/min) rates gravimetrically. The resulting hydraulic heads at the inflow chamber and the outflow chamber were 0.36 m and 0.32 m, respectively. The injection points, the sampling points and the screen depths are shown in figure 4.1.

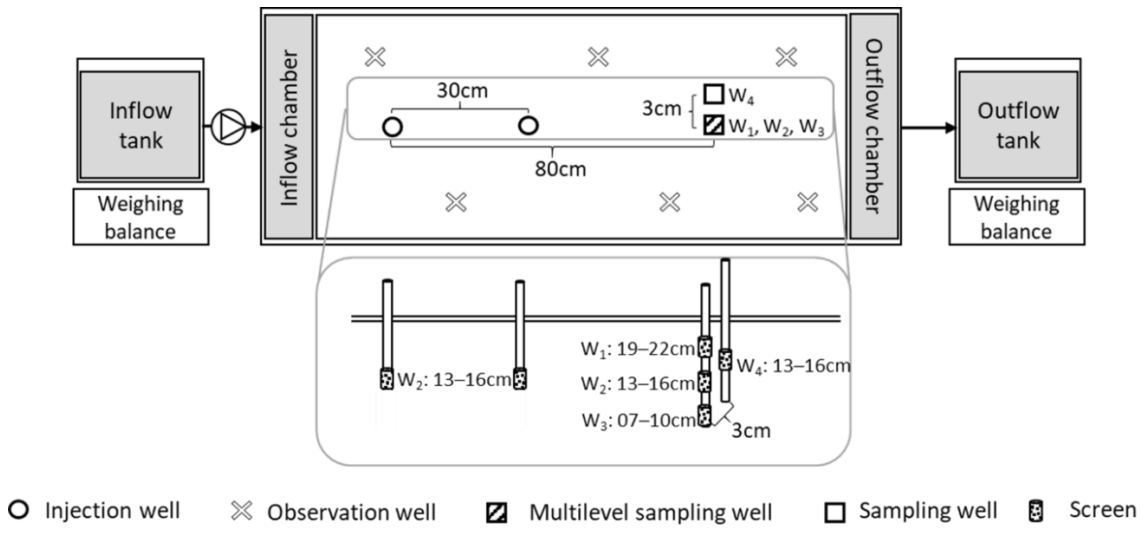

Figure 4.1: Schematic experimental setup

We injected 400ml of salt (1.8g/L) and 100ml of SiDNAmag (~10^6 particles/ml) sequentially at injection rates of 400ml / min and 100ml/min, respectively. Further, we determined the concentration of the salt and the SiDNAmags as a function of time by measuring electric conductivity (WTW-Portable conductivity meter ProfiLine Cond 3310, Germany) and the DNA concentration using qPCR (Bio-Rad laboratories, USA), respectively, in samples collected at a 5 minutes interval. The sampling was done intermittently slow abstraction using plastic syringes in order to avoid the effect on the flow near the well. The protocol followed for qPCR had been detailed in Chakraborty et al., (2022). For representing, analysing and transport modelling of the salt breakthrough curves, we considered the datapoints above the background salt concentration by subtracting the background electric conductivity (EC_{BG}) from observed concentration (EC) and injection concentration (EC_0) using

$$\frac{EC}{EC_0} = \frac{EC - EC_{BG}}{EC_0 - EC_{BG}} \quad (4.1)$$

For simulation of the SiDNAmag breakthrough curves, we considered only the rising limbs, time to peak and the declining limbs. We did not consider the datapoints at the breakthrough tails because the concentrations were near the no template control (NTC) and similar to the scattered datapoints prior to the breakthrough. Therefore, we treated the breakthrough tail datapoints as uncertainty in sample analysis and did not include in the parameter estimation process (for k_{det}). For the breakthrough tails, we did not present the simulated breakthrough curves as well.

4.2.3 Breakthrough curve analysis and 3D modelling

We analysed the BTCs for both the salt tracer and the SiDNAmags in terms of time to peak (t_{peak}) and the maximum effluent concentration (C_{max}/C_0) for all the sampling locations. Then, we determined the k, n_e, and α_L parameter uncertainty, by subjecting the breakthrough curves to 3-dimensional convective-diffusive transport modelling, adopting a Monte-Carlo inverse approach,

considering the first order kinetic non-equilibrium attachment and detachment processes primarily controlling the SiDNAmag transport through saturated porous media.

4.2.4 Groundwater, the salt and the SiDNAmag transport modelling

Encapsulated DNA particles and silica colloids' transport through saturated porous media were descrived using classical convection-dispersion equation for solute transport with first order kinetic attachment – detachment process/term (Chakraborty et al., 2022). The partial differential equation used to simulate the (pore water flow equation not shown) convective-dispersive salt and SiDNAmag transport along with first order kinetic mass transfer from aqueous to solid phase was (Zheng and Wang, 1999)

$$n_e \frac{\partial C}{\partial t} + k_{att} n_e C - k_{det} \rho_b S = \frac{\partial}{\partial x_i}\left(n_e D_{ij} \frac{\partial C}{\partial x_j}\right) - \frac{\partial}{\partial x_i}(n_e v_i C) \quad (4.2)$$

Where C is the salt tracer or SiDNAmag concentration in the water, n_e is the effective porosity [-], D_{ij} is the hydrodynamic dispersion coefficient tensor [m^2/min], k_{att} is the first order attachment rate [1/min] and k_{det} is the first order detachment rate of the colloids [1/min], v_i is the pore water velocity [m/min] and represent the hydraulic conductivity (k) as $v_i = - (k / n_e)* (\delta h/ \delta l)$, where v_i is the pore water velocity [m/min], K is the hydraulic conductivity [m/min], n_e is the effective porosity [-] and $\delta h/ \delta l$ is the hydraulic gradient [-]. S is the SiDNAmag concentration of attachment SiDNAmags [kg/kg], ρ_b is the bulk density of the sand [kg/m^3] and t is the time of transport [min]. In the SiDNAmag transport module, k_{att} is represented by β/n_e [1/min], where β is the mass transfer rate from water to the sand [1/min]. k_{det} is represented by $\beta/\rho_b k_d$ [1/min], where k_d is the distribution coefficient [m^3/kg] (Babakhani, 2019).

We considered straining not to be an important process in the SiDNAmag transport because the colloid to sand grain diameter ratio was 0.0003, which was well below the threshold of 0.003 (Bradford and Bettahar, 2006) and 0.004 (Johnson et al., 2010). Also, the salt and the SiDNAmag

concentration in the injection suspension did not alter the viscosity and density of the injection water, therefore, we did not include density effect in the modelling process.

4.2.5 Monte Carlo simulation and parameter uncertainty analysis

We performed the simulations using a finite difference groundwater flow model, Modflow-2005 (Harbaugh, 2005) in conjunction with a solute transport module, MT3DMS (Zheng and Wang, 1999) in a python package, Flopy (Bakker et al., 2016). We spatially discretized the 1.3m x 0.7m x 0.36m tank model into 12 layers of equal thickness, each layer thickness corresponding to the length of the injection or sampling screen. The first layer was assigned as unconfined and rest of the 11 layers as unconfined/confined. We temporally discretized the mass transport in three stress periods for stabilizing the hydraulic heads (50 minutes), injection period (1 minute) and the sampling period (200 minutes). The input ranges of k, ne and α_L, were 0.05 – 0.15 [m/min], 0.2 – 0.5 [-], and 10^{-8} – 10^{-1} [m], respectively. We estimated the input K and the n_e ranges as ±50% of the average K and n_e estimated from observed hydraulic heads and Darcy's law. The hydraulic heads and therefore, the hydraulic gradients were measured at the observation, injection and the sampling wells. Then we estimated the K by dividing the Darcy flux by the hydraulic gradients ($q = -k * i$), where q is the Darcy flux [m/min] and i is the hydraulic gradient [-]. We approximated the initial n_e by dividing q by average linear velocity (v) obtained from the initially conducted small scale salt tracer experiments. The input range for β was 0.001 – 0.1 [1/min] and the k_d was set to 1 [1/min]. The solute and SiDNAmag transport equation (equation 1) was solved for 20,000 uniformly distributed random realization sets of K, n_e, α_L, and k_{att} for each of the ionic strength conditions. The goodness of fit of the parameter sets were evaluated based on minimized $RMSE_{log}$ combined for all sampling locations and transport distance. We did not emphasize on the coefficient of correlation (R^2) as an objective function because a higher R^2 could be achieved even when the BTC magnitudes are not matched (Ward et al., 2016). Based on the minimized objective

function, we considered the top 1% as the best parameter value sets. Then, we evaluated the normality of the parameter distributions through Kolmogorov – Smirnov test and Quantile – Quantile plot (QQ plot). Because not all the distributions followed a normal distribution, we assessed the statistical differences of the parameter distributions using the distribution non-specific Mann Whitney U test (significance level = 0.05). The simulated breakthrough curves (figure 4.2) are presented based on the median values obtained for each parameter.

4.3 Results

4.3.1 SiDNAmag and sand characterization

The ζ potential of the SiDNAmags decreased with increasing IS of phosphate buffer *(table 1)*. The ζ potentials of the $SiDNAmag_1$ (injected for 0.5m transport length) were -47.7, -44.1, and -39.9 mV, while dispersed in 1mM, 5mM and 20mM phosphate buffer, respectively. The ζ potentials of the $SiDNAmag_2$ (injected for 0.8m transport length) were -43, -40.7, and -38.5 mV, while dispersed in 1mM, 5mM and 20mM phosphate buffer, respectively. In tap water, the ζ potentials of both the SiDNAmags were ~ - 22 mV. The ζ potentials indicated acceptable stability (-20mV < ζ < +20mV) in all water types. The ζ potentials of sand were -26.3, -37.7, -50.7, and -49.3 mV in tap water, 1, 5, and 20mM phosphate buffer, respectively. The negative ζ potentials of both the sand and the SiDNAmag under all ionic strength conditions indicated that colloid transport was conducted under unfavourable condition for colloid attachment onto the sand grains (repulsive double layer interaction). D_{hyd} of the $SiDNAmag_1$ were 442.3, 644.6, and 652.3 nm, while dispersed in 1mM, 5mM and 20mM phosphate buffer, respectively. D_{hyd} of the $SiDNAmag_2$ were 516.9, 660.5, and 655.8 nm, while dispersed in 1mM, 5mM and 20mM phosphate buffer, respectively. The D_{hyd} of the SiDNAmags did not change significantly throughout the experiment interval (240 minutes), indicating that particle aggregation was unlikely to occur (table 4.1).

Table 4.1: Differently DNA-tagged injected particles ($SiDNAmag_1$ and $SiDNAmag_2$) characterization and experimental conditions. The zeta (ζ) potentials were measured at particle concentrations ~4E+5 and 6E+5 particles ml^{-1}, for $SiDNAmag_1$ and $SiDNAmag_2$, respectively

me min)	Injection suspension									Sand
	Salt		$SiDNAmag_1$			$SiDNAmag_2$				
	NaCl	Uranine	1mM	5mM	20mM	1mM	5mM	20mM	1mM	5mM
	3120	517	183	860	2930	183	860	2930		-
		6.8				7.1				
	-	-	-47.7 ± 3.8	-44.1 ± 3.8	-39.9 ± 2.2	-43.0 ± 4.3	-40.7 ± 2.9	-38.5 ± 3.0	-37.7 ± 19.3	-50.7 ± 11
0	-	-	442.3 ± 39.1	644.6 ± 101	652.6 ± 125	516.9 ± 91.9	660.5 ± 108	655.8 ± 84.6		
60	-	-	591.2 ± 98	691.4 ± 41	729.3 ± 118	523 ± 56.1	656.6 ± 87.4	608.22 ± 101		-
120	-	-	478.6 ± 58	678.5 ± 59	698.4 ± 99	577.5 ± 77	698.1 ± 104	688.65 ± 88.2		
240	-	-	505.2 ± 102	623.5 ± 121	702.5 ± 79	528.7 ± 117	602.7 ± 97.1	622 ± 98.7		

† injected at 0.5m transport length, ‡ injected at 0.8m transport lengthSalt and SiDNAmag breakthrough curves

All the sampling locations combined, the time to peaks (t_{peaks}) for salt tracer at 0.5 m and 0.8m transport distances ranged between 75 – 80 minutes and 120 – 125 minutes, respectively (figure 4.2).

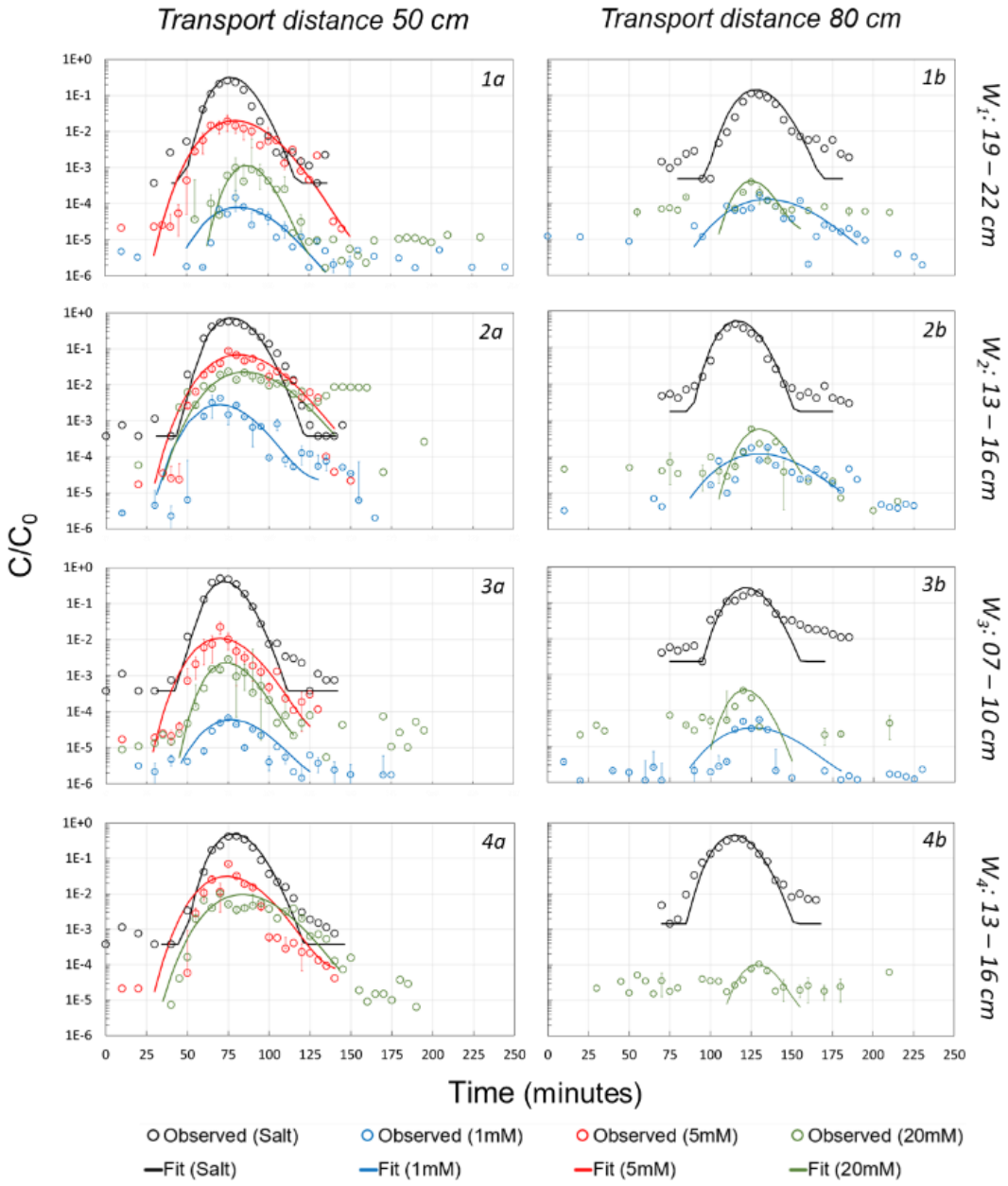

Figure 4.2: BTCs of conservative and SiDNAmag at sampling location W_1 (above injection depth, central flow line); W_2 (at injection depth, central flow line); W_3 (below injection depth, central flow line), and W_4 (at injection depth, transverse horizontally perpendicular to central flow line); at 50cm (left column) and 80cm (right column) transport distance, respectively, for injection suspension of 1mM, 5mM and 20mM PO_4 buffer. All reported depths were measured from the bottom of the tank. The BTCs include the relative SiDNAmag concentrations above no template control (NTC)

The t_{peaks} of the SiDNAmag dispersed in 1mM suspension for 0.5 m and 0.8 m transport distances were 75 – 80 minutes and 130 – 135 minutes respectively. SiDNAmags suspended in 5mM suspension reached the maximum effluent concentration at 70 – 75 minutes for 0.5 m transport distance. The t_{peaks} of the SiDNAmags suspended in 20mM injection suspension were 75 – 80 minutes and 120 – 130 minutes, for 0.5m and 0.8 m transport distances, respectively. Though the t_{peak} of SiDNAmags, under all ionic strength conditions, were similar to the salt tracer, the maximum effluent concentrations (C_{max}/C_0) of SiDNAmags were 1 – 4 log units lower than the salt tracer. At 0.5m transport distance, the C_{max}/C_0 of the salt tracer, SiDNAmags in 1mM, 5mM and 20mM ranged between 0.26 – 0.57, 0.000067 – 0.0042, 0.019 – 0.088, and 0.001 – 0.023 [-], respectively. At 0.8 m transport distance, C_{max}/C_0 for the salt, SiDNAmags in 1mM, and 20mM were 0.11 – 0.43, 0.000018 – 0.00015, and 0.0001 – 0.0024 [-], respectively. In comparison with 50cm transport distance, the lower C_{max}/C_0, and fewer datapoints near the centre of SiDNAmag mass indicated that under our experimental conditions, the transport of SiDNAmag was limited. The maximum C_{max}/C_0 of salt and SiDNAmag concentration were observed at W_2 because W_2 was installed at the injection depth. The SiDNAmag to salt ratio of area under the breakthrough curves were in the order of magnitude of 10^{-3} - 10^{-4}, 10^{-1} – 10^{-2}, and 10^{-2} – 10^{-3}, for 1mM, 5mM, and 20mM injection suspension, respectively. The 5^{th} – 95^{th} percentile ranges of the parameters estimated from the salt and the SiDNAmag BTCs are summarised in table 4.2.

4.3.2 Estimation of parameter uncertainty

The median K values for the salt tracers and SiDNAmags dispersed in 1mM, 5mM, and 20mM phosphate buffer injection water were 0.072, 0.077 – 0.078, 0.074, and 0.08 [m/min], respectively (figure 4.3). The statistical test showed that the parameter distributions (5^{th} – 95^{th} percentile) were not statistically significantly different from each other. The median n_e for the salt tracers,

SiDNAmags dispersed in 1mM, 5mM, and 20mM phosphate buffer injection water were 0.36, 0.34 – 0.35, 0.36, and 0.34 [-], respectively.

Table 4.2: Breakthrough curve characteristics (C_{max}/C_0 and t_{peak}) at different sampling locations and the hydraulic conductivity (K), effective porosity (n_e), longitudinal dispersivity (α_L), horizontal transverse (α_{TH} / α_L), and vertical transverse (α_{TV} / α_L) dispersivity estimated from the salt tracer and the SiDNAmag

		Transport distance [m]	Sampling location	C_{max}/C_0 [-]	t_{peak} [min]	K [m/min]	n_e [-]	α_L [m]	K_{att} [1/min]
Salt tracer		0.5	W_1	0.26	75	0.074 (0.074 – 0.082)†	0.36 (0.31 – 0.38)	9.16e-4 (3.2e-5 – 9.34e-4)	-
			W_2	0.57	75				
			W_3	0.5	75				
			W_4	0.42	80				
		0.8	W_1	0.11	125				
			W_2	0.43	120				
			W_3	0.39	120				
			W_4	0.19	125				
SiDNAmag	1mM	0.5	W_1	1.48e-4	80	0.078 (0.07 – 0.08)	0.35 (0.31 – 0.38)	2.6e-4 (8.8e-5 – 4.72e-4)	0.061 (0.055 – 0.068)
			W_2	4.2e-3	70				
			W_3	6.77e-5	75				
			W_4	-	-				
		0.8	W_1	1.64e-4	130	0.077 (0.07 – 0.1)	0.34 (0.33 – 0.37)	5.5e-4 (9.9e-5 – 7.84e-4)	0.05 (0.041 – 0.058)
			W_2	1.78e-5	135				
			W_3	5.47e-5	130				
			W_4	-	-				
	5mM	0.5	W_1	1.9e-2	75	0.074 (0.07 – 0.084)	0.36 (0.32 – 0.37)	1e-4 (6.2e-5 – 7.87e-4)	0.019 (0.013 – 0.022)
			W_2	8.8e-2	75				
			W_3	2.2e-2	70				

		W_4	7e-2	75				
	0.8	W_1	-	-	-	-	-	-
		W_2	-	-				
		W_3	-	-				
		W_4	-	-				
20mM	0.5	W_1	9.9e-4	80				
		W_2	2.4e-2	75	0.08	0.34	9.7e-4	0.035
		W_3	2.8e-3	75	(0.075 – 0.082)	(0.33 – 0.37)	(8e-5 – 6.9e-4)	(0.031 – 0.042)
		W_4	1e-2	70				
	0.8	W_1	3.94e-4	125				
		W_2	5.77e-4	120	0.08	0.34	1.8e-4	0.054
		W_3	3.61e-4	120	(0.076 – 0.081)	(0.31 – 0.38)	(3.2e-5 – 9.6e-4)	(0.051 – 0.063)
		W_4	1.04e-4	130				

† 5^{th} – 95^{th} percentile of the parameter uncertainty

- Not analysed

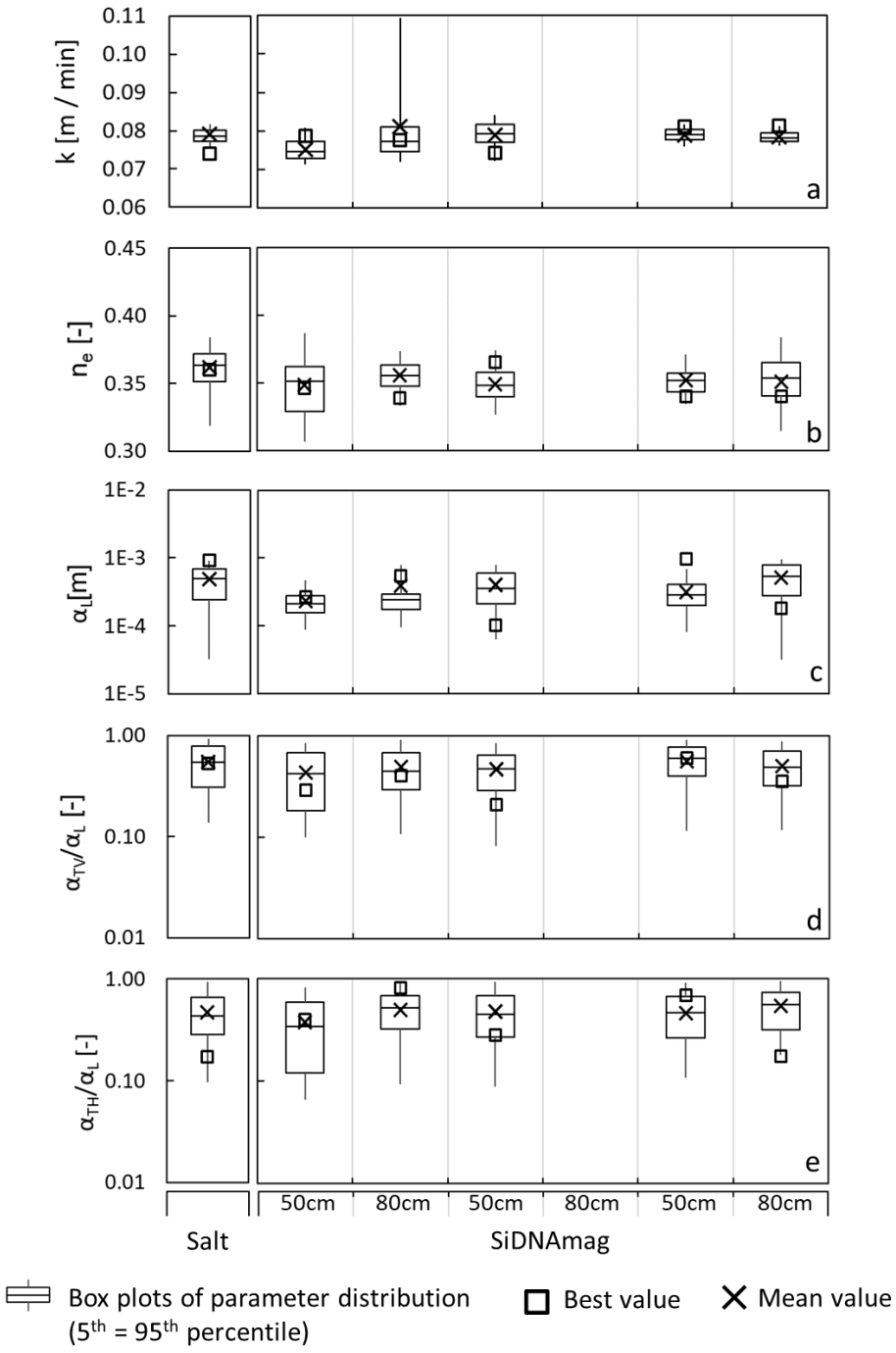

Figure 4.3: Estimated value ranges of (a) hydraulic conductivity, (b) effective porosity, (c) longitudinal dispersivity for salt tracer (NaCl, fluorescein) and SiDNAmag dispersed in phosphate buffer of varying ISs (1mM, 5mM and 20mM).

The n_e of SiDNAmags, like k, increased slightly as compared to the salt tracer, however, the n_e distributions were not statistically different from each other. The median α_L for the salt tracers, SiDNAmags dispersed in 1mM, 5mM, and 20mM phosphate buffer injection water were 9.16 x 10^{-}

^{4}, 2.6 x 10^{-4} – 5.5 x 10^{-4}, 1 x 10^{-4}, and 1.8 x 10^{-4} - 9.7 x 10^{-4} [m], respectively. The parameter distribution of SiDNAmags within the 5th – 95th percentile for all the ionic strength condition, were statistically not different than those of the salt tracer. The attachment rate (K_{att}) of the SiDNAmags dispersed in 1mM, 5mM and 20mM, onto the sand grains were 0.05 – 0.061, 0.019, and 0.035 – 0.054 [1/min], respectively, which was reflected on the order of maximum effluent concentration as a function of ionic strength of the injection water.

4.4 Discussion

The average velocity of salt (6.4 x 10^{-3} – 6.7 x 10^{-3} m/min) and the SiDNAmag (6 x 10^{-3} - 7 x 10^{-3} m/min) at both 50cm and 80cm transport distances were similar to each other irrespective of the ionic strength of the injection water. The similar time of maximum concentration (t_{peak}) of the salt and SiDNAmags dispersed in the injection water of 1mM, 5mM, and 20mM ionic strengths indicated that size exclusion or velocity enhancement did not occur. Our observation was similar to Wu et al., (2020), where within a range of 1mM – 20mM NaCl suspension, no early arrival or velocity enhancement was observed for 100nm polystyrene nanoparticles transporting through dessert soil (86% sand). In a 15cm column, with similar colloid and collector grain size, Chakraborty et al., (2022) observed similar time of maximum effluent concentration indicating absence of velocity enhancement. In fine sand (180 – 250 µm) and at a linear velocity of 0.009 m/min, Harter and Wagner, (2000) did not observe earlier breakthrough or velocity enhancement for 4500 – 5500 µm Cryptosporidium Parvum oocysts, though at larger grain sizes the velocity enhancement was apparent. Absence of size exclusion of velocity enhancement of colloids in our experiments was possibly due to the collector size being 3 orders of magnitude higher, and the average pore throat size being ~2 orders of magnitude higher as compared to the SiDNAmags. This ratio was much higher than the threshold of 1.5, observed by Sirivithayapakorn and Keller, (2003). In contrast to our observation, earlier arrival and velocity enhancement, with similar colloid size and grain size, as used in this study, had been reported by Mikutis et al., (2018), which could be due to

the difference in the linear velocity used. There are other studies (Nocito-Gobel and Tobiason, 1996; Higgo et al., 1993; Grolimund et al., 1998; Keller et al., 2004) which reported the occurrences of size exclusion and velocity enhancement at varying colloid size, collector size and average linear velocities.

Considering the maximum SiDNAmag concentration in the effluent, the SiDNAmags showed least attachment (k_{att}) and highest mobility while dispersed in 5mM phosphate buffer, followed by 20mM and 1mM phosphate buffer injection suspension. The slightly higher attachment rate, and therefore, the 0.5 – 1 log unit reduction in the maximum effluent concentration for SiDNAmags in 20mM phosphate suspension as compared to 5mM injection suspension agreed with most of the studies on the effect of ionic strength on the colloid transport (Xu et al., 2021; Wu et al., 2020; Bolster et al., 2001). Nocito-Gobel and Tobiason, (1996), observed least attachment and maximum mobility of latex particles at an NaCl concentration of 0.1 and 1 mM as compared to 5mM and 10mM. Similar decrease in the attachment efficiency was reported by Bolster et al., (2001) for bacterial transport upon reduction of ionic strength from 100mM to 10mM of KCl. Reduction in attachment efficiency and attachment rates with decreasing ionic strength were attributed to the compression of electric double layer leading to reduced depth of secondary energy minimum and weakened electrostatic repulsion between the colloids and the collector grains (Xu et al., 2021, Wu et al., 2020; Bolster et al., 2001). Therefore, we attributed the increase in attachment with increasing ionic strength of the injection suspension to the compression of electric double layer resulting in weakened electrostatic repulsion. However, a decrease in SiDNAmag attachment in 5mM injection water as compared to 1mM was in contradiction with the widely reported observations (Nocito-Gobel and Tobiason, 1995; Wu et al., 2020, Tufenkji and Elimelech, 2005). This contrast with our result can be explained by the competitive attachment of phosphate ions on the favourable attachment sites onto the collector grains. As reported by Chen et al., (2021), addition of 0.5mM phosphate suspension in saturated columns increased the maximum effluent

concentration by ~3% and ~17% in clean and goethite coated sand, respectively. When phosphate concentration increased form 0.1mM to 1mM, Wang et al., (2011), reported an increase in *E. coli* recovery from ~45% to ~77% at an NaCl concentration of 10mM. Silica colloid transport increased from ~11% to ~48% in a quartz sand column in the presence of 0.5mM phosphate due to a reduction in zeta potential of the colloids (Liu et al., 2017). Such reduction in attachment and enhancement in colloid transport in the presence of phosphate had been attributed to the adsorption of phosphate onto the colloids and collector grains leading to an increased colloid – colloid and colloid – collector repulsion (Chen et al., 2015; Liu et al., 2017). This increase in the repulsion increased primary energy barrier for attachment (Wang et al., 2019; Zhang et al., 2018; Li and Schuster, 2014).

Our results indicated that the hydraulic parameter (k, n_e, and α_L) distributions estimated from the salt tracers and the SiDNAmags were statistically similar and therefore, were independent to the ionic strengths used in this study. In this regard, our results were similar to the Mesticou et al., (2013), where reduction in K did not occur at ionic strengths ranged between 0 to 13.68mM, with similar sand grain size and silica colloids of 1.3 – 22 µm diameter. Similarly, Soma and Papadopoulos, (1995), observed only a small (7%) reduction in K at lower ionic strengths (0.5 and 5mM). The K reduction had been attributed to the pore constriction clogging due to straining (Ochi and Vernouz, 1999; Torkzaban et al., 2015), aggregation of colloids (Won et al., 2020; Xinqiang et al., 2019; Dikinya et al., 2008), and colloid aggregation on the collector surface (Ye et al., 2019). Because the colloid aggregation increases with increasing ionic strength, therefore pore clogging and the reduction in K were reported to increase with increasing ionic strength as well (Xinqiang et al., 2019; Ye et al., 2019; Won et al., 2020). However, the highly negative ζ – potentials and the constant D_{hyd} of the SiDNAmags suspended in all ionic strengths throughout the experiment interval implied that SiDNAmag aggregation was unlikely to occur. In addition, the colloid and collector ratio (0.0003 [-]) in our experiments was an order of magnitude lower than

the threshold of 0.004 (Johnson et al., 2010) or 0.003 (Bradford and Bettahar, 2006) for straining. Overall, at the experimental conditions and the range of ionic strengths used in our work, the 3D transport behaviour of the salt tracers and the SiDNAmags dispersed 1mM, 5mM and 20mM phosphate buffer suspension were statistically not different.

However, under our experimental condition, we identified a limitation of using the SiDNAmag. The particles showed limited travel at 80cm transport distance, reflected on the low effluent concentration. Therefore, only a small number of datapoints could be modelled to estimate the conductivity and the effective porosity. The low SiDNAmag injection concentration was possibly limiting our findings and should be considered in the future work.

4.5 Conclusion

- Under all ionic strength conditions, the recovery of SiDNAmags were 1 – 4 log units reduced as compared to the salt tracers due to colloid attachment onto the collector grains. We observed the maximum SiDNAmag transport under 5mM ionic strength injection suspension followed by 20mM and 1mM injection water ionic strength.
- We conclude that lower attachment rate of SiDNAmags at 5mM injection suspension as compared to 1mM injection water was due to the competitive adsorption of negatively charged phosphate ions on the favourable attachment sites of collector grains. At comparatively higher ionic strength, i.e. 20mM injection suspension, the attachment rate increased due to the compression of electric double layer resulting in lower energy barrier.
- Comparing the salt tracers and colloids (SiDNAmags) transport breakthrough curves, we found that at all ionic strength of injection water, the estimated hydraulic parameter distributions (hydraulic conductivity, effective porosity, and longitudinal dispersivity) were not statistically significantly different. Therefore, we can accept our null hypothesis that the ionic strengths do not have effect on the hydraulic parameter distributions

- We did not observe size exclusion or velocity enhancement of the SiDNAmags resulting in earlier breakthrough of the SiDNAmags. This was possibly due to the three orders of magnitude higher grain size diameter as compared to the SiDNAmags, therefore, high pore size to SiDNAmag size ratio.
- The implication of this study lies in that, under homogeneous, saturated, and unconsolidated sand and within the ionic strength range used in this work, the SiDNAmags have similar three dimensional transport properties as the salt and can be applied for determining the hydraulic parameters of a 3D system

4.6 Acknowledgement

This research had been funded by the Dutch Research Council (NWO), TTW grant 14514. We would like to thank Dr. Sulalit Bandyopadhyay, Department of Chemical Engineering, Faculty of Natural Sciences, NTNU, Norway for the kind contribution with SiDNAmag particles. We would like extend our gratitude to thank Dr. Thom Bogaard, Department of Civil Engineering and Geosciences, TU-Delft, the Netherlands, for his contribution and support with experimental setup preparation and modelling. We would like to thank Hortus Botanicus, TU-Delft, the Netherlands; and IHE-Delft, the Netherlands for the laboratory work support.

CHAPTER 5: QUANTIFYING AQUIFER HETEROGENEITY USING SUPERPARAMAGNETIC DNA PARTICLES

Chakraborty, S., Alqrinawi, F., Foppen, J. W., & Schijven, J. Quantifying aquifer heterogeneity using superparamagnetic DNA particles (Under review)

Abstract

Determining hydraulic parameters of physical heterogeneity of aquifers is pivotal for flow field analysis, contaminant migration and risk assessment. In this research, we quantified hydraulic parameter distributions of a sand tank with lens shaped physical heterogeneity using Silica encapsulated DNA tagged superparamagnetic particles (SiDNAmag). We conducted three sets of multi – point injection experiments in unconsolidated (1) homogeneous (zone 0), (2) heterogeneous with a no-conductivity-zone (zone 1), and (3) heterogeneous with a high-conductive-zone (zone 2) sand tank. At 0.6m downstream, we determined the conservative salt tracer and SiDNAmag concentration at three vertically distributed sampling points. From the breakthrough curves (BTC), we estimated the parameters distributions of hydraulic conductivity (k), effective porosity (n_e), longitudinal dispersivity (α_L), transverse vertical (α_{TV}), and transverse horizontal dispersivities (α_{TH}) applying Monte Carlo simulation approach for BTC fitting. Attributing to the hydraulic conductivity and effective porosity, the effect of heterogeneities was reflected on the arrival and magnitude of maximum salt and SiDNAmag concentration and shape of the BTCs. In all scenarios, a significant fraction of SiDNAmag was retained in the tank due to first order kinetic attachment on the sand. The parameter distributions of k, n_e, α_L, α_{TV}, and α_{TH}, determined from SiDNAmag BTCs were not statistically significantly different to the salt tracer in the three individual experiment systems. Current work demonstrates the applicability of SiDNAmag in identifying aquifer heterogeneity and quantifying the hydraulic parameters of each hetero – domains of a heterogeneous aquifer.

Keywords: Colloids, aquifer heterogeneity, conductivity, porosity, sand tank

5.1 Introduction

Estimation of spatial variability of aquifer hydraulic parameters is essential to accurately predict groundwater flow fields, migration of contaminant plumes, design groundwater remediation strategies, and manage groundwater resources sustainably (Cardenas and Jiang, 2010; Vincent Henri and Harter, 2019; Cardiff et al., 2013; Liu et al., 2020; Torkzaban et al., 2019; Harvey et al., 1993). Multi-point pumping tests, hydraulic head response observations, flowmeter tests (Cardiff et al., 2013; Maier et al., 2022; Song et al., 2023; D'Oria and Zanini, 2019; Zha et al., 2019), and application of tracers (Müller et al., 2010; Moeck et al., 2017; Song et al., 2023; Hartog et al., 2010; Hoffmann et al., 2019) are the common approaches to assess aquifer physical heterogeneities.

In laboratory and field scales, conservative tracers (e.g. tritium, chloride) have been applied to determine the spatial variations in hydraulic conductivity (Salamon et al., 2007; Ronayne et al., 2010; Danquigny et al., 2004), dispersivity (Vereecken et al., 2000; Castro-Alcala et al., 2012; Jose et al., 2004), and colloids (e.g. bacteria, virus, microspheres) to identify the effect of physical heterogeneity on contaminant transport (Wang et al., 2013; Fontes et al., 1991; Yin et al., 2022; Sarris et al., 2018; Baumann and Werth, 2005). The effect of physical heterogeneity on the tracer transport were commonly analysed through moment analysis (Vereecken et al., 2000); deterministic or stochastic breakthrough curve fitting (Salamon et al., 2007; Ronayne et al., 2010; Dann et al., 2008; Levy and Berkowitz, 2003), tracer transport imaging (Castro-Alcala et al., 2012; Jose et al., 2004; Baumann and Werth, 2005), or hydraulic tomography (Illman et al., 2012). The variety of investigated physical heterogeneities included discrete or clustered lenses (Salamon et al., 2007; Ronayne et al., 2010; Illman et al., 2012), sand blocks (Levy and Berkowitz, 2003; Castro-Alcala et al., 2012; Danquigny et al., 2008), and variably conductive channels (Vereecken et al., 2000; Dann et al., 2008; Derouane and Dassarhues, 1998; Wang et al., 2013). Columns were typically

constructed with contrasting permeability at the core, surrounded by matrix (Morley et al., 1998; Baumann and Werth, 2005). Larger sand grains typically constituted the higher conductivity or velocity zones due to higher void to solid ratio (Ren and Santamarina, 2018), and lower effective porosity for the sand grain larger than ~700 - 800µm (Urumović and Urumović Sr, 2014). Based on the scale of heterogeneous domains, both the solute tracers and colloid breakthrough curves reflected the effect of differential flow fields in its' asymmetry with long tailings (Bradford et al., 2004), or multi-peaked breakthrough curves (Wang et al., 2013; Yin et al., 2022). The multi – peaks were due to high velocity of solute and colloid through high conductivity zones followed by a second peak due to transport through low conductivity zones (Wang et al., 2013; Dong et al., 2019; Fontes et al., 1991; Torkzaban et al., 2019; Bhattacharjee et al., 2002). Dispersion coefficient of both the solute and colloids increased in high conductivity zones because plume expansion was directly proportional to the advection velocity (Sun et al., 2001). Colloid deposition coefficient, in most cases, were lower in high conductivity regions as compared to the low conductivity zones (Sun et al., 2001; Dong et al., 2019; Morley et al., 1998), due to enhanced hydrodynamic forces exerted on the colloids by higher flow velocity and larger voids to migrate through (Zhang et al., 2015; Bradford et al., 2009). In columns, colloid deposition profiles explained that along with the column inlet, the interface of the high and low conductive domains (Bradford et al., 2004; Wang et al., 2013) were pivotal for colloid retention. In the systems free from colloid size dependent exclusion, colloid aggregation, and pore clogging, which often lead to velocity enhancement, reduction in hydraulic conductivity and effective porosity (Oudega et al., 2021; Mikutis et al., 2018; Won et al., 2020), hydraulic parameters (hydraulic conductivity and effective porosity) estimated from salt breakthrough curves could explain colloid transport velocity well (Bradford et al., 2004; Wang et al., 2013; Morley et al., 1998; Baumann and Werth, 2005, Maxwell et al., 2003).

Due to spatial variation of hydraulic parameters in a heterogeneous aquifer, a unique deterministic description of the system is not possible (Ptak et al., 2004; Fu and Gómez-Hernández, 2009). Neglecting the hydraulic parameter uncertainties might lead to erroneous description of the system (Rojas et al., 2008), and eventually inaccurate groundwater flow or solute transport predictions. Therefore, stochastic methods are required to acknowledge and identify the simulation, prediction and hydraulic parameter uncertainties (Ptak et al., 2004; Varouchakis and Hristopolus, 2013; Renard et al., 2013; Pool et al., 2015). Monte Carlo algorithm is one such robust stochastic tool to assess aquifer hydraulic parameter values and associated uncertainties (Fu and Gómez-Hernández, 2009; Hoffmann et al., 2019, Chakraborty et al., 2023), or spatial variations of hydraulic parameters (Herrick et al., 2002; Liang and Zhang, 2013) to predict state variables (Hoffmann et al., 2019) or assess pollution risk (Neshat et al., 2015).

Over the last fifteen years, DNA particles, encapsulated in polylactic acid, silica, or alginate (Foppen, 2023), had been used in determining subsurface flow properties, contaminant transport and characterizing aquifer hydraulic parameters (Mikutis et al., 2018; Pang et al., 2020; Zhang et al., 2021; Kong et al., 2018; Kianfar et al., 2022). Encapsulated DNA particles, unlike conventional salt tracers, could be used for concurrent injection experiments due to the uniqueness of DNA sequences without background concentration interference (Pang et al., 2020; Chakraborty et al., 2023). The additional advantages of the encapsulated DNA particles were high detection specificity in polymerase chain reaction (Dahlke et al., 2015; Foppen et al., 2011), and stability against physico – chemical parameters (pH, radiation, and enzymatic activities) because of the encapsulation (Pang et al., 2020; Mikutis et al., 2018; Sharma et al., 2012).

We previously demonstrated the suitability of SiDNAmag for hydraulic parameters estimation of a homogeneous system (Chakraborty et al., 2023). In this study, our objective

was to assess the suitability of using SiDNAmag to estimate hydraulic parameter values (k, n_e, and α_L) and associated uncertainties in a homogeneous aquifer and each of the heterogeneous domains of a heterogeneous sand tank, and statistically compare the parameter value distributions with the salt tracer. To our knowledge, this is the first attempt to apply SiDNAmag to quantify the hydraulic parameter distributions (k, n_e, and α_L) of each of the hetero – domains in a heterogeneous aquifer using Monte Carlo. Based on the observed transport behaviour of SiDNAmag in a homogeneous sand tank, with similar sand grain size to this study (Chakraborty et al., 2023), we hypothesize that in aquifer, with simple lens shaped physical heterogeneity, the hydraulic parameter distributions estimated from SiDNAmag breakthrough curves would be statistically similar to the salt tracer. Thus, SiDNAmag would be a suitable candidate to identify and determine the hydraulic parameters values and associated uncertainties of each of the heterogeneous – domains in an aquifer.

5.2 Materials and methodology

5.2.1 SiDNAmag

Sharma et al., (2021), synthesized the SiDNAmag by binding negatively charged double stranded DNA (ds – DNA) onto positively charged iron oxide nanoparticles, followed by encapsulation in a silicate layer. We acquired two uniquely sequenced SiDNAmag ($SiDNAmag_1$ and $SiDNAmag_2$) stock suspensions (~10^{10} particles/ml) (NTNU, Norway) dispersed in demineralized water. The diameters of the two SiDNAmag were 184 ± 58 and 206 ± 86nm, respectively. The zeta potentials (ζ) were – 14 and -11 mV, when dispersed in demineralized water.

5.2.2 Conservative salt tracer and SiDNAmag suspension

We prepared the injection NaCl (J. T. Baker, the Netherlands) salt solution at a concentration of 1.8g/L (pH ~7; EC ~2950µS/cm; 0.03M) to ensure sufficient contrast against the background tap water (EC ~480 µS/cm) in the sand tank. SiDNAmag injection suspensions were prepared as detailed in Chakraborty et al., (2023). In brief, we diluted the SiDNAmag stock suspensions with 5ml demineralized water and treated with 1µL commercial bleach to digest any non-encapsulated DNA present in the suspension. Then, we magnetically separated the SiDNAmags and washed twice with demineralized water to remove traces of bleach. Finally, we dispersed the magnetically separated and washed SiDNAmags in 500ml of 5mM phosphate buffer (~10^6 particles/ml) and used as injection suspensions. 5mM phosphate buffer was prepared by dissolving 0.77g/L of $Na_2HPO_4 \cdot 7H_2O$ (2.9mM) (EMSURE®, Merck KgaA, Germany) and 0.29g/L of $Na_2HPO_4 \cdot 7H_2O$ (2.1mM) (J. T. Baker, Spain) in demineralized water. We used 100mM NaOH (J. T. Baker, Poland) to adjust the pH to 7 – 7.1. We measured the hydrodynamic diameters (D_{hyd}) and the zeta (ζ) – potentials (at a particle concentration ~10^7 particles/ml) of SiDNAmags in 5mM phosphate buffer using Smoluchowski's equation (Malvern Panalytical Zetasizer Nano-Zs ZEN 3600, the Netherlands). The D_{hyd} were measured using 173° dynamic light backscattering. To explore the interaction behaviour between the SiDNAmag and sand, we also measured the ζ – potentials of the ground sand fractions dispersed in 5mM phosphate buffer at a w/v of 0.1g/ml for both the sand fractions (500 – 700µm and 1300 – 1600µm) used to create the heterogeneity.

5.2.3 Sand tank experiments and sample analysis

We wet packed a PVC tank (1.3m x 0.7m x 0.4m) with coarse grain (d = 500 - 700 µm; d_{50} = 630 µm) quartz sand (Sibelco, Belgium) to represent a homogeneous unconsolidated aquifer (zone 0) To create the no conductivity zone (zone 1) in the heterogeneous tank, we

embedded a ~6cm thick and ~28cm long solid lens, shape adopted from Lu et al., (2018), at a height of ~14 - 20cm from the bottom of the tank (figure 5.1).

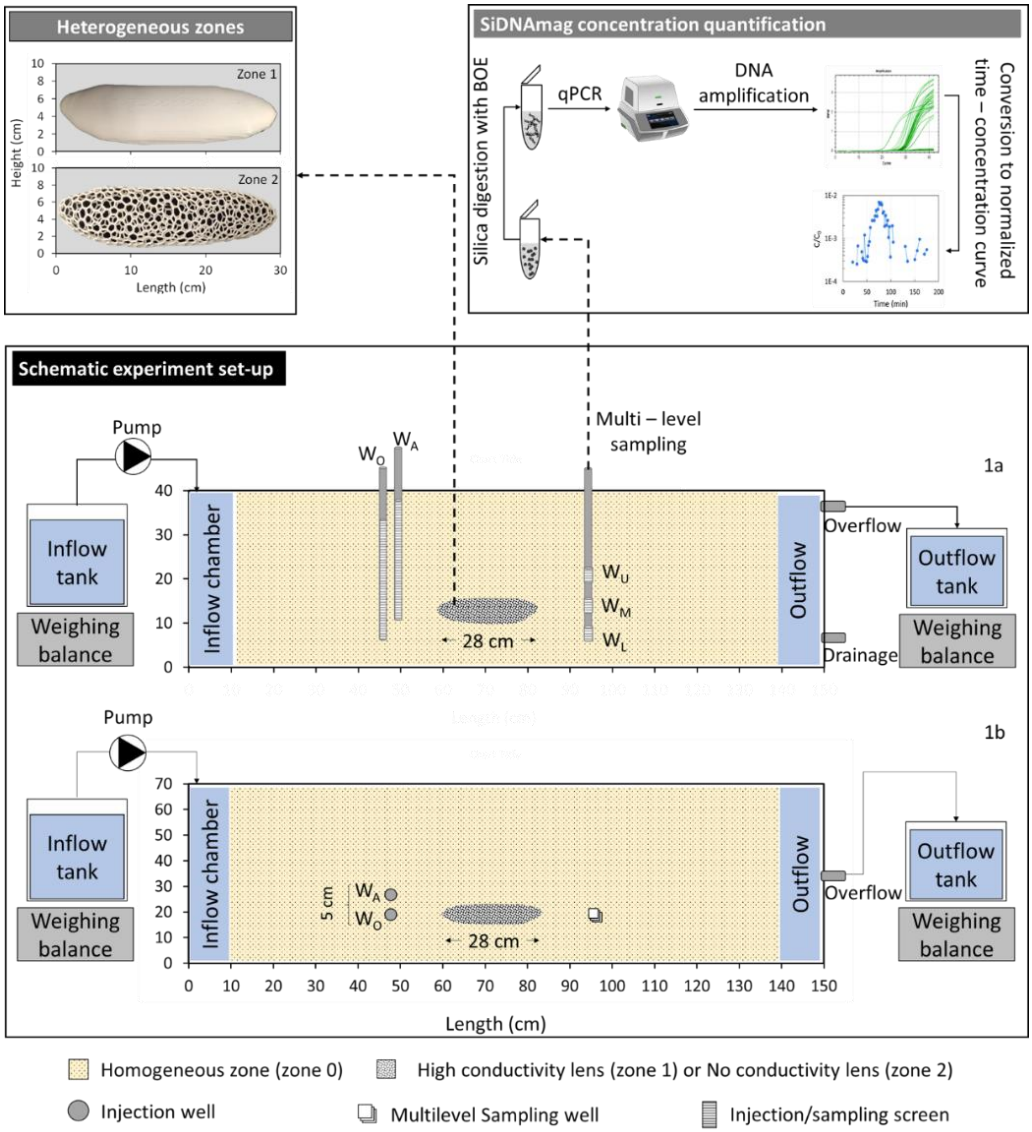

Figure 5.1: Schematic vertical cross-section (1a) and top (1b) view of the experimental setup. The ~28 cm long high conductivity zone (HCZ) and no conductivity zone (NCZ) were embedded at the depth of ~ 14 – 20 cm from the bottom of the tank. The high permeability zone contained very coarse grain sand (1300 – 1600 µm diameter) surrounded by the coarse grain matrix (500 – 700 µm).

A wireframe of the same lens as zone 1 filled with very coarse (1300 – 1600µm) quartz sand grains, was embedded at a height of ~14 - 20cm from the bottom of the tank to create a high conductivity zone (zone 2). In the heterogeneous systems, the zone 1 and 2 were

installed in the middle of the transport length, flanked by a strip of 0.15m of 500 – 700 µm sand (i.e. zone 0). We installed two fully penetrating injection wells (W_O and W_A) 0.4m downstream of the inflow chamber. We placed a multi-level sampling well at 0.6m downstream of the injection point on the same flowline as W_O. W_A was installed ~0.05 m transverse - perpendicularly distant from W_O (figure 5.1). We maintained a constant flow at the inflow and outflow chambers by pumping in ~796 ± 18 ml/min in the inflow chamber. The average outflow was ~781 ± 19 ml/min (measured gravimetrically) with an overall water balance percentage discrepancy of 1 – 4.4%. The constant hydraulic heads were ~0.35m and ~0.3m the inflow and outflow chambers, respectively, with an overall hydraulic gradient of 0.037. At first, we injected 500ml of the salt tracer into each of the injection wells at a rate of ~83 ml/min for all three set ups, followed by the SiDNAmag injection experiments. Because concurrent multi – point salt injection would interfere with the electric conductivity measurements, we carried out the injections at W_O and W_A sequentially, after the first salt breakthrough had reduced to background concentration. Due to the advantage that SiDNAmags were uniquely sequenced, we carried out SiDNAmag injection concurrently.

At the multi – level sampling well, as a function of time, we determined the salt concentrations as electric conductivity (WTW-Portable conductivity meter ProfiLine Cond 3310, Germany) and the SiDNAmags as ds-DNA concentration in qPCR. The qPCR protocol for DNA concentration enumeration was as described by Chakraborty et al., (2022). Briefly, we treated 20µL of sample with 1µL of Buffered Oxide Etch (BOE) to dissolve the SiDNAmag. Then the sample was mixed with primers (Biolegio B.V., Nijmegen, the Netherlands) and qPCR enzyme master mix (KAPA SYBR® FAST, South Africa). Finally, the dsDNA amplification and quantification were carried out in CFX96 Touch Real Time PCR detection system (Bio-Rad laboratories, Singapore). As quality assurance, we included No Template Control (NTC) and positive controls with each set of sample analysis. In figure 5.3, the salt tracer

breakthrough curve datapoints, normalized by injection concentration, were background concentration subtracted as

$$\frac{EC}{EC_0} = \frac{EC - EC_{BG}}{EC_0 - EC_{BG}} \quad (5.1)$$

where *EC*, EC_0 and EC_{BG} represented the observed, injected, and, background electric conductivity. The normalized SiDNAmag breakthrough curves present the datapoints only above NTC.

5.2.4 Breakthrough curve analysis

We compared the salt and the SiDNAmag breakthrough curves obtained at all three sampling locations (W_U, W_M, and W_L) form both the injection points (W_O and W_A) with regard to the shape of the breakthrough curves, time of maximum effluent concentration (t_{peak}), and maximum effluent concentrations (C_{max}/C_0). In addition, we analysed the effect of lens heterogeneities on the salt and the SiDNAmag breakthrough shapes between homogeneous, heterogeneous with NCZ and heterogeneous HCZ sand tanks.

5.2.5 Salt and SiDNAmag transport modelling

SiDNAmag transport through saturated porous media has been explained by classical convection – dispersion equation for solute transport integrated with first order attachment – detachment term (Chakraborty et al., 2022, 2023). We simulated the salt and the SiDNAmag transport in a 3D block – centred finite difference groundwater flow model, MODFLOW-2005 (Harbaugh et al., 2017), in conjunction with the mass transport module, MT3D (Zheng and Wang, 1999) using the partial differential equation

$$n_e \frac{\partial C}{\partial t} + k_{att} n_e C - k_{det} \rho_b S = \frac{\partial}{\partial x_i}\left(n_e D_{ij} \frac{\partial C}{\partial x_j}\right) - \frac{\partial}{\partial x_i}(n_e v_i C) \quad (5.2)$$

Where n_e is the effective porosity of the sand [-], C is the concentration of the salt tracer or SiDNAmag in the water [kg/m^3], D_{ij} is the hydrodynamic dispersion coefficient tensor

[m^2/min], k_{att} and k_{det} are the first order kinetic attachment and detachment rates of the colloids [1/min], v_i is the pore water velocity [m/min], S is the SiDNAmag concentration at the solid surface of the sand [kg/kg], ρ_b is the bulk density of the sand [kg/m^3] and t is the time because injection [min]. k_{att} and k_{det} are the attachment rate coefficient and detachment rate coefficients [1/min], respectively. The hydraulic conductivity (k) [m/min] was incorporated in the equation through v_i as $v_i = -(k/n_e) * i$, where i is the hydraulic gradient [-]. We used method of characteristics (MOC) scheme of advection to reduce numerical dispersion.

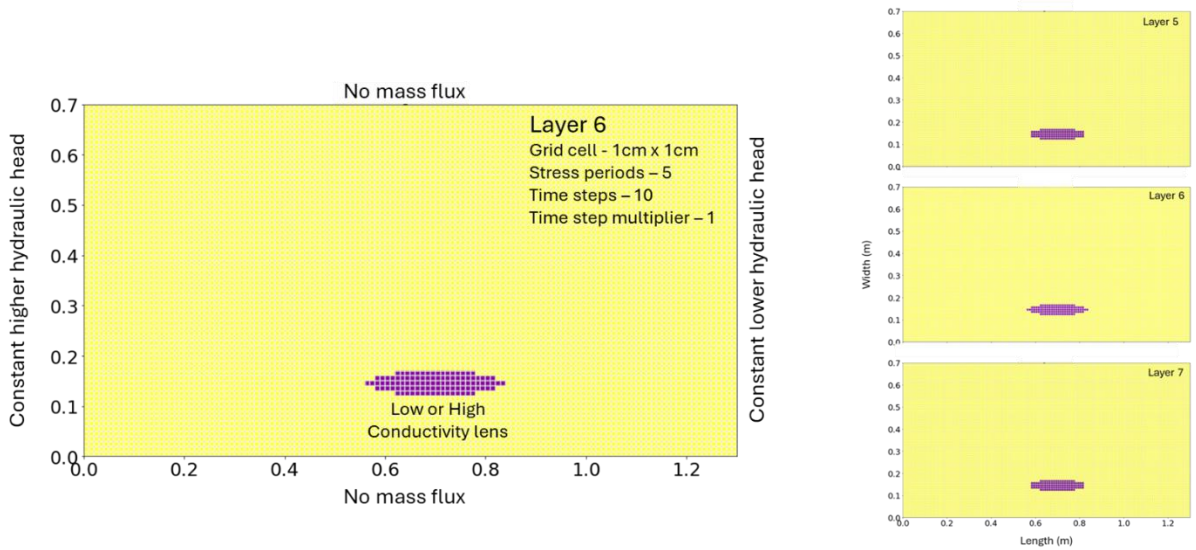

Figure 5.2: Model discretization containing no conductivity amd high conductivitiy lens

In the mass transport module MT3D, k_{att} and k_{det} were expressed in terms of as β [1/min] and k_d [m^3/kg] (Babakhani, 2019) as

$$k_{att} = \frac{\beta}{n_e} \quad (5.3a)$$

and $$k_{det} = \frac{\beta}{\rho_{b*}\, k_d} \quad (5.3b)$$

where β is the mass transfer rate from water to sand [1/min] and k_d is the distribution coefficient [m^3/kg]. We considered straining to be insignificant because the SiDNAmag to Sand ratios for the coarse grain and very coarse grain sand were 0.0003, and 0.000013,

respectively, which were well below the threshold of 0.004 (Johnson et al., 2010) or 0.003 (Bradford and Bettahar, 2006). The salt and SiDNAmag concentration in the injection water were too low to alter the viscosity and density of the injection water, therefore, we constant density transport in the modelling exercise.

5.2.6 Model description

We spatially discretised a 1.3m x 0.7m x 0.36m model grid (resolution of 1cm x 1cm) into 12 layers with the first layer as unconfined and other layers as unconfined/confined. Each layer thickness was set to 2 – 3 cm corresponding to the height of the sampling screens used in the experiment. Layer 8 was set to ~1cm to accommodate the lens height accurately. To simulate the homogeneous sand tank, the whole flow model was discretized as zone 0, which was also used as the background sand for heterogeneous sand tanks. To simulate the no conductivity (zone 1) and high conductivity (zone 2) lenses (we discretized the lenses into 1cm x 1cm grids and embedded within zone 0, spanning over three layers corresponding to the height of the lens (~6cm). We temporally discretized the total mass transport simulation time into three stress periods for hydraulic head stabilization (50 min), injection (6 min), and sampling period (200 min). Because the injection points were fully penetrating, we determined the injection flow rates of each layer proportional to the thickness of the model layers such that the sum of the injection rates at each layer (Q_L) equaled to the total injection rate (Q_{Tot}) (Konikow et al., 2009), according to

$$Q_{Tot} = \sum_{L=1}^{12} Q_L \quad (5.4)$$

The sampling screens were specified at layer 5, 7, and 9. However, we did not specify any pumping rate for the sampling points because the sampling was done intermittently without constant pumping.

5.2.7 Parameter estimation (Monte Carlo simulation)

We simulated the groundwater, salt, and SiDNAmag transport in MODFLOW-2005 and MT3D using a python package, Flopy (Bakker et al., 2016). We determined the k, n_e, α_L, α_{TH}/α_L, and α_{TV}/α_L parameter distributions through Monte – Carlo simulation approach. Thereto, the convection – dispersion equation (eq 5.2) was solved for 5000 parameter sets random – uniformly drawn from predefined input ranges. The input ranges were defined for zone 0, and 2 individually instead of considering a resultant homogeneous system. All parameters for no conductivity zone (zone 1) were considered to be zero. To determine the input range of *k*, at first, we approximated the K for all three systems (homogeneous and heterogeneous systems with zone 1 and 2) by dividing the Darcy flux by hydraulic gradients measured at 6 different observation wells in the tank. Possibly due to the small scale of the experiments and heterogeneity, we did not observe any measurable effect of heterogeneity on the hydraulic heads. Therefore, for the high conductive zone, we approximated the K (~0.13m/min) using Kozeny – Carman equation from the grain size distribution considering a d_{10} of 1.3 mm. The gravimetric approximation of n_e, for the coarse grain (zone 0) and the very coarse grain (zone 2) sand were 0.37 and 0.25 [-], respectively. Finally, we considered ±25 – 30 % of averaged K and n_e as the input ranges for Monte Carlo simulation. For no conductive zone, we set all the parameters as 'no flow'. The input range of α_L was 10^{-6} – 10^{-1} [m] for both the HCZ and the matrix. The input of both α_{TH}/α_L, and α_{TV}/α_L were set to a wide range of 0.01 – 1 [-]. The input ranges have been summarized in table 5.1.

Table 5.1: Input ranges of hydraulic conductivity (k), effective porosity (n_e), longitudinal dispersivitiy (α_L), transverse vertical dispersivitiy (α_{TV}/α_L), and transverse horizontal dispersivity (α_{TH}/α_L) for salt and SiDNAmag transport Monte Carlo simulations

	Homogeneous (zone 0)	Heterogeneous (NCZ, zone 0)	Heterogeneous (HCZ, zone 2)
k [m/min]	0.048 – 0.081		
k_{het} [m/min]	-	-	0.1 – 0.21
n_e [-]	0.27 – 0.46		
$n_{e\text{-}het}$ [-]	-	-	0.17 – 0.33

α_L [m]		$10^{-6} – 10^{-1}$	
$\alpha_{L\text{-het}}$ [m]	-	-	$10^{-6} – 10^{-1}$
α_{TV}/α_L [-]		0.01 – 1	
$\alpha_{TV}/\alpha_{L\text{-het}}$ [-]	-	-	0.01 – 1
α_{TH}/α_L [-]		0.01 – 1	
$\alpha_{TH}/\alpha_{L\text{-het}}$ [-]	-	-	0.01 – 1

Because the number of datapoints, specifically for *k,* were limited and defining its' distribution was not possible, we decided that the parameter sets, to be drawn for Monte Carlo simulation, to be uniformly distributed. In the post – processing, we selected the best 1% parameter sets as the parameter distributions based on minimized Root Mean Squared Error (RMSE), both for individual sampling levels as well as for combined for all three sampling levels. RMSE was a preferred objective function over R^2 because a higher R^2 could be achieved even when the breakthrough magnitudes were not well matched (Ward et al., 2017). We evaluated the normality of the parameter distributions using Kolmogorov – Smirnov test. Because not all the distributions were normal, we applied distribution non – specific Mann Whitney U test ($\alpha = 0.05$) to evaluate the statistical difference between the parameter distributions. At first, we statistically compared the parameter distributions obtained from individual sampling locations with the distributions obtained from all the sampling locations combined. This was to confirm whether the distributions estimated from all sampling locations combined were good representatives of the individual sampling locations. Further, we compared the distributions estimated from the salt and the SiDNAmag breakthrough curves.

5.3 Results

5.3.1 SiDNAmag and sand characterization

The hydrodynamic diameters (D_{hyd}) of the $SiDNAmag_1$ and $SiDNAmag_2$ dispersed in 5mM phosphate buffer were 644 ± 101, and 660 ± 108 nm, respectively. Throughout the experiment interval of 240 minutes, under quiescent condition, the D_{hyd} of $SiDNAmag_1$

varied between 644 – 691nm, and 660 – 698nm for SiDNAmag$_2$. Time dependent D_{hyd} had been detailed in our previous work (Chakraborty et al., 2023). The SiDNAmag$_1$ and SiDNAmag$_2$, dispersed in 5mM phosphate buffer were negatively charged, with ζ-potentials of -44 ± 3.8, and -41 ± 2.9 mV, respectively. The ζ-potential of the coarse grain (500 - 700µm; used in zone 0) and very coarse grain (1300 - 1600µm; used in zone 2) sand were -50.7 ± 11.5 and -48.3 ± 13.3 mV, respectively.

5.3.2 Salt and SiDNAmag breakthrough curves

In the homogeneous sand tank, both the salt and the SiDNAmag breakthrough curves were symmetric in shape. The time of maximum effluent concentration (t_{peak}) for the salt tracer and the SiDNAmags at upper (W_U), middle (W_M), and lower (W_L), sampling levels were similar. For the salt tracer injected on the sampling flowline (W_O), the t_{peaks} were 77 minutes at all three sampling levels. For the injection at W_A the t_{peaks} were 75 - 79 minutes. The t_{peaks} for the SiDNAmag injected at W_O and W_A were 75 – 77 minutes and 75 – 79 minutes, respectively, and were similar to the salt tracer (figure 5.3, table 5.2).

However, maximum effluent concentration (C_{max}/C_0) of SiDNAmag BTCs were 1 – 2 log units lower as compared to the salt tracer, for both the injection points. The ratio of SiDNAmag and the salt recovery, calculated by integrating the area under BTC, were 0.01 – 0.02 [-]. The C_{max}/C_0 of the BTCs observed for the injection at W_A were ~50% reduced because the centre of the plume was beyond the flowline of the sampling points. In the heterogeneous tank with no conductive lens (zone 1), the t_{peaks} of the salt BTCs observed for both the injection points were 60 – 66 minutes as compared to the 56 – 64 minutes for the SiDNAmag at all three sampling levels (table 5.2). While the t_{peaks} of salt and SiDNAmag BTCs were visually similar, the C_{max}/C_0 of SiDNAmag were 2 – 3 log units lower than the salt tracer. The recovery ratio of SiDNAmag to the salt were 0.014 – 0.092 [-]. As compared to the homogeneous system, there was no prominent effect of the zone 1 on the breakthrough

curve observed from injection at W_0. However, the maximum effluent concentration of both the salt and the SiDNAmag BTCs observed from injection at W_A were reduced by 50 – 90% as compared to the homogeneous system, and was the only visible effect of the no conductivity lens.

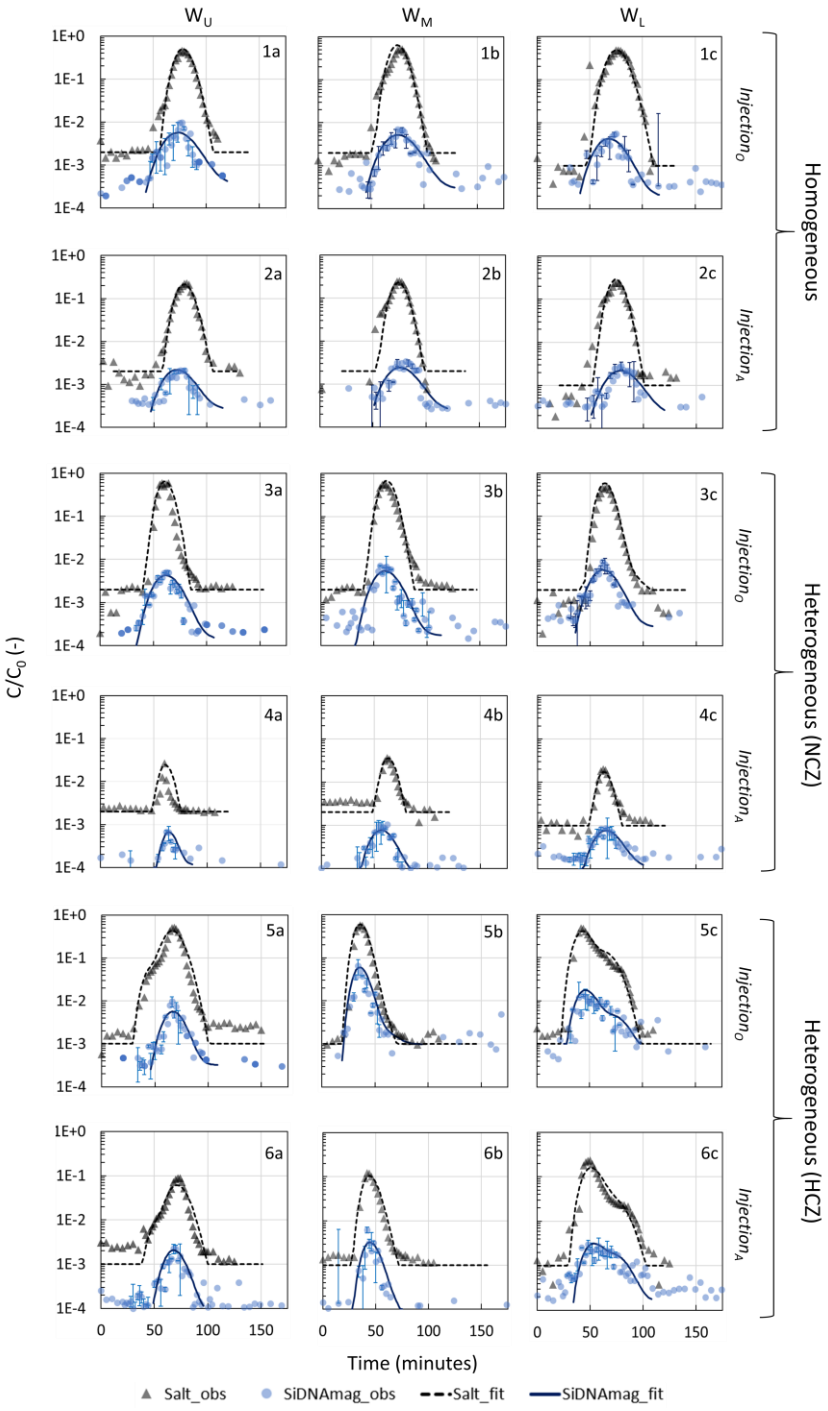

Figure 5.3: Observed (_obs) and model fitted (_fit) breakthrough curves (BTCs) of the salt and the SiDNAmag transport in homogeneous (1a – 2c), no conductivity zone (NCZ and zone

1) embedded (3a – 4c), and high conductivity zone (HCZ and zone 2) embedded (5a – 6c) sand tank. $Injection_O$ and $Injection_A$ represent the BTCs observed corresponding to the injection point On and horizontally perpendicularly Away to the flow line of sampling well, respectively.

Table 5.2: Salt and SiDNAmag breakthrough curve characteristics (maximum concentration and time to peak) in homogeneous, heterogeneous medium with a no permeability zone (NCZ), and heterogeneous medium with a high permeability zone (HCZ) for two injection points. 'O' and 'A' represent breakthrough curves observed from injection on the sampling flowline and injection on horizontally perpendicularly away from the sampling flow line, respectively.

		Homogeneous				**Heterogeneous (NCZ)**				**Heterogeneous (HCZ)**			
		C_{max}/C_0 [-]		t_{peak} [min]		C_{max}/C_0 [-]		t_{peak} [min]		C_{max}/C_0 [-]		t_{peak} [min]	
		O	A	O	A	O	A	O	A	O	A	O	A
Salt	W_U	0.45	0.17	77	79	0.65	0.03	64	60	0.5	0.09	68	72
	W_M	0.52	0.25	77	75	0.57	0.04	60	62	0.57	0.12	36	42
	W_L	0.48	0.24	77	75	0.48	0.02	66	62	0.48	0.25	42	46
SiDNAmag	W_U	0.01	0.002	77	79	0.005	0.0006	62	62	0.01	0.002	66	68
	W_M	0.007	0.002	75	75	0.007	0.001	56	62	0.03	0.006	34	40
	W_L	0.005	0.002	75	79	0.009	0.0009	62	64	0.013	0.003	44	48

This indicated the advantage of multi – point injection scheme, especially in a heterogeneous system. There was an obvious effect of the high conductivity lens (zone 2) on the t_{peak} and the breakthrough shape. For both the injection points W_O and W_A, the t_{peaks} of salt and the SiDNAmag BTCs in the W_M and W_L were 34 – 42, and 42 – 48 minutes, respectively, reflected the effect of HCZ (table 5.2). At W_O, the BTC falling limb sharply declined with little or no tailing, whereas, at W_L, the salt and the SiDNAmag concentrations, at the falling limb, declined with a lower slope followed by sharper decline till the background concentration (figure 5.3). The t_{peaks} of the salt and the SiDNAmag BTCs at W_U were 66 – 72 minutes because this sampling point was above the layers comprising the zone 2. However, the salt BTC at W_U was asymmetric with only a minor influence of the zone 2 on the rising limb. The SiDNAmag BTC did not capture the effect of high conductive lens at W_U. C_{max}/C_0 of SiDNAmag were reduced by 1 – 2 log units as compared to salt, with recovery ratio of SiDNAmag to salt of 0.015 – 0.087.

5.3.3 Parameter distributions

In this section, we present the 5^{th} – 95^{th} percentile ranges of k, n_e, α_L, α_{TH}, and α_{TV} for zone 0, and 2 for the homogeneous and the heterogeneous sand tanks (figure 5.3). The median values of the hydraulic parameters estimated in homogeneous and heterogeneous systems have been summarized in table 5.3.

In the homogeneous tank, estimated K range for the salt tracer were 0.06 – 0.07 [m/min] for the injection point W_O and W_A combined. The K range estimated from SiDNAmag BTCs were 0.061 – 0.068 [m/min], and were statistically not significantly different to the salt tracer. The n_e ranges estimated from the salt and the SiDNAmag were 0.34 – 0.41, and 0.37 – 0.42[-], respectively. The α_L ranges estimated from the salt and the SiDNAmag ranged 3×10^{-5} – 8×10^{-4} and 1×10^{-4} – 2.8×10^{-3} [m].

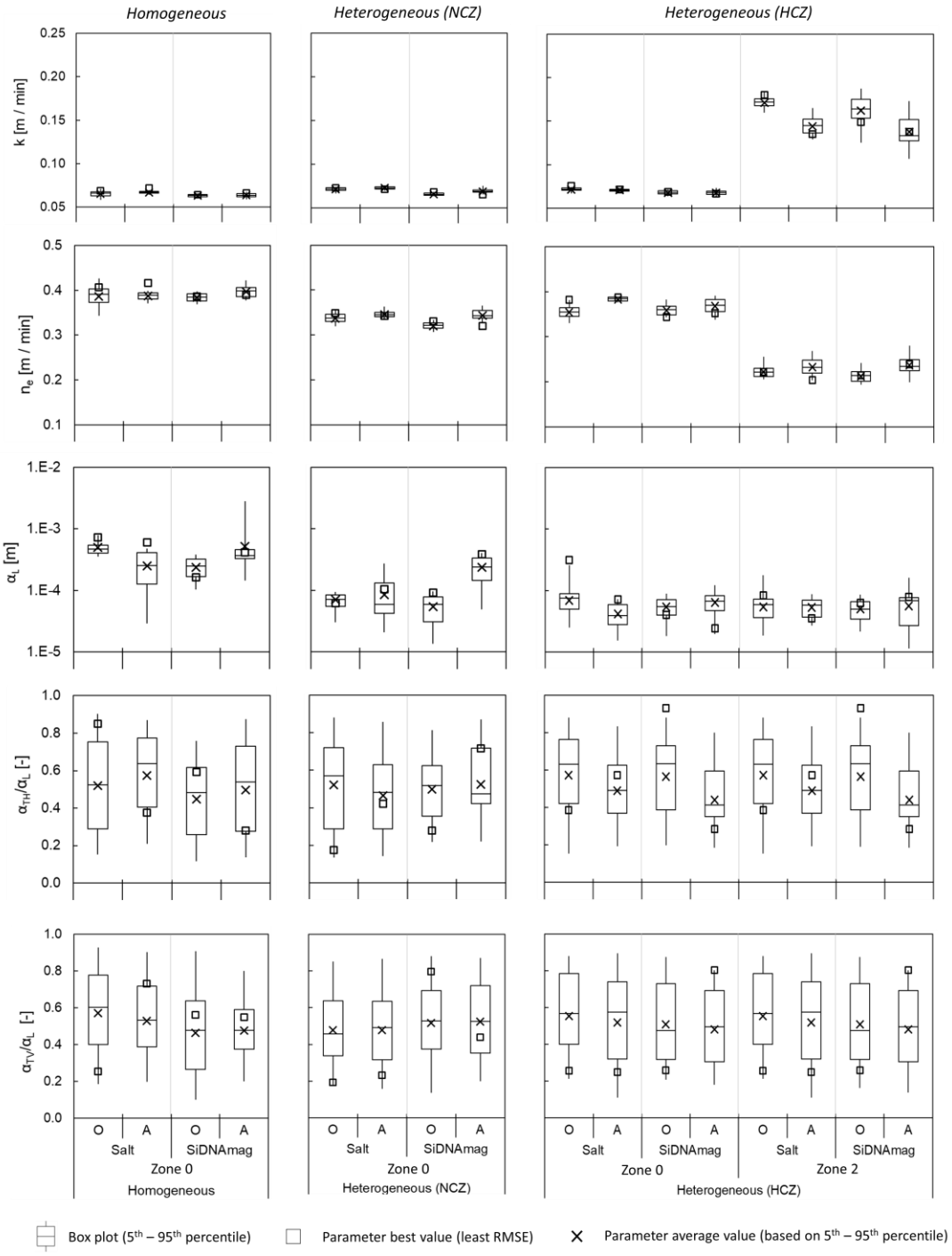

Figure 5.4: Hydraulic parameter (k, n_e, α_L, α_{TH}/α_L, and α_{TV}/α_L) ranges estimated from the observed salt and SiDNAmag breakthrough curves through Monte Carlo simulation approach. 'O' and 'A' indicate the parameter distributions estimated from the injection on the sampling flowline and injection on horizontally perpendicularly away from the sampling flowline experiments. Zone 0 and Zone 2 represent the background sand (500 - 700µm) and high conductive lens (1300 - 1600µm).

Table 5.3: Hydraulic parameter ranges estimated from the salt and the SiDNAmag breakthrough curves through Monte Carlo approach in the homogeneous, heterogeneous with no conductivity zone (NCZ) and high conductivity zone (HCZ) systems. The parameter values are represented as median (5^{th} – 95^{th} percentile range). $A_{SiDNAmag/Salt}$ is the SiDNAmag to salt ratio of area under the curve (recovery).

Hydraulic parameters		**Homogeneous**		**Heterogeneous (NCZ)**		**Heterogeneous (HCZ)**	
		Salt	SiDNAmag	Salt	SiDNAmag	Salt	SiDNAmag
k [m/min]	O	0.066 (0.06 – 0.07)	0.064 (0.061 – 0.066)	0.071 (0.066 – 0.074)	0.066 (0.063 – 0.068)	0.072 (0.067 – 0.075)	0.068 (0.064 – 0.071)
	A	0.067 (0.064 – 0.07)	0.063 (0.06 – 0.068)	0.073 (0.069 – 0.075)	0.069 (0.065 – 0.075)	0.071 (0.069 – 0.074)	0.068 (0.064 – 0.073)
k_{het} [m/min]	O	-	-	-	-	0.17 (0.16 – 0.184)	0.16 (0.12 – 0.187)
	A	-	-	-	-	0.145 (0.13 – 0.17)	0.133 (0.11 – 0.17)
n_e [-]	O	0.39 (0.34 – 0.41)	0.38 (0.37 – 0.4)	0.34 (0.32 – 0.35)	0.32 (0.31 – 0.34)	0.35 (0.33 – 0.38)	0.36 (0.34 – 0.38)
	A	0.39 (0.34 – 0.4)	0.4 (0.38 – 0.42)	0.34 (0.33 – 0.36)	0.34 (0.33 – 0.37)	0.38 (0.38 – 0.39)	0.37 (0.34 – 0.39)
$n_{e\text{-}het}$ [-]	O	-	-	-	-	0.22 (0.21 – 0.26)	0.21 (0.19 – 0.24)
	A	-	-	-	-	0.23 (0.2 – 0.27)	0.23 (0.2 – 0.28)

α_L [m]	O	4.7×10^{-4} (3.5×10^{-4}–8×10^{-4})	2.5×10^{-4} (1×10^{-4}–3.8×10^{-4})	7.2×10^{-5} (3×10^{-5}–9×10^{-5})	5.9×10^{-5} (1.3×10^{-5}– 9.5×10^{-5})	7.5×10^{-5} (2.5×10^{-5}– 8.6×10^{-5})	5.5×10^{-5} (1.8×10^{-5}– 8.9×10^{-5})
	A	2.5×10^{-4} (3×10^{-5}–2.8×10^{-4})	3.6×10^{-4} (1.4×10^{-4}– 2.8×10^{-3})	6×10^{-5} (2.1×10^{-5}–2.7×10^{-4})	9.4×10^{-5} (4.9×10^{-5}– 4×10^{-4})	3.9×10^{-5} (1.1×10^{-5}– 7.2×10^{-5})	6.7×10^{-5} (1.9×10^{-5}– 8.6×10^{-5})
$\alpha_{L\text{-het}}$ [m]	O	-	-	-	-	5.9×10^{-5} (1.9×10^{-5}– 3.8×10^{-4})	5×10^{-5} (2.1×10^{-5}– 1.2×10^{-4})
	A	-	-	-	-	5.7×10^{-5} (2.7×10^{-5}– 2.6×10^{-4})	6.8×10^{-5} (1.1×10^{-5}– 1.6×10^{-4})
α_{TH}/α_L [-]	O	0.52 (0.15 – 0.9)	0.48 (0.12 – 0.76)	0.57 (0.13 – 0.88)	0.52 (0.22 – 0.81)	0.63 (0.15 – 0.88)	0.63 (0.2 – 0.88)
	A	0.64 (0.21 – 0.87)	0.54 (0.14 – 0.88)	0.48 (0.14 – 0.86)	0.47 (0.22 – 0.87)	0.49 (0.19 – 0.83)	0.41 (0.19 – 0.8)
$\alpha_{TH}/\alpha_{L\text{-het}}$ [-]	O	-	-	-	-	0.63 (0.15 – 0.88)	0.63 (0.2 – 0.83)
	A	-	-	-	-	0.49 (0.19 – 0.83)	0.41 (0.19 – 0.8)
α_{TV}/α_L [-]	O	0.6 (0.19 – 0.93)	0.48 (0.1 – 0.9)	0.46 (0.18 – 0.85)	0.53 (0.14 – 0.88)	0.57 (0.21 – 0.88)	0.47 (0.2 – 0.88)
	A	0.53 (0.2 – 0.9)	0.48 (0.2 – 0.8)	0.49 (0.16 – 0.86)	0.53 (0.2 – 0.87)	0.58 (0.11 – 0.89)	0.49 (0.18 – 0.8)
$\alpha_{TV}/\alpha_{L\text{-het}}$ [-]	O	-	-	-	-	0.57 (0.21 – 0.88)	0.47 (0.16 – 0.88)
	A	-	-	-	-	0.58 (0.11 – 0.89)	0.49 (0.14 – 0.8)

β [1/min]	O	-	0.021 (0.02 – 0.021)	-	0.023 (0.022 – 0.023)	-	0.021 (0.018 – 0.021)
	A	-	0.017 (0.015 – 0.02)	-	0.025 (0.024 – 0.028)	-	0.018 (0.015 – 0.022)
β_{het} [1/min]	O	-	-	-	-	-	0.022 (0.013 – 0.033)
	A	-	-	-		-	0.025 (0.013 – 0.033)
k_{att} [1/min]	O	-	0.055 (0.052 – 0.057)	-	0.073 (0.07 – 0.077)	-	0.06 (0.049 – 0.071)
	A	-	0.042 (0.036 – 0.048)	-	0.073 (0.067 – 0.078)	-	0.049 (0.042 – 0.065)
$k_{att-het}$ [1/min]	O	-	-	-	-	-	0.11 (0.058 – 0.163)
	A	-	-	-	-	-	0.11 (0.056 – 0.153)
RMSE [-]	O	0.02 – 0.042	0.0007 – 0.00072	0.034 – 0.041	0.0005 – 0.0006	0.041 – 0.055	0.0033 – 0.0043
	A	0.014 – 0.018	0.00028 – 0.00035	0.002 – 0.003	0.00009 – 0.0001	0.004 – 0.006	0.00037 – 0.00042
$A_{SiDNAmag/Salt}$ [-]	O	0.01 - 0.02		0.014 - 0.023		0.015 - 0.087	
	A	0.014 – 0.02		0.029 – 0.092		0.25 – 0.029	

4

The overall ranges of α_{TV}/α_L, and α_{TV}/α_L of the salt and the SiDNAmag were 0.1 – 0.9 [-]. According to the Mann Whitney U test, the parameter distributions of n_e, α_L, α_{TH}/α_L, and α_{TV}/α_L determined from the SiDNAmag BTCs were statistically not different from the salt tracer. The first order mass transfer rate (β) of SiDNAmag onto the coarse grain sand were 0.021 and 0.017 [1/min] for W_O and W_A, respectively, corresponding to the attachment rate coefficients (K_{att}) of 0.055 and 0.042 [1/min]. The SiDNAmag to salt recovery ratio, combined for both the injection points W_O and W_A, ranged between 0.01 – 0.02 [-].

In the heterogeneous system (with embedded zone 1), we estimated the hydraulic and mass transport parameters only for the zone 0, because we considered all parameters to be zero for no conductivity zone 1. The K ranges estimated from salt BTCs for both injection points combined were 0.066 – 0.075 [m/min] as compared to 0.063 - 0.075 [m/min] estimated from SiDNAmag BTCs. The n_e range estimated from the salt tracer BTCs for both the injection points were 0.33 – 0.36[-]in comparison with 0.31 – 0.37 [-] estimated from the SiDNAmag. The α_L range of the salt tracer BTCs estimated from both the injection points were 2.1×10^{-5}– 2.7×10^{-4} [m] as compared to 1.3×10^{-5} – 4×10^{-4} [m] estimated from SiDNAmag BTCs. The α_L of the SiDNAmag and salt tracer in heterogeneous (NCZ) tank were ~40 – 50% lower than the homogeneous tank. The α_{TV}/α_L, and α_{TV}/α_L of the salt tracer ranged between 0.13 – 0.88 [-], whereas, the α_{TH}/α_L, and α_{TV}/α_L of the SiDNAmag ranged between 0.14 – 0.88 [-], and were statistically not different from the salt tracer. According to the Mann Whitney U test, the parameter distributions of k, n_e, α_L, α_{TV}/α_L, and α_{TV}/α_L of zone 0, determined from the SiDNAmag BTCs were statistically not significantly different from the salt tracer. The first order mass transfer rate (β) of SiDNAmag onto the coarse grain sand in matrix were 0.023 and 0.025 [1/min] for W_O and W_A, respectively, both corresponding to a K_{att} of 0.073 [1/min]. The SiDNAmag to salt recovery ratio, combined for both the injection points W_O and W_A, ranged between 0.014 – 0.092 [-] (table 5.3).

In the heterogeneous tank with embedded zone 2, the K range of the zone 0 estimated from the salt BTCs for two injection points was 0.067 – 0.075 [m/min] The K range of the high conductivity lens (zone 2) estimated from salt tracer BTCs was 0.13 – 0.18 [m/min]. The K range of the zone 0 estimated from the SiDNAmag BTCs was 0.064 – 0.073 [m/min]. The K range of the zone 2 estimated from the SiDNAmag BTCs was 0.11 – 0.18 [m/min]. The n_e range of the zone 0 and 2, estimated from the salt tracer were 0.33 – 0.39 and 0.2 and 0.27[-], respectively. The range of n_e for zone 0 and 2, estimated from SiDNAmag were 0.34 – 0.39, and 0.2 – 0.28 [-], respectively. The median n_e of the zone 2, estimated from both the salt tracer and the SiDNAmag, were ~40 – 50% lower than the zone 0. The α_L range of the zone 0 and 2, estimated from the salt tracer BTCs, were 1.1 x 10^{-5} - 8.6 x 10^{-5}, and 1.9 x 10^{-5}– 3.8 x 10^{-4} [m], respectively. The α_L range of the zone 0 and 2, estimated from the SiDNAmag BTCs, were 1.8 x 10^{-5} – 8.9 x 10^{-5}, and 1.1 x 10^{-5}– 1.6 x 10^{-4} [m], respectively. The 5^{th} – 95^{th} range of α_L of the zone 2 were in the same order of magnitude as the zone 0 and were statistically similar. The α_{TH}/α_L, and α_{TV}/α_L ranges of the zone 0 estimated from the salt and the SiDNAmag 0.11 – 0.89, and 0.18 – 0.88 [-], respectively. The α_{TH}/α_L, and α_{TV}/α_L ranges of the zone 2 estimated from the salt and the SiDNAmag 0.11 – 0.89, and 0.14 – 0.88 [-], respectively. According to the Mann Whitney U test, the k, n_e, α_L, α_{TH}/α_L, and α_{TV}/α_L ranges of the salt and the SiDNAmag, both in the zone 0 and 2, were statistically not significantly different. The first order mass transfer rate (β) of SiDNAmag onto the coarse grain sand in zone 0 were 0.021 and 0.018 [1/min] for W_O and W_A, respectively, corresponding to K_{att}s of 0.06 and 0.049 [1/min]. In the very coarse grain sand in zone 2, β were 0.022 and 0.025 [1/min], both corresponding to a K_{att} of 0.11 [1/min]. The recovery ratio of SiDNAmag to salt tracer, combined for both the injection points W_O and W_A, ranged between 0.015 – 0.087 [-] (Table 3). The RMSE ranges corresponding to each set up and injection points are summarized in table 5.3.

Based on the minimized objective function (RMSE) and best 1% of the Monte – Carlo simulation parameter sets, the parameter distributions estimated from BTCs observed at individual sampling depth (W_U, W_M, and W_L) were statistically similar to the parameter distributions estimated from all sampling depths combined. Therefore, here we presented only the parameter distributions estimated from the sampling points combined.

5.4 Discussion

The convective – dispersive flow and solute transport module could satisfactorily explain the salt BTCs, and the SiDNAmag BTCs with first order kinetic attachment rate coefficient incorporated. The similar time to peak (t_{peak}s), and statistically similar uncertainties of k, n_e, α_L, α_{TH}, and α_{TV} values estimated from the salt tracer and SiDNAmag in zone 0 and zone 2 of the homogeneous and heterogeneous sand tanks indicated that in our experimental condition, SiDNAmag and salt tracer exhibited similar convective – dispersive transport behaviour, and complied with our hypothesis.

The similar t_{peak}s of the salt tracer and the SiDNAmag BTCs in both the homogeneous and heterogeneous sand tanks (with zone 1 and 2) at all sampling points indicated that the SiDNAmags migrated with the velocity almost identical to the salt tracer. With the sand grain size to colloid ratio similar to this study (3000 and 7000 [-] for coarse grain and very coarse grain sand, respectively), similar mean transport velocity of conservative tracer and colloids were reported by Chakraborty et al., (2023); Chrysikopoulos and Katzourakis, (2015); Solovitch et al., (2010); and Leij and Bradford, (2018). Therefore, the often observed phenomenon of size exclusion and velocity enhancement (Mikutis et al., 2018; Grolimund et al., 1998) did not occur visibly in both the coarse grain (zone 0) and very coarse grain (zone 2) sand, possibly due to the pore throat to SiDNAmag ratio being atleast two orders of magnitude higher than the threshold value of ~1.5 (Sirivithayapakorn and Keller, 2003).

5.4.1 Breakthrough behaviour

In the homogeneous tank, both the salt and the SiDNAmag BTCs were almost symmetric with little or no tailing, suggesting uniform homogeneous flow of the salt and SiDNAmag (Ghosh et al., 2022; Chakraborty et al., 2022). Though we measured few samples with near – NTC SiDNAmag concentrations in the SiDNAmag BTC tails, however, we considered these datapoints as sample analysis error because we observed SiDNAmag concentrations of similar order of magnitude prior to the breakthrough as well. The effect of heterogeneity (with zone 1) was not apparent on the salt and SiDNAmag BTCs observed for injection at W_O, which was due to the re-mergence of salt and SiDNAmag plume past the no conductivity zone and migrating similar to the homogeneous zone. Therefore, a reduction in the maximum effluent concentration by 50 – 90% observed in the BTCs for injection at W_A demonstrated the significance of conducting multi – point tracing in identifying a no conductivity zone. Breakthrough tailing of conservative tracers and colloids were commonly observed due to slow release of the tracers or back diffusion from low permeability zones (Chapman et al., 2012; Tatti et al., 2016; Qin et al., 2020). Breakthrough tailings were not observed in our experiment because the lens used in our work was 'no' flow lens, as also observed by Leij and Bradford, (2013), when low permeability lens had little or no flow velocity. As compared to the lower sampling screen, slightly earlier (5 – 6 minutes) breakthrough peaks of the salt and the SiDNAmag in the middle sampling screen was possibly due to the formation of preferential flow around the zone 1 (Lyon – Marion et al., 2017; Hitzelberger et al., 2022). The flow and solute transport model showed a minor increase in flow velocity in the grid cells around the zone 1 as well. The effect of zone 2 on the BTCs, observed at W_U and W_L, were obvious in the breakthrough shape. In W_L, the first peaks were due to the influence of higher conductivity and flow velocity in the high conductivity zone 2 followed by the second peaks due to the lower conductivity matrix. This was similar to the multi – peaked BTCs observed by Wang et al., (2013); Yin et al., (2022);

and, Dong et al., (2019) due to faster tracer transport through high conductivity zones or lenses. In W_M, like heterogeneity with zone 1, there was not prominent effect of the high conductivity zone 2 on the breakthrough shape other than overall faster transport (faster t_{peak}), due to the plumes transported similar to the homogeneous system once past the HCZ. As compared to the homogeneous matrix, a faster arrival and slower increase in the breakthrough concentration in W_U was possibly due to the velocity shear effect (Joodi et al., 2010) of the high flow velocity in high conductivity zone 2 on the low conductivity matrix at the interface.

5.4.2 Estimated parameter value uncertainties

The initial input ranges and the estimated hydraulic conductivity of the coarse grain (zone 0) and very coarse grain (zone 2) sand were well within the realistic ranges of 0.00006 – 0.6 [m/min] for clean sand and 0.006 – 60 [m/min] for gravelly sand (Freeze and Charry, 1979; Sosa et al., 2022). While a number of studies have reported enhancement or reduction in hydraulic conductivity due to adaptation of preferential flow paths or colloid attachment onto the sand grains or pore clogging (Oudega et al., 2021; Keller et al., 2004; Dikinya et al., 2008; Won and Burns, 2017), Wang et al., (2013), demonstrated that colloids migrated more or less like conservative tracer when the colloid size is sufficiently small. Though Hong et al., (2009), and Roychoudhury et al., (2014), demonstrated that even for smaller colloids aggregation played a pivotal role in straining or pore clogging, we did not observe significant change in the D_{HYD} throughout the experiment duration. Chakraborty et al., (2023), in a homogeneous sand tank, demonstrated that hydraulic conductivity estimated from NaCl tracer was statistically similar to SiDNAmag. Both in the homogeneous and heterogeneous systems, studies with ~1 order of magnitude lesser collector to colloid ratio as compared to the present work, could explain the colloid transport using the hydraulic conductivity estimated from conservative tracer (Bradford et al., 2004; Baumann and Werth, 2005; Lyon

– Marion et al., 2017; Leij and Bradford, 2013). Transport length could also be an important factor as the effect of preferential flow path, impacting the estimation of hydraulic conductivity, can diminish with colloid transport length (Ahfir et al., 2009). Because the viscosity and density of the injection suspension were not significantly different than the background water in the tank, a reduction in the estimation of hydraulic conductivity by resisting the plume movement (Li et al., 2016; Mondal et al., 2018) was not expected.

In homogeneous, heterogeneous (with zone 1), and heterogeneous (with zone 2) sand tanks, the effective porosity and associated uncertainty ranges estimated from SiDNAmag BTCs were statistically similar to the salt tracer in both the coarse grain and very coarse grain sand. This agreed with the findings that, when the colloid diameter was sufficiently small to migrate similar to a conservative tracer (Wang et al., 2013), effective porosity estimated from conservative tracers could explain colloid BTCs satisfactorily (Tian et al., 2010; Tosco et al., 2009). Though colloid attachment had been reported to reduce effective porosity (Li et al., 2016; Chrysikopoulos and Katzourakis, 2015), and SiDNAmag attachment occurred in our experiments, however, was probably not enough to influence the pore structure and the effective porosity (Liu et al., 2016). In our previous work as well (Chakraborty et al., 2023), using the same SiDNAmag and coarse grain sand as in this study, the effective porosity parameter distribution obtained through a Monte – Carlo approach from conservative tracer was statistically similar to the SiDNAmag. The estimated effective porosity of the very coarse grain sand (zone 2) (~0.22 [-]) was less than the coarse grain (zone 0) effective porosity (~0.37 [-]), which agreed with the observation that effective porosity reduced for sand grain diameter >700 – 800µm as per Castany, 1967 (Huysmans and Dassargues, 2005).

Both in the coarse grain (zone 0) and very coarse grain (zone 2) sand, in the homogeneous and heterogeneous sand tanks, the longitudinal dispersivities and associated uncertainties

of SiDNAmag were statistically not significantly different from the conservative salt tracer. Chakraborty et al., (2023) reported statistically similar longitudinal dispersivity uncertainties of SiDNAmag and salt tracer in a homogeneous coarse grain sand tank. Similar observations were also reported by Tian et al., (2010) and Keller et al., (2004). This was possibly due to the small size of SiDNAmag, because smaller particles took more detours as compared to larger colloids (Auset and Keller, 2004; Keller et al., 2004; Sirivithayapakorn and Keller, 2003; Chrysikopoulos and Katzourakis, 2015), and migrated similar to a conservative tracer (Syngouna and Chrysikopoulos, 2011). The longitudinal dispersivity had been reported to increase in the high permeable region because dispersivity proportionally increases with advection velocity (Sun et al., 2001). Though we estimated the 95th percentile of the longitudinal dispersivity range of the salt tracer and SiDNAmag to be ~0.5 order of magnitude higher in high conductive very coarse grain (zone 2) sand as compared to zone 0, the overall value uncertainties were not statically significantly different. Therefore, our experimental and analysis method were inefficient to distinguish the longitudinal dispersivity between the lower and higher permeability regions. The α_{TV}/α_L, and α_{TH}/α_L associated uncertainty ranges, estimated from the SiDNAmag BTCs, in zone 0 both in the homogeneous and heterogeneous sand tank, and zone 2 in the heterogeneous sand tank were statistically not different than the salt tracer. The median α_{TV}/α_L, and α_{TH}/α_L values of both the salt tracer and SiDNAmag, however, were higher than the usually accepted value of 0.1 (Bijeljic and Blunt, 2007). This was possibly due to low peclet number (0.5 – 1) and flow velocity conditions where the ratio of transverse and longitudinal dispersion coefficients could reach as high as 1 (Bijeljic and Blunt, 2007), pertaining to colloids following more tortuous flow path (He et al., 2014). However, to understand the similarity of SiDNAmag transverse dispersion with the salt tracer, and higher than usually applied value of 0.1, a pore scale observation would be required (Baumann et al., 2010).

5.4.3 SiDNAmag attachment

First order kinetic attachment of SiDNAmag onto the coarse grain (zone 0) and very coarse grain sand (zone 2) resulted in 1 – 2 orders of magnitude reduction in SiDNAmag recovery as compared to the salt tracer, which was a limitation to overcome for subsurface application of SiDNAmag (Pang et al., 2020). The SiDNAmag mass transfer rate and attachment rate coefficient (k_{att}) were similar in the coarse grain sand (zone 0) in homogeneous, heterogeneous (with zone 1), and heterogeneous (with zone 2) tanks. In the heterogenous tank (zone 2), k_{att} in the very coarse grain sand was ~1.5 – 2.6 times higher as compared to the zone 0 with lower hydraulic conductivity. Considering our experimental conditions (e.g. grain size, Darcy flux) this is in accordance with the relation that particle deposition was directly proportional to the pore water velocity, inversely proportional to the effective porosity (Tufenkji and Elimelech, 2004), and directly proportional to $k^{1/3}$ (Sun et al., 2001). Though, many studies observed lesser colloid k_{att} in high conductivity zones with higher flow velocity (Dong et al., 2019; Qin et al., 2020; Wang et al., 2013; Phenrat et al., 2010; Torkzaban et al., 2019), due to enhanced hydrodynamic forces increasing pore voids for increased colloid migration (Zhang et al., 2015; Bradford et al., 2009) or by creating larger shadow zones (Ko and Elimelech, 2000). Probably our experimental condition was below a critical velocity (Ahfir et al., 2009) beyond which k_{att} would decrease at higher flow velocity. Overall, the higher K_{att} in the high conductivity zone were possibly a combined effect of grain size and the flow velocity (Ren et al., 2000).

5.4.4 Sensitivity to transport length and velocity

Because the BTC shapes were a prominent indicator of the high conductive channel in the heterogeneous tank with zone 2, as also observed by Wang et al., (2013); and Yin et al., (2022), we evaluated the effect of different hypothetical length of zone 0 (L_M) to length of zone 2 (L_{HCZ}) ratio (0.33 – 2.33 [-]) on the BTC shape indicator. We used the median k, n_e, α_L,

α_{TH}/α_L, and α_{TV}/α_L for salt and SiDNAmag along with the median k_{att} for SiDNAmag. In these hypothetical L_M/L_{HCZ} ratio, the L_{HCZ} was kept constant flanked by increasing L_M. The simulated breakthrough curves indicated that increase in L_M/L_{HCZ} results in diminished multi – peak behaviour of the BTCs, resembling tracer breakthrough of a homogeneous system for both the NaCl and SiDNAmag BTCs. Therefore, in order to identify the heterogeneity and further estimate hydraulic parameters of each hetero – domains using the current method, it is important to conduct lengthwise multi – point injection and sampling experiments. Because the salt and colloid transport were velocity dependent (Dong et al., 2019; Qin et al., 2020), in addition to the transport length, we also evaluated the breakthrough behaviour as a function of different hypothetical velocity scenarios (a ratio of experimental and hypothetical velocity ranging between 0.16 – 1.32) considering the estimated median k, n_e, α_L, α_{TH}/α_L, and α_{TV}/α_L values. Though Darcy velocity can influence the large colloid dispersivities (Sun et al., 2001), we assumed our colloid size was small enough not to influence the dispersivity significantly. For SiDNAmag transport, we calculated the k_{att} at different velocity using (Tufenkji and Elimelech, 2004) -

$$k_{att} = 1.5 \frac{(1-n_e)}{d_c n_e} v\alpha\eta_0 \quad (5.5)$$

where v was the Darcy velocity [m/min], α was the attachment efficiency [-], and η_0 was the single collector contact efficiency [-]. We considered a constant α for all velocities because theoretically α is independent of linear velocity (Tufenkji and Elimelech, 2004), and same for similar sand and colloid material (Bradford et al., 2004). The k_{att} were only an approximation because the equation is applicable for 1D system. The simulated breakthrough curves show that reduction in velocity results in visibly smoother curves with reduced effect of the high conductivity zone 2 on the breakthrough shape. Therefore, a SiDNAmag BTC resembling a homogeneous transport path does not guarantee the homogeneity of the system and it is important to conduct multi – point injection and sampling experiments at different

velocities to identify the heterogeneous lens and estimate parameter ranges for each hetero – domains.

5.5 Conclusion

- Multi – point injection and sampling approach in homogeneous, heterogeneous (with no conductivity lens), and heterogeneous (with high conductivity lens) sand tanks indicated that the convective – dispersive transport behaviour of SiDNAmag was similar to the salt tracer.
- The hydraulic parameters (k, n_e, α_L, α_{TH}/α_L, and α_{TV}/α_L) and associated uncertainties estimated from SiDNAmag BTCs using Monte – Carlo simulations approach in homogeneous (zone 0), heterogeneous (with zone 1), and heterogeneous (with zone 2) sand tanks were statistically not significantly different than the salt tracer.
- Though the α_L, α_{TH}/α_L, and α_{TV}/α_L value uncertainty ranges estimated form the salt tracer and the SiDNAmag in the heterogeneous sand tank for both the low conductivity zone (zone 0) and higher conductivity lens (zone 2) were statistically not different, we did not observe a clear distinction of longitudinal dispersivity between the zone 0 and zone 2 in the heterogeneous sand tank.
- In the heterogeneous tank, the effect of high conductivity lens (zone 2) was observed as a faster peak concentration for both the salt and the SiDNAmag followed by a slower peak due to the lower conductivity zone 0.
- In the heterogeneous sand tank with no conductivity zone (zone 1), the effect of zone 1 was not evident on the breakthrough time and shape observed for the injection on the flowline of sampling well. However, for the injection point horizontally perpendicularly away from the flowline, the maximum salt and SiDNAmag concentrations were ~1 log unit lower as compared to the homogeneous sand tank. This indicated the relevance of

multi – point injection approach for identifying heterogeneous domains and in turn, the advantage of applying uniquely sequenced SiDNAmag.

- SiDNAmag attachment resulted in lesser mass recovery as compared to the salt tracer, a limitation of SiDNAmag application in long distance transport in subsurface.
- Overall, under current experiment conditions, SiDNAmag was a suitable candidate for identifying and determining hydraulic conductivity and effective porosity values and associated uncertainty ranges in homogeneous and each heterogeneous domains of the heterogeneous sand tank.

5.6 Acknowledgement

This research had been funded by the Dutch Research Council (NWO), TTW grant 14514. We would like to thank Dr. Sulalit Bandyopadhyay, Department of Chemical Engineering, Faculty of Natural Sciences, NTNU, Norway for the kind contribution with SiDNAmag particles. We would like extend our gratitude to Dr. Thom Bogaard, Department of Civil Engineering and Geosciences, TU-Delft, the Netherlands, for his contribution and support with experimental setup preparation and modelling. We would like to thank Dr. Ahmed Mahmoud (PostDoc); Ms. Yuchen Tang (PhD student); Hortus Botanicus, TU-Delft, the Netherlands; and IHE-Delft, the Netherlands for laboratory work support

CHAPTER 6: CONCLUSION AND FUTURE RESEARCH

6.1 General conclusion

In this thesis, we demonstrated theapplicability of silica encapsulated DNA tagged particles (SiDNASi and SiDNAmag) in determining hydraulic properties (hydraulic conductivity, effective porosity, and 3D dispersivities) of saturated, medium grained and coarse-grained sand. Overall, though SiDNA recovery, irrespective of the experimental physico-chemical conditions, was significantly less as compared to the conservative salt and dye tracers, the experimental and numerical analysis method could be successfully implemented to determine hydraulic properties of medium and coarse grained homogeneous and heterogeneous 3D sand tanks using the microparticles. However, SiDNA or colloid mobility was influenced by particle concentration and ionic strength of injection water.

6.1.1 Importance of SiDNA concentration

In controlled saturated column experiments, we demonstrated that increasing injection concentrations of SiDNA, when varied between ~10^2 – 10^8 particles/ml, facilitated particle mobility with log-linearly decreasing attachment rate coefficients, from $1.7x10^{-3}$ to $4.4x10^{-2}$ [1/min], onto the medium diameter collector sand grains. Therefore, an overall reduction in the colloid removal efficiency was observed with increasing injection particle concentration. Though the existing literature pool had investigated the effect of particle concentration on the particle transport through saturated porous media, however, majority of the experimental conditions resulted in particle aggregation, retention at pore constriction, colloid straining or blocking. Our work contributed to the understanding of the concentration effect where colloids were stable and therefore, free from colloid aggregation and pore clogging, and within an injection range where blocking did not occur. For such concentration range and under unfavourable conditions for colloid deposition, the removal

efficiency was considered to be concentration independent, because the removal efficiency, a product of single collector attachment efficiency and single collector collision efficiency, depends on experimental variables e.g. colloid size, collector size, solution chemistry, and colloid – collector surface charges (Tufenkji and Elimelech, 2004), whereas, we observed a decrease in the removal efficiency with increasing injection particle concentration. Our breakthrough curves and estimated parameters did not indicate occurrence of blocking and experimental conditions did not faciliatate particle aggregation (ζ potential > -40mV) and pore clogging. Therefore, we speculated that an increase in aqueous phase – solid phase colloid collision with increasing injection particle concentration, resulting in increased removal of attached colloids could be a plausible explanation of decreased removal efficiency with increasing injection particle concentration, a mechanism hypothesized by Bradford et al., (2009). However, direct visualization of the effect of particle concentration on the pore scale mechanisms of colloid transport and retention using methods, e.g. laser scanning confocal microscopy (Wu et al., 2023), fluorescent dark field phase contrast microscopy imaging (Lanning and Ford, 2002), or synchrotron X-ray tomography (DiCarlo et al, 2006) would be required to determine the underlying mechanisms of the particle concentration dependent SiDNASi retention.

6.1.2 Significance of ionic strength of injection water

In controlled laboratory sand tank steady state experiments with multi-point injection and sampling, we demonstrated that ionic strength of the injection water significantly impacted the SiDNAmag mobility at a transport distance of 0.5 and 0.8m. Highest SiDNAmag transport with least attachment rate was observed at an ionic strength of 5mM followed by 20mM and 1mM. The widely observed effect of ionic strength on colloid transport was an increase

in attachment rate with increasing ionic strength (Espinasse et al., 2007; Compere et al., 2001) due to compression of electrostatic double layer thickness promoting favourable deposition and aggregation (Bradford et al., 2002; Torkzaban et al., 2008). We hypothesize that our observation of enhanced SiDNAmag transport at 5mM as compared to 1mM was possibly due to competitive adsorption of phosphate onto collector grain and phosphate adsorption onto SiDNAmags enhancing colloid-colloid and colloid-collector electrostatic repulsion, and in turn, facilitating SiDNAmag transport. Similar observations and explanations were reported for different types of colloids in the presence of phosphate (Xu et al., 2018; Guo et al., 2018; Chen et al., 2015). The advective – dispersive transport parameters and associated uncertainties of SiDNAmag, however, were not statistically influenced by the ionic strength of the injection water. The hydraulic parameter and associated uncertainty distributions of SiDNAmag were also statistically not different compared to conservative tracers. Our results connotate that under environmentally relevant ionic strength conditions (~1 – 20mM) and in medium grain sand, SiDNAmag can be applied for determining the hydraulic parameters of a homogeneous system. However, the ionic strength dependent SiDNAmag attachment limits the transport distance as we observed in SiDNAmag breakthrough at 0.8 m transport distances, where maximum effluent concentrations were significantly reduced with higher DNA concentration uncertainty. Therefore, for longer transport distances an optimum injection concentration must be adapted.

6.1.3 SiDNAmag applicability in hydraulic parameter estimation

6.1.3.1 Homogeneous sand system

In a homogeneous medium grain sand system, the hydraulic parameters responsible for mass transport velocity (hydraulic conductivity, and effective porosity) and mass spread

(longitudinal dispersivity, transverse horizontal, and transverse vertical dispersivities) could be successfully estimated using SiDNAmag breakthrough curves (Chapter 3) by using the advective – dispersive transport equation and incorporating first order, one site kinetic attachment – detachment term. Though mass loss of SiDNAmag was present throughout, the hydraulic parameters and associated uncertainties were statistically similar to the conservative salt tracers. Our results indicated that SiDNAmag is a suitable candidate for characterizing a medium grain homogeneous aquifer where the pore water chemistry does not facilitate colloidal instability and aggregation. Highest SiDNAmag mobility was achieved at 5mM phosphate buffer injection suspension, and depending on the transport distance the injection concentration must be optimized.

6.1.3.2 Heterogeneous system with lens shape heterogeneity

In addition to a homogeneous system, we demonstrated the applicability of SiDNAmag in identifying and characterizing lens shaped heterogeneity through multi-source and multi-plexed sampling. The applicability of SiDNAmag was tested both in case of the no conductivity lens and high conductivity lens, respectively. In heterogeneous sand tank with embedded high conductivity lens, and packed with coarse grain sand, the hydraulic conductivity and effective porosity and associated uncertainties of both the lens and background zone were successfully estimated using advective – dispersive transport model with first order kinetic attachment – detachment through stochastic Monte – Carlo approach. In contrast to the homogeneous system, the bi-peaked breakthrough curves for both the salt tracers and the SiDNAmag indicated the presence of a preferential flow zone resulting in a faster, higher concentration peak followed by a second peak. However, our current experimental and modeling approach was ineffective in distinctively determining longitudinal dispersivities and transverse dispersivities for the high conductivity lens and the

background zone. Similarly, in the heterogeneous system with no conductive lens, application of SiDNAmag could successfully estimate the hydraulic conductivity, effective porosity and dispersivities and associated uncertainties, and were statistically similar to the salt tracers. Unlike the high conductive lens, the SiDNAmag multi-point injection approach was more effective in identifying the no conductivity lens, because the breakthrough curves observed from injection on the sampling flow line did not differ from the breakthrough curves of the homogeneous zone.

6.2 Challengesand limitation

6.2.1. Particle mass lossOne of the most important limitation was the SiDNA mass loss due to first order kinetic attachment onto the collctor grains under all experimental conditions. The recovery of SiDNAmag was 1 – 3 order of magnitude lesser as compared to the conservative salt and dye tracers, as presented in chapter 3, 4, and 5. At the highest injection concentration of SiDNASi, i.e. ~10^8 particles/ml, with highest particle mobility through medium grain sand column, was 83%. Such mass losses indicate a significant hindrance for hydrogeological applications of SiDNA for longer transport distances (and field scale) to obtain breakthrough curves which could be subjected to numerical modelling for parameter estimation process, as we observed in medium grain sand for a 0.8m transport distance (chapter 3, and 4). Based on our experiment conditions and observation, this limitation of obtaining SiDNA breakthrough curves suitable for hydraulic parameter estimation process can be addressed by adjusting the injection concentration of SiDNA (chapter 2).

6.3 Future research trajectories

Several research directions can be developed further in terms of underlying SiDNA transport processes under different physico-chemical conditions and investigating the applicability of

the SiDNA particles in varied homogeneous and heterogeneous systems in order to standardize and validate the real world applications of the particles.

6.3.1 Physico-chemical variables

In order to determine the diverse environmental conditions where SiDNA application would be suitable for determining hydraulic parameters, systematic studies are required to investigate the transport characteristics of SiDNA under different physico-chemical environments such as sand grain size (Bradford et al., 2002; Xie et al., 2018; Zhang et al., 2022; Sun et al., 2015), groundwater inorganic ions (Zhang and Selim, 2007; Torkzaban et al., 2015), flow velocity (Zhang et al., 2022; Kermani et al., 2020), salinity (Magal et al., 2011; Pierve et al., 2019), and dissolved organic matter (Morales et al., 2011; Yang et al., 2015; Cheng and Siers, 2015; Kianfar et al., 2023). Transport characteristics of diverse natural or engineered colloids as a function of different physico-chemical conditions have been extensively reported in literature, however, SiDNA specific investigations under environmentally relevant varying physico-chemical conditions are required in order to broaden the spectrum of environmental conditions, e.g. lithology, groundwater chemistry, physical and chemical heterogeneity etc. where SiDNA can be successfully applied for aquifer hydraulic parameter estimation.

6.3.2 Aquifer heterogeneity

In this thesis, we demonstrated the applicability of SiDNAmag in characterizing hydraulic parameters and associated uncertainties in heterogeneous system with no conductive and high conductive lens in order to contribute to the methodology of SiDNAmag application in identifying a preferential flow zone embedded in otherwise a homogeneous system. However, physical heterogeneity of an aquifer can be of wide variety e.g. multiple heterogeneous lenses (Berg and Illman, 2011), or layers (Sommers et al., 2013), and

therefore, require further experimentations under those complex heterogeneous systems in order to demonstrate the applicability of SiDNAmag for hydraulic parameter estimation of each of the heterogeneous domains, i.e. preferential flow paths, multiple lenses, and heterogeneous layers.

7. References

1. Abascal, E., Gómez-Coma, L., Ortiz, I., & Ortiz, A. (2022). Global diagnosis of nitrate pollution in groundwater and review of removal technologies. Science of the total environment, 810, 152233. https://doi.org/10.1016/j.scitotenv.2021.152233
2. Abiriga, D., Jenkins, A., Vestgarden, L. S., & Klempe, H. (2021). A nature-based solution to a landfill-leachate contamination of a confined aquifer. Scientific Reports, 11(1), 14896. https://doi.org/10.1038/s41598-021-94041-7
3. Acar, Ö., Klammler, H., Hatfield, K., Newman, M. A., Annable, M. D., Cho, J., ... & Kroeker, R. (2013). A stochastic model for estimating groundwater and contaminant discharges from fractured rock passive flux meter measurements. Water Resources Research, 49(3), 1277-1291. https://doi.org/10.1002/wrcr.20109
4. Adamczyk, Z., Nattich-Rak, M., Sadowska, M., Michna, A., & Szczepaniak, K. (2013). Mechanisms of nanoparticle and bioparticle deposition–Kinetic aspects. Colloids and Surfaces A: Physicochemical and Engineering Aspects, 439, 3-22. https://doi.org/10.1016/j.colsurfa.2012.12.060
5. Ahfir, N. D., Benamar, A., Alem, A., & Wang, H. (2009). Influence of internal structure and medium length on transport and deposition of suspended particles: a laboratory study. Transport in porous media, 76, 289-307. https://doi.org/10.1007/s11242-008-9247-3
6. Alcalá, F. J., & Custodio, E. (2008). Using the Cl/Br ratio as a tracer to identify the origin of salinity in aquifers in Spain and Portugal. Journal of Hydrology, 359(1-2), 189-207. https://doi.org/10.1016/j.jhydrol.2008.06.028

7. Alves Júnior, J., & Baldo, J. (2014). The Behavior of Zeta Potential of Silica Suspensions. New Journal of Glass and Ceramics, 04, 29-37. http://www.scirp.org/journal/PaperInformation.aspx?PaperID=45415&#abstract
8. Amme, M., Aldave de las Heras, L., Betti, M., Lang, H., & Stöckl, M. (2004). Effects of colloidal and dissolved silica on the dissolution of UO2 nuclear fuel in groundwater leaching tests. Journal of radioanalytical and nuclear chemistry, 261(2), 327-336. https://doi.org/10.1023/b:jrnc.0000034867.55260.a7
9. Aquilanti, L., Clementi, F., Nanni, T., Palpacelli, S., Tazioli, A., & Vivalda, P. M. (2016). DNA and fluorescein tracer tests to study the recharge, groundwater flowpath and hydraulic contact of aquifers in the Umbria-Marche limestone ridge (central Apennines, Italy). Environmental Earth Sciences, 75(7), 626. https://doi.org/10.1007/s12665-016-5436-5
10. Assari, A., & Mohammadi, Z. (2017). Assessing flow paths in a karst aquifer based on multiple dye tracing tests using stochastic simulation and the MODFLOW-CFP code. Hydrogeology Journal, 25(6), 1679. https://doi.org/10.1007/s10040-017-1595-z
11. Auset, M., & Keller, A. A. (2004). Pore-scale processes that control dispersion of colloids in saturated porous media. Water resources research, 40(3). https://doi.org/10.1029/2003WR002800
12. Babakhani, P. (2019). The impact of nanoparticle aggregation on their size exclusion during transport in porous media: One-and three-dimensional modelling investigations. Scientific reports, 9(1), 1-12. https://doi.org/10.1038/s41598-019-50493-6

13. Bai, H., Cochet, N., Drelich, A., Pauss, A., & Lamy, E. (2016). Comparison of transport between two bacteria in saturated porous media with distinct pore size distribution. Rsc Advances, 6(18), 14602-14614. https://doi.org/10.1039/C5RA21695H

14. Bakker, M., Post, V. +., Langevin, C. D., Hughes, J. D., White, J. T., Starn, J. J., & Fienen, M. N. (2016). Scripting MODFLOW model development using Python and FloPy. Groundwater, 54(5), 733-739. https://doi.org/10.1111/gwat.12413

15. Banks, E. W., Cook, P. G., Owor, M., Okullo, J., Kebede, S., Nedaw, D., ... & MacDonald, A. M. (2021). Environmental tracers to evaluate groundwater residence times and water quality risk in shallow unconfined aquifers in sub Saharan Africa. Journal of Hydrology, 598, 125753. https://doi.org/10.1016/j.jhydrol.2020.125753

16. Baskaran, S., Ransley, T., Brodie, R. S., & Baker, P. (2009). Investigating groundwater–river interactions using environmental tracers. Australian Journal of Earth Sciences, 56(1), 13-19. https://doi.org/10.1080/08120090802541887

17. Baumann, T., & Werth, C. J. (2005). Visualization of colloid transport through heterogeneous porous media using magnetic resonance imaging. Colloids and surfaces A: Physicochemical and engineering aspects, 265(1-3), 2-10. https://doi.org/10.1016/j.colsurfa.2004.11.052

18. Baumann, T., Toops, L., & Niessner, R. (2010). Colloid dispersion on the pore scale. water research, 44(4), 1246-1254. https://doi.org/10.1016/j.watres.2009.11.035

19. Becker, M. W., Collins, S. A., Metge, D. W., Harvey, R. W., & Shapiro, A. M. (2004). Effect of cell physicochemical characteristics and motility on bacterial transport in groundwater. Journal of Contaminant Hydrology, 69(3-4), 195-213. https://doi.org/10.1016/j.jconhyd.2003.08.001

20. Bennacer, L., Ahfir, N. D., Bouanani, A., Alem, A., & Wang, H. (2013). Suspended particles transport and deposition in saturated granular porous medium: particle size effects. Transport in Porous Media, 100(3), 377-392. https://doi.org/10.1007/s11242-013-0220-4

21. Beryani, A., Moghaddam, M. R. A., Tosco, T., Bianco, C., Hosseini, S. M., Kowsari, E., & Sethi, R. (2020). Key factors affecting graphene oxide transport in saturated porous media. Science of The Total Environment, 698, 134224. https://doi.org/10.1016/j.scitotenv.2019.134224

22. Bhattacharjee, S. (2016). DLS and zeta potential–what they are and what they are not? Journal of controlled release, 235, 337-351. https://doi.org/10.1016/j.jconrel.2016.06.017

23. Bhattacharjee, S., Ryan, J. N., & Elimelech, M. (2002). Virus transport in physically and geochemically heterogeneous subsurface porous media. Journal of Contaminant Hydrology, 57(3-4), 161-187. https://doi.org/10.1016/S0169-7722(02)00007-4

24. Bijeljic, B., & Blunt, M. J. (2007). Pore-scale modeling of transverse dispersion in porous media. Water Resources Research, 43(12). https://doi.org/10.1029/2006WR005700

25. Bjerg, P. L., Hinsby, K., Christensen, T. H., & Gravesen, P. (1992). Spatial variability of hydraulic conductivity of an unconfined sandy aquifer determined by a mini slug test. Journal of hydrology, 136(1-4), 107-122. https://doi.org/10.1016/0022-1694(92)90007-I

26. Boadu, F. K. (2000). Hydraulic conductivity of soils from grain-size distribution: new models. Journal of Geotechnical and Geoenvironmental Engineering, 126(8), 739-746. https://doi.org/10.1061/(ASCE)1090-0241(2000)126:8(739)

27. Bolster, C. H., Mills, A. L., Hornberger, G. M., & Herman, J. S. (2001). Effect of surface coatings, grain size, and ionic strength on the maximum attainable coverage of bacteria on sand surfaces. Journal of contaminant hydrology, 50(3-4), 287-305. https://doi.org/10.1016/S0169-7722(01)00106-1

28. Bradford, S. A., & Bettahar, M. (2006). Concentration dependent transport of colloids in saturated porous media. Journal of Contaminant Hydrology, 82(1-2), 99-117. https://doi.org/10.1016/j.jconhyd.2005.09.006

29. Bradford, S. A., Bettahar, M., Simunek, J., & Van Genuchten, M. T. (2004). Straining and attachment of colloids in physically heterogeneous porous media. Vadose Zone Journal, 3(2), 384-394. https://doi.org/10.2113/3.2.384

30. Bradford, S. A., Kim, H. N., Haznedaroglu, B. Z., Torkzaban, S., & Walker, S. L. (2009). Coupled factors influencing concentration-dependent colloid transport and retention in saturated porous media. Environmental science & technology, 43(18), 6996-7002. https://doi.org/10.1021/es900840d

31. Bradford, S. A., Simunek, J., & Walker, S. L. (2006). Transport and straining of E. coli O157: H7 in saturated porous media. Water Resources Research, 42(12). https://doi.org/10.1029/2005WR004805

32. Bradford, S. A., Simunek, J., Bettahar, M., Van Genuchten, M. T., & Yates, S. R. (2003). Modeling colloid attachment, straining, and exclusion in saturated porous media. Environmental science & technology, 37(10), 2242-2250. https://doi.org/10.1021/es025899u

33. Bradford, S. A., Torkzaban, S., & Walker, S. L. (2007). Coupling of physical and chemical mechanisms of colloid straining in saturated porous media. Water research, 41(13), 3012-3024. https://doi.org/10.1016/j.watres.2007.03.030

34. Bradford, S. A., Torkzaban, S., Kim, H., & Simunek, J. (2012). Modeling colloid and microorganism transport and release with transients in solution ionic strength. Water Resources Research, 48(9). https://doi.org/10.1029/2012WR012468

35. Bradford, S. A., Yates, S. R., Bettahar, M., & Simunek, J. (2002). Physical factors affecting the transport and fate of colloids in saturated porous media. Water resources research, 38(12), 63-1. https://doi.org/10.1029/2002WR001340

36. Bridge, J. S., & Hyndman, D. W. (2004). Aquifer characterization. https://doi.org/10.2110/pec.04.80.0001

37. Butler, K. E. (2009). Trends in waterborne electrical and EM induction methods for high resolution sub-bottom imaging. Near Surface Geophysics, 7(4), 241-246. https://doi.org/10.3997/1873-0604.2009002

38. Cardenas, M. B., & Jiang, X. W. (2010). Groundwater flow, transport, and residence times through topography-driven basins with exponentially decreasing permeability and porosity. Water Resources Research, 46(11). https://doi.org/10.1002/wrcr.20064

39. Cardiff, M., Bakhos, T., Kitanidis, P. K., & Barrash, W. (2013). Aquifer heterogeneity characterization with oscillatory pumping: Sensitivity analysis and imaging potential. Water Resources Research, 49(9), 5395-5410. https://doi.org/10.1002/wrcr.20356

40. Cardiff, M., Bakhos, T., Kitanidis, P. K., & Barrash, W. (2013). Aquifer heterogeneity characterization with oscillatory pumping: Sensitivity analysis and imaging potential. Water Resources Research, 49(9), 5395-5410. https://doi.org/10.1002/wrcr.20356

41. Cary, L., Pauwels, H., Ollivier, P., Picot, G., Leroy, P., Mougin, B., ... & Labille, J. (2015). Evidence for TiO_2 nanoparticle transfer in a hard-rock aquifer. Journal of

Contaminant Hydrology, 179, 148-159. https://doi.org/10.1016/j.jconhyd.2015.06.007

42. Castro-Alcalá, E., Fernàndez-Garcia, D., Carrera, J., & Bolster, D. (2012). Visualization of mixing processes in a heterogeneous sand box aquifer. Environmental science & technology, 46(6), 3228-3235. https://doi.org/10.1021/es201779p
43. Chai, J. C., Hossain, M. J., Carter, J., & Shen, S. L. (2014). Cone penetration-induced pore pressure distribution and dissipation. Computers and Geotechnics, 57, 105-113. https://doi.org/10.1016/j.compgeo.2014.01.008
44. Chakraborty, S., Elhaj, R., Foppen, J. W., & Schijven, J. (2023). Effect of injection water ionic strength on estimating hydraulic parameters in a 3D sand tank using silica encapsulated magnetic DNA particles. Advances in Water Resources, 104507. https://doi.org/10.1016/j.advwatres.2023.104507
45. Chakraborty, S., Foppen, J. W., & Schijven, J. F. (2022). Effect of concentration of silica encapsulated ds-DNA colloidal microparticles on their transport through saturated porous media. Colloids and Surfaces A: Physicochemical and Engineering Aspects, 651, 129625. https://doi.org/10.1016/j.colsurfa.2022.129625
46. Chan Hilton, A. B., & Culver, T. B. (2005). Groundwater remediation design under uncertainty using genetic algorithms. Journal of water resources planning and management, 131(1), 25-34. https://doi.org/10.1061/(ASCE)0733-9496(2005)131:1(25)
47. Chandrasekaran, A. R., & Halvorsen, K. (2020). Nuclease degradation analysis of DNA nanostructures using gel electrophoresis. Current protocols in nucleic acid chemistry, 82(1), e115. https://doi.org/10.1002/cpnc.115

48. Chapman, S. W., Parker, B. L., Sale, T. C., & Doner, L. A. (2012). Testing high resolution numerical models for analysis of contaminant storage and release from low permeability zones. Journal of contaminant hydrology, 136, 106-116. https://doi.org/10.1016/j.jconhyd.2012.04.006

49. Chen, G., & Walker, S. L. (2012). Fecal indicator bacteria transport and deposition in saturated and unsaturated porous media. Environmental Science & Technology, 46(16), 8782-8790. https://doi.org/10.1021/es301378q

50. Chen, J., Chen, W., Lu, T., Song, Y., Zhang, H., Wang, M., ... & Lu, M. (2021). Effects of phosphate on the transport of graphene oxide nanoparticles in saturated clean and iron oxide-coated sand columns. journal of environmental sciences, 103, 80-92. https://doi.org/10.1016/j.jes.2020.10.011

51. Chen, M., Xu, N., Cao, X., Zhou, K., Chen, Z., Wang, Y., & Liu, C. (2015). Facilitated transport of anatase titanium dioxides nanoparticles in the presence of phosphate in saturated sands. Journal of colloid and interface science, 451, 134-143. https://doi.org/10.1016/j.jcis.2015.04.010

52. Chen, X., Zhang, Y. F., Xue, X., Zhang, Z., & Wei, L. (2012). Estimation of baseflow recession constants and effective hydraulic parameters in the karst basins of southwest China. Hydrology Research, 43(1-2), 102-112. https://doi.org/10.2166/nh.2011.136

53. Chowdhury, I., Hong, Y., Honda, R. J., & Walker, S. L. (2011). Mechanisms of TiO_2 nanoparticle transport in porous media: Role of solution chemistry, nanoparticle concentration, and flowrate. Journal of colloid and interface science, 360(2), 548-555. https://doi.org/10.1016/j.jcis.2011.04.111

54. Chrysikopoulos, C. V., & Katzourakis, V. E. (2015). Colloid particle size-dependent dispersivity. Water Resources Research, 51(6), 4668-4683. https://doi.org/10.1002/2014WR016094

55. Chrysikopoulos, C. V., & Syngouna, V. I. (2014). Effect of gravity on colloid transport through water-saturated columns packed with glass beads: modeling and experiments. Environmental science & technology, 48(12), 6805-6813. https://doi.org/10.1021/es501295n

56. Chu, Y., Jin, Y., Baumann, T., & Yates, M. V. (2003). Effect of soil properties on saturated and unsaturated virus transport through columns. Journal of Environmental Quality, 32(6), 2017-2025. https://doi.org/10.2134/jeq2003.2017

57. Cosgrove, T. (Ed.). (2010). Colloid science: principles, methods and applications. John Wiley & Sons.

58. Crowe, C., Sommerfeld, M., & Tsuji, Y. (1998). Multiphase Flows with droplets and particles: Ž.

59. D'Oria, M., & Zanini, A. (2019). Characterization of hydraulic heterogeneity of alluvial aquifer using natural stimuli: a field experience of northern Italy. Water, 11(1), 176. https://doi.org/10.3390/w11010176

60. Dahlke, H. E., Williamson, A. G., Georgakakos, C., Leung, S., Sharma, A. N., Lyon, S. W., & Walter, M. T. (2015). Using concurrent DNA tracer injections to infer glacial flow pathways. Hydrological Processes, 29(25), 5257-5274. https://doi.org/10.1002/hyp.10679

61. Dann, R. L., Close, M. E., Pang, L., Flintoft, M. J., & Hector, R. P. (2008). Complementary use of tracer and pumping tests to characterize a heterogeneous

channelized aquifer system in New Zealand. Hydrogeology Journal, 16, 1177-1191. https://doi.org/10.1007/s10040-008-0291-4

62. Danquigny, C., Ackerer, P., & Carlier, J. P. (2004). Laboratory tracer tests on three-dimensional reconstructed heterogeneous porous media. Journal of Hydrology, 294(1-3), 196-212. https://doi.org/10.1016/j.jhydrol.2004.02.008
63. Davis, J. A., Kent, D. B., Coston, J. A., Hess, K. M., & Joye, J. L. (2000). Multispecies reactive tracer test in an aquifer with spatially variable chemical conditions. Water Resources Research, 36(1), 119-134. https://doi.org/10.1029/1999WR900282
64. Davis, S. N., Fabryka-Martin, J. T., & Wolfsberg, L. E. (2004). Variations of bromide in potable ground water in the United States. Ground Water, 42(6), 902-909. https://www.proquest.com/scholarly-journals/variations-bromide-potable-ground-water-united/docview/236916765/se-2
65. Davis, S. N., Thompson, G. M., Bentley, H. W., & Stiles, G. (1980). Ground-water tracers—A short review. Groundwater, 18(1), 14-23. https://doi.org/10.1111/j.1745-6584.1980.tb03366.x
66. de Almeida, A., Maciel, D. F., Sousa, K. F., Nascimento, C. T. C., & Koide, S. (2021). Vertical electrical sounding (VES) for estimation of hydraulic parameters in the porous aquifer. Water, 13(2), 170. https://doi.org/10.3390/w13020170
67. Deichmann, U. (2007). “Molecular” versus “colloidal”: controversies in biology and biochemistry, 1900–1940. Bulletin for the History of Chemistry, 32(2).
68. DeNovio, N. M., Saiers, J. E., & Ryan, J. N. (2004). Colloid movement in unsaturated porous media: Recent advances and future directions. Vadose Zone Journal, 3(2), 338-351. https://doi.org/10.2113/3.2.338

69. Derouane, J., & Dassargues, A. (1998). Delineation of groundwater protection zones based on tracer tests and transport modeling in alluvial sediments. Environmental Geology, 36, 27-36. https://doi.org/10.1007/s002540050317

70. Devic, G., Djordjevic, D., & Sakan, S. (2014). Natural and anthropogenic factors affecting the groundwater quality in Serbia. Science of the Total Environment, 468, 933-942.

71. Dibyanshu, K., Chhaya, T., & Raychoudhury, T. (2022). A review on the fate and transport behavior of engineered nanoparticles: Possibility of becoming an emerging contaminant in the groundwater. International Journal of Environmental Science and Technology, 1-24. https://doi.org/10.1007/s13762-021-03835-9

72. Dikinya, O., Hinz, C., & Aylmore, G. (2008). Decrease in hydraulic conductivity and particle release associated with self-filtration in saturated soil columns. Geoderma, 146(1-2), 192-200. https://doi.org/10.1016/j.geoderma.2008.05.014

73. Divine, C. E., & McDonnell, J. J. (2005). The future of applied tracers in hydrogeology. Hydrogeology journal, 13, 255-258. https://doi.org/10.1007/s10040-004-0416-3

74. Doetsch, J., Linde, N., Vogt, T., Binley, A., & Green, A. G. (2012). Imaging and quantifying salt-tracer transport in a riparian groundwater system by means of 3D ERT monitoring. Geophysics, 77(5), B207-B218. https://doi.org/10.1190/geo2012-0046.1

75. Dong, S., Gao, B., Sun, Y., Guo, H., Wu, J., Cao, S., & Wu, J. (2019). Visualization of graphene oxide transport in two-dimensional homogeneous and heterogeneous porous media. Journal of hazardous materials, 369, 334-341. https://doi.org/10.1016/j.jhazmat.2019.02.042

76. Dujardin, J., Anibas, C., Bronders, J., Jamin, P., Hamonts, K., Dejonghe, W., ... & Batelaan, O. (2014). Combining flux estimation techniques to improve characterization of groundwater–surface-water interaction in the Zenne River, Belgium. Hydrogeology Journal. https://doi.org/10.1007/s10040-014-1159-4

77. Elimelech, M. (1992). Predicting collision efficiencies of colloidal particles in porous media. Water research, 26(1), 1-8. https://doi.org/10.1016/0043-1354(92)90104-C

78. Elimelech, M., Nagai, M., Ko, C. H., & Ryan, J. N. (2000). Relative insignificance of mineral grain zeta potential to colloid transport in geochemically heterogeneous porous media. Environmental science & technology, 34(11), 2143-2148. https://doi.org/10.1021/es9910309

79. Elliot, T. (2014). Environmental tracers. Water, 6(11), 3264-3269. https://doi.org/10.3390/w6113264

80. Ersenkal, D. A., Ziylan, A., Ince, N. H., Acar, H. Y., Demirer, M., & Copty, N. K. (2011). Impact of dilution on the transport of poly (acrylic acid) supported magnetite nanoparticles in porous media. Journal of contaminant hydrology, 126(3-4), 248-257. https://doi.org/10.1016/j.jconhyd.2011.09.005

81. Esfahani, A. R., Firouzi, A. F., Sayyad, G., & Kiasat, A. R. (2014). Transport and retention of polymer-stabilized zero-valent iron nanoparticles in saturated porous media: Effects of initial particle concentration and ionic strength. Journal of Industrial and Engineering Chemistry, 20(5), 2671-2679. https://doi.org/10.1016/j.jiec.2013.10.054

82. Everett, D. H. (2007). Basic principles of colloid science. Royal society of chemistry. ISBN 0-85186-443-0

83. Fazeli Sangani, M., Owens, G., & Fotovat, A. (2019). Transport of engineered nanoparticles in soils and aquifers. Environmental Reviews, 27(1), 43-70. https://doi.org/10.1139/er-2018-0022

84. Fernàndez-Garcia, D., Illangasekare, T. H., & Rajaram, H. (2004). Conservative and sorptive forced-gradient and uniform flow tracer tests in a three-dimensional laboratory test aquifer. Water Resources Research, 40(10). https://doi.org/10.1029/2004WR003112

85. Ferrer, N., Folch, A., Masó, G., Sanchez, S., & Sanchez-Vila, X. (2020). What are the main factors influencing the presence of faecal bacteria pollution in groundwater systems in developing countries?. Journal of contaminant hydrology, 228, 103556. https://doi.org/10.1016/j.jconhyd.2019.103556

86. Flint, L. E., & Flint, A. L. (2002). 2.3 Porosity. Methods of Soil Analysis: Part 4 Physical Methods, 5, 241-254. ISBN:089118841X, 9780891188414

87. Fontes, D. E., Mills, A. L., Hornberger, G. M., & Herman, J. (1991). Physical and chemical factors influencing transport of microorganisms through porous media. Applied and Environmental Microbiology, 57(9), 2473-2481. https://doi.org/10.1128/aem.57.9.2473-2481.1991

88. Foppen, J. W. (2023). Artificial DNA in hydrology. Wiley Interdisciplinary Reviews: Water, e1681. https://doi.org/10.1002/wat2.1681

89. Foppen, J. W., Orup, C., Adell, R., Poulalion, V., & Uhlenbrook, S. (2011). Using multiple artificial DNA tracers in hydrology. Hydrological Processes, 25(19), 3101-3106. https://doi.org/10.1002/hyp.8159

90. Foppen, J. W., Seopa, J., Bakobie, N., & Bogaard, T. (2013). Development of a methodology for the application of synthetic DNA in stream tracer injection

experiments. Water Resources Research, 49(9), 5369-5380. https://doi.org/10.1002/wrcr.20438

91. Foppen, J. W., van Herwerden, M., & Schijven, J. (2007). Transport of Escherichia coli in saturated porous media: Dual mode deposition and intra-population heterogeneity. Water Research, 41(8), 1743-1753. https://doi.org/10.1016/j.watres.2006.12.041
92. Freeze, R. A., & Cherry, J. A. (1979). Groundwater. New Jersey: Prentice-Hall geochemical parameter distribution in a ground water system contaminated with petroleum hydrocarbons. Journal of Environmental Quality, 30, 1548-1563.
93. Fu, J., & Gómez-Hernández, J. J. (2009). Uncertainty assessment and data worth in groundwater flow and mass transport modeling using a blocking Markov chain Monte Carlo method. Journal of Hydrology, 364(3-4), 328-341. https://doi.org/10.1016/j.jhydrol.2008.11.014
94. Gao, B., Saiers, J. E., & Ryan, J. (2006). Pore-scale mechanisms of colloid deposition and mobilization during steady and transient flow through unsaturated granular media. Water Resources Research, 42(1). https://doi.org/10.1029/2005WR004233
95. Genereux, D., & Guardiario Jr, J. (2001). A borehole flowmeter investigation of small-scale hydraulic conductivity variation in the Biscayne Aquifer, Florida. Water Resources Research, 37(5), 1511-1517. https://doi.org/10.1029/2001WR900023
96. Gentile, G. J., & de Cortalezzi, M. M. F. (2016). Enhanced retention of bacteria by TiO2 nanoparticles in saturated porous media. Journal of contaminant hydrology, 191, 66-75. https://doi.org/10.1016/j.jconhyd.2016.05.004
97. Gerke, K. M., Sidle, R. C., & Tokuda, Y. (2008). Sorption of Uranine on forest soils. Hydrological Research Letters, 2, 32-35. https://doi.org/10.3178/hrl.2.32

98. Geyer, T., Birk, S., Licha, T., Liedl, R., & Sauter, M. (2007). Multitracer test approach to characterize reactive transport in karst aquifers. Groundwater, 45(1), 36-45. https://doi.org/10.1111/j.1745-6584.2006.00261.x

99. Ghosh, D., Das, S., Gahlot, V. K., Pulimi, M., Anand, S., Chandrasekaran, N., ... & Mukherjee, A. (2022). Nano-SiO2 transport and retention in saturated porous medium: Influence of pH, ionic strength, and natural organics. Journal of Contaminant Hydrology, 248, 104029. https://doi.org/10.1016/j.jconhyd.2022.104029

100. Godinez, I. G., & Darnault, C. J. (2011). Aggregation and transport of nano-TiO2 in saturated porous media: effects of pH, surfactants and flow velocity. Water research, 45(2), 839-851. https://doi.org/10.1016/j.watres.2010.09.013

101. Goeppert, N., & Goldscheider, N. (2021). Experimental field evidence for transport of microplastic tracers over large distances in an alluvial aquifer. Journal of hazardous materials, 408, 124844. https://doi.org/10.1016/j.jhazmat.2020.124844

102. Grisey, E., Belle, E., Dat, J., Mudry, J., & Aleya, L. (2010). Survival of pathogenic and indicator organisms in groundwater and landfill leachate through coupling bacterial enumeration with tracer tests. Desalination, 261(1-2), 162-168. https://doi.org/10.1016/j.desal.2010.05.007

103. Grolimund, D., Elimelech, M., Borkovec, M., Barmettler, K., Kretzschmar, R., & Sticher, H. (1998). Transport of in situ mobilized colloidal particles in packed soil columns. Environmental Science & Technology, 32(22), 3562-3569. https://doi.org/10.1021/es980356z

104. Gross, M. J., Albinger, O., Jewett, D. G., Logan, B. E., Bales, R. C., & Arnold, R. G. (1995). Measurement of bacterial collision efficiencies in porous media. Water research, 29(4), 1151-1158. https://doi.org/10.1016/0043-1354(94)00235-Y

105. Guo, Y., Huang, J., Xiao, F., Yin, X., Chun, J., Um, W., ... & Wu, N. (2016). Bead-based microfluidic sediment analogues: fabrication and colloid transport. Langmuir, 32(36), 9342-9350. https://pubs.acs.org/doi/abs/10.1021/acs.langmuir.6b02184

106. Guo, Z., Ma, R., Zhang, Y., & Zheng, C. (2021). Contaminant transport in heterogeneous aquifers: A critical review of mechanisms and numerical methods of non-Fickian dispersion. Science China Earth Sciences, 64, 1224-1241. https://doi.org/10.1007/s11430-020-9755-y

107. Hahn, M. W., & O'Melia, C. R. (2004). Deposition and reentrainment of Brownian particles in porous media under unfavorable chemical conditions: Some concepts and applications. Environmental science & technology, 38(1), 210-220. https://doi.org/10.1021/es030416n

108. Harbaugh, A. W., Langevin, C. D., Hughes, J. D., Niswonger, R. N., & Konikow, L. F. (2017). MODFLOW-2005 version 1.12. 00, the US Geological Survey modular groundwater model. US Geological Survey Software Release, 3.

109. Harbaugh, A.W., 2005, MODFLOW-2005, the U.S. Geological Survey modular ground-water model -- the Ground-Water Flow Process: U.S. Geological Survey Techniques and Methods 6-A16

110. Hartog, N., Cho, J., Parker, B. L., & Annable, M. D. (2010). Characterization of a heterogeneous DNAPL source zone in the Borden aquifer using partitioning and interfacial tracers: residual morphologies and background sorption. Journal of

contaminant hydrology, 115(1-4), 79-89. https://doi.org/10.1016/j.jconhyd.2010.04.004

111. Harvey, R. W. (1997). Microorganisms as tracers in groundwater injection and recovery experiments: a review. FEMS Microbiology Reviews, 20(3-4), 461-472. https://doi.org/10.1111/j.1574-6976.1997.tb00330.x

112. Harvey, R. W., & Harms, H. (2002). Tracers in groundwater: use of microorganisms and microspheres. Encyclopedia of environmental microbiology, 6, 3194-3202. https://doi.org/10.1002/0471263397.env157

113. Harvey, R. W., Kinner, N. E., MacDonald, D., Metge, D. W., & Bunn, A. (1993). Role of physical heterogeneity in the interpretation of small-scale laboratory and field observations of bacteria, microbial-sized microsphere, and bromide transport through aquifer sediments. Water Resources Research, 29(8), 2713-2721. https://doi.org/10.1029/93WR00963

114. Hassan, P. A., Rana, S., & Verma, G. (2015). Making sense of Brownian motion: colloid characterization by dynamic light scattering. Langmuir, 31(1), 3-12. https://doi.org/10.1021/la501789z

115. Hassanizadeh, S. M., & Schijven, J. F. (2000). Use of bacteriophages as tracers for the study of removal of viruses. In Tracers and modelling in hydrogeology. Proceedings of TraM'2000, the International Conference on Tracers and Modelling in Hydrogeology held at Liège, Belgium, May 2000 (pp. 167-174). IAHS Press.

116. Haznedaroglu, B. Z., Kim, H. N., Bradford, S. A., & Walker, S. L. (2009). Relative transport behavior of Escherichia coli O157: H7 and Salmonella enterica serovar pullorum in packed bed column systems: Influence of solution chemistry and

cell concentration. Environmental science & technology, 43(6), 1838-1844. https://doi.org/10.1021/es802531k

117. He, K., Retterer, S. T., Srijanto, B. R., Conrad, J. C., & Krishnamoorti, R. (2014). Transport and dispersion of nanoparticles in periodic nanopost arrays. ACS nano, 8(5), 4221-4227. https://doi.org/10.1021/nn404497z

118. He, S. H., Ding, Z., Hu, H. B., & Gao, M. (2021). Effect of grain size on microscopic pore structure and fractal characteristics of carbonate-based sand and silicate-based sand. Fractal and Fractional, 5(4), 152. https://doi.org/10.3390/fractalfract5040152

119. Herrick, M. G., Benson, D. A., Meerschaert, M. M., & McCall, K. R. (2002). Hydraulic conductivity, velocity, and the order of the fractional dispersion derivative in a highly heterogeneous system. Water Resources Research, 38(11), 9-1. https://doi.org/10.1029/2001WR000914

120. Higgo, J. J. W., Williams, G. M., Harrison, I., Warwick, P., Gardiner, M. P., & Longworth, G. (1993). Colloid transport in a glacial sand aquifer. Laboratory and field studies. In Colloids in the Aquatic Environment (pp. 179-200). Elsevier. https://doi.org/10.1016/B978-1-85861-038-2.50016-4

121. Hitzelberger, M., Khan, N. A., Mohamed, R. A., Brusseau, M. L., & Carroll, K. C. (2022). PFOS Mass Flux Reduction/Mass Removal: Impacts of a Lower-Permeability Sand Lens within Otherwise Homogeneous Systems. Environmental Science & Technology, 56(19), 13675-13685. https://doi.org/10.1021/acs.est.2c02193

122. Hoffmann, R., Dassargues, A., Goderniauxf, P., & Hermans, T. (2019). Heterogeneity and prior uncertainty investigation using a joint heat and solute tracer

experiment in alluvial sediments. Frontiers in Earth Science, 7, 108. https://doi.org/10.3389/feart.2019.00108

123. Honeyman, B. D. (1999). Colloidal culprits in contamination. Nature, 397(6714), 23-24. https://doi.org/10.1038/16150

124. Hong, Y., Honda, R. J., Myung, N. V., & Walker, S. L. (2009). Transport of iron-based nanoparticles: role of magnetic properties. Environmental science & technology, 43(23), 8834-8839. https://doi.org/10.1021/es9015525

125. Hosono, T., Tokunaga, T., Tsushima, A., & Shimada, J. (2014). Combined use of δ13C, δ15N, and δ34S tracers to study anaerobic bacterial processes in groundwater flow systems. Water Research, 54, 284-296. https://doi.org/10.1016/j.watres.2014.02.005

126. Hou, J., Zhang, M., Wang, P., Wang, C., Miao, L., Xu, Y., ... & Liu, Z. (2017). Transport, retention, and long-term release behavior of polymer-coated silver nanoparticles in saturated quartz sand: The impact of natural organic matters and electrolyte. Environmental Pollution, 229, 49-59. https://doi.org/10.1016/j.envpol.2017.05.059

127. Huysmans, M., & Dassargues, A. (2005). Review of the use of Péclet numbers to determine the relative importance of advection and diffusion in low permeability environments. Hydrogeology Journal, 13, 895-904. https://doi.org/10.1007/s10040-004-0387-4

128. Illman, W. A., Berg, S. J., & Yeh, T. C. J. (2012). Comparison of approaches for predicting solute transport: Sandbox experiments. Groundwater, 50(3), 421-431. https://doi.org/10.1111/j.1745-6584.2011.00859.x

129. Jain, P., Powell, J., Townsend, T. G., & Reinhart, D. R. (2006). Estimating the hydraulic conductivity of landfilled municipal solid waste using the borehole permeameter test. Journal of Environmental Engineering, 132(6), 645-652. https://doi.org/10.1061/(ASCE)0733-9372(2006)132:6(645)

130. James, S. C., & Chrysikopoulos, C. V. (2003). Effective velocity and effective dispersion coefficient for finite-sized particles flowing in a uniform fracture. Journal of colloid and interface science, 263(1), 288-295. https://doi.org/10.1016/S0021-9797(03)00254-6

131. Johnson, & Elimelech. (1995). Dynamics of colloid deposition in porous media: Blocking based on random sequential adsorption. Langmuir, 11(3), 801-812. https://doi.org/10.1021/la00003a023

132. Johnson, P. R., Sun, N., & Elimelech, M. (1996). Colloid transport in geochemically heterogeneous porous media: Modeling and measurements. Environmental science & technology, 30(11), 3284-3293. https://doi.org/10.1021/es960053+

133. Johnson, W. P., Pazmino, E., & Ma, H. (2010). Direct observations of colloid retention in granular media in the presence of energy barriers, and implications for inferred mechanisms from indirect observations. water research, 44(4), 1158-1169. https://doi.org/10.1016/j.watres.2009.12.014

134. Joodi, A. S., Sizaret, S., Binet, S., Bruand, A., Alberic, P., & Lepiller, M. (2010). Development of a Darcy-Brinkman model to simulate water flow and tracer transport in a heterogeneous karstic aquifer (Val d'Orléans, France). Hydrogeology journal, 18(2), 295. http://dx.doi.org/10.1007%2Fs10040-009-0536-x

135. Jose, S. C., Rahman, M. A., & Cirpka, O. A. (2004). Large-scale sandbox experiment on longitudinal effective dispersion in heterogeneous porous media. Water Resources Research, 40(12). https://doi.org/10.1029/2004WR003363

136. Joun, W. T., Lee, K. K., Ha, S. W., Lee, S. S., Kim, Y., Do, H. K., ... & Ju, Y. (2023). A modified and rapid method for the single-well push-pull (SWPP) test using SF6, Kr, and uranine tracers. Water Research, 236, 119955. https://doi.org/10.1016/j.watres.2023.119955

137. Kamai, T., Nassar, M. K., Nelson, K. E., & Ginn, T. R. (2015). Colloid filtration prediction by mapping the correlation-equation parameters from transport experiments in porous media. Water Resources Research, 51(11), 8995-9012. https://doi.org/10.1002/2015WR017403

138. Kasteel, R., Vogel, H. J., & Roth, K. (2002). Effect of non-linear adsorption on the transport behaviour of Brilliant Blue in a field soil. European journal of soil science, 53(2), 231-240. https://doi.org/10.1046/j.1365-2389.2002.00437.x

139. Keller, A. A., Sirivithayapakorn, S., & Chrysikopoulos, C. V. (2004). Early breakthrough of colloids and bacteriophage MS2 in a water-saturated sand column. Water Resources Research, 40(8). https://doi.org/10.1029/2003WR002676

140. Kermani, M. S., Jafari, S., Rahnama, M., & Raoof, A. (2020). Direct pore scale numerical simulation of colloid transport and retention. Part I: Fluid flow velocity, colloid size, and pore structure effects. Advances in Water Resources, 144, 103694. https://doi.org/10.1016/j.advwatres.2020.103694

141. Khatri, N., & Tyagi, S. (2015). Influences of natural and anthropogenic factors on surface and groundwater quality in rural and urban areas. Frontiers in life science, 8(1), 23-39.

142. Kianfar, B., Tian, J., Rozemeijer, J., van der Zaan, B., Bogaard, T. A., & Foppen, J. W. (2022). Transport characteristics of DNA-tagged silica colloids as a colloidal tracer in saturated sand columns; role of solution chemistry, flow velocity, and sand grain size. Journal of Contaminant Hydrology, 246, 103954. https://doi.org/10.1016/j.jconhyd.2022.103954

143. Kim, J. W., Choi, H., & Lee, J. Y. (2005). Characterization of hydrogeologic properties for a multi-layered alluvial aquifer using hydraulic and tracer tests and electrical resistivity survey. Environmental geology, 48, 991-1001. https://doi.org/10.1007/s00254-005-1299-x

144. Kimambo, V., Bhattacharya, P., Mtalo, F., Mtamba, J., & Ahmad, A. (2019). Fluoride occurrence in groundwater systems at global scale and status of defluoridation–state of the art. Groundwater for Sustainable Development, 9, 100223. https://doi.org/10.1016/j.gsd.2019.100223

145. Klepikova, M., Wildemeersch, S., Hermans, T., Jamin, P., Orban, P., Nguyen, F., ... & Dassargues, A. (2016). Heat tracer test in an alluvial aquifer: Field experiment and inverse modelling. Journal of Hydrology, 540, 812-823. https://doi.org/10.1016/j.jhydrol.2016.06.066

146. Ko, C. H., & Elimelech, M. (2000). The “shadow effect” in colloid transport and deposition dynamics in granular porous media: measurements and mechanisms. Environmental Science & Technology, 34(17), 3681-3689. https://doi.org/10.1021/es0009323

147. Kong, X. Z., Deuber, C. A., Kittilä, A., Somogyvári, M., Mikutis, G., Bayer, P., ... & Saar, M. O. (2018). Tomographic reservoir imaging with DNA-labeled silica

nanotracers: the first field validation. Environmental science & technology, 52(23), 13681-13689. https://doi.org/10.1021/acs.est.8b04367

148. Konikow, L. F., Hornberger, G. Z., Halford, K. J., Hanson, R. T., & Harbaugh, A. W. (2009). Revised multi-node well (MNW2) package for MODFLOW ground-water flow model. US Geological Survey Techniques and Methods, 67(10.3133). http://pubsdata.usgs.gov/pubs/tm/tm6a30/index.html

149. Kosakowski, G. (2004). Anomalous transport of colloids and solutes in a shear zone. Journal of Contaminant Hydrology, 72(1-4), 23-46. https://doi.org/10.1016/j.jconhyd.2003.10.005

150. Lanning, L. M., & Ford, R. M. (2002). Glass micromodel study of bacterial dispersion in spatially periodic porous networks. Biotechnology and bioengineering, 78(5), 556-566. https://doi.org/10.1002/bit.10236

151. Lapcevic, P. A., Novakowski, K. S., & Sudicky, E. A. (1999). The interpretation of a tracer experiment conducted in a single fracture under conditions of natural groundwater flow. Water resources research, 35(8), 2301-2312. https://doi.org/10.1029/1999WR900143

152. Larocque, M., Cook, P. G., Haaken, K., & Simmons, C. T. (2009). Estimating flow using tracers and hydraulics in synthetic heterogeneous aquifers. Groundwater, 47(6), 786-796. https://doi.org/10.1111/j.1745-6584.2009.00595.x

153. Lauber, U., & Goldscheider, N. (2014). Use of artificial and natural tracers to assess groundwater transit-time distribution and flow systems in a high-alpine karst system (Wetterstein Mountains, Germany). Hydrogeology Journal, 22(8), 1807. DOI:10.1007/s10040-014-1173-6

154. Lecoanet, H. F., & Wiesner, M. R. (2004). Velocity effects on fullerene and oxide nanoparticle deposition in porous media. Environmental science & technology, 38(16), 4377-4382. https://doi.org/10.1021/es035354f

155. Lee, J. Y., Kim, J. W., Cheon, J. Y., Yi, M. J., & Lee, K. K. (2003). Combined performance of pumping and tracer tests: A case study. Geosciences Journal, 7, 237-241. https://doi.org/10.1007/BF02910290

156. Leij, F. J., & Bradford, S. A. (2013). Colloid transport in dual-permeability media. Journal of contaminant hydrology, 150, 65-76. https://doi.org/10.1016/j.jconhyd.2013.03.010

157. Levy, M., & Berkowitz, B. (2003). Measurement and analysis of non-Fickian dispersion in heterogeneous porous media. Journal of contaminant hydrology, 64(3-4), 203-226. https://doi.org/10.1016/S0169-7722(02)00204-8

158. Li, J., Rajajayavel, S. R. C., & Ghoshal, S. (2016). Transport of carboxymethyl cellulose-coated zerovalent iron nanoparticles in a sand tank: Effects of sand grain size, nanoparticle concentration and injection velocity. Chemosphere, 150, 8-16. https://doi.org/10.1016/j.chemosphere.2015.12.075

159. Li, L., & Schuster, M. (2014). Influence of phosphate and solution pH on the mobility of ZnO nanoparticles in saturated sand. Science of the total environment, 472, 971-978. https://doi.org/10.1016/j.scitotenv.2013.11.057

160. Li, M., Zhang, X., Yi, K., He, L., Han, P., & Tong, M. (2021). Transport and deposition of microplastic particles in saturated porous media: Co-effects of clay particles and natural organic matter. Environmental Pollution, 287, 117585. https://doi.org/10.1016/j.envpol.2021.117585

161. Li, Y., Wang, Y., Pennell, K. D., & Abriola, L. M. (2008). Investigation of the transport and deposition of fullerene (C60) nanoparticles in quartz sands under varying flow conditions. Environmental science & technology, 42(19), 7174-7180. https://doi.org/10.1021/es801305y

162. Liang, X., & Zhang, Y. K. (2013). Temporal and spatial variation and scaling of groundwater levels in a bounded unconfined aquifer. Journal of hydrology, 479, 139-145. https://doi.org/10.1016/j.jhydrol.2012.11.044

163. Liao, R., Yang, P., Wu, W., Luo, D., & Yang, D. (2018). A DNA tracer system for hydrological environment investigations. Environmental science & technology, 52(4), 1695-1703. https://doi.org/10.1021/acs.est.7b02928

164. Lile, O. B., Morris, M., & Rønning, J. S. (1997). Estimating groundwater flow velocity from changes in contact resistance during a saltwater tracer experiment. Journal of Applied Geophysics, 38(2), 105-114. https://doi.org/10.1016/S0926-9851(97)00018-9

165. Lin, D., Bradford, S., Hu, L., & MC Lo, I. (2021). Impact of phosphate adsorption on the mobility of PANI-supported nano zero-valent iron. Vadose Zone Journal, 20(2), e20091. https://doi.org/10.1002/vzj2.20091

166. Liu, C., Xu, N., Feng, G., Zhou, D., Cheng, X., & Li, Z. (2017). Hydrochars and phosphate enhancing the transport of nanoparticle silica in saturated sands. Chemosphere, 189, 213-223. https://doi.org/10.1016/j.chemosphere.2017.09.066

167. Liu, F., Yeh, T. C. J., Wang, Y. L., Hao, Y., Wen, J. C., & Wang, W. (2020). Characterization of basin-scale aquifer heterogeneity using transient hydraulic tomography with aquifer responses induced by groundwater exploitation reduction. Journal of Hydrology, 588, 125137. https://doi.org/10.1016/j.jhydrol.2020.125137

168. Liu, Q., Cui, X., Zhang, C., & Huang, S. (2016). Experimental investigation of suspended particles transport through porous media: particle and grain size effect. Environmental technology, 37(7), 854-864. https://doi.org/10.1080/09593330.2015.1088578

169. Liu, Q., Lazouskaya, V., He, Q., & Jin, Y. (2010). Effect of particle shape on colloid retention and release in saturated porous media. Journal of environmental quality, 39(2), 500-508. https://doi.org/10.2134/jeq2009.0100

170. Liu, X., O'Carroll, D. M., Petersen, E. J., Huang, Q., & Anderson, C. L. (2009). Mobility of multiwalled carbon nanotubes in porous media. Environmental science & technology, 43(21), 8153-8158. https://doi.org/10.1021/es901340d

171. Loveland, J. P., Bhattacharjee, S., Ryan, J. N., & Elimelech, M. (2003). Colloid transport in a geochemically heterogeneous porous medium: aquifer tank experiment and modeling. Journal of contaminant hydrology, 65(3-4), 161-182. https://doi.org/10.1016/S0169-7722(02)00238-3

172. Lu, C., Yao, C., Su, X., Jiang, Y., Yuan, F., & Wang, M. (2018). The influences of a clay lens on the hyporheic exchange in a sand dune. Water, 10(7), 826. https://doi.org/10.3390/w10070826

173. Lu, H., Dong, J., Xi, B., Cai, P., Xia, T., & Zhang, M. (2021). Transport and retention of porous silicon-coated zero-valent iron in saturated porous media. Environmental Pollution, 276, 116700. https://doi.org/10.1016/j.envpol.2021.116700

174. Lyon-Marion, B. A., Becker, M. D., Kmetz, A. A., Foster, E., Johnston, K. P., Abriola, L. M., & Pennell, K. D. (2017). Simulation of magnetite nanoparticle mobility

in a heterogeneous flow cell. Environmental Science: Nano, 4(7), 1512-1524. https://doi.org/10.1039/C7EN00152E

175. Ma, H. (2014). Mercury intrusion porosimetry in concrete technology: tips in measurement, pore structure parameter acquisition and application. Journal of porous materials, 21, 207-215. https://doi.org/10.1007/s10934-013-9765-4

176. Maier, R., Leven, C., Sánchez-León, E., Strasser, D., Stoll, M., & Cirpka, O. A. (2022). Revealing vertical aquifer heterogeneity and hydraulic anisotropy by pumping partially penetrating wells. Hydrogeology Journal, 30(2), 463-477. https://doi.org/10.1007/s10040-022-02458-9

177. Maliva, R. G. (2016). Aquifer characterization techniques (Vol. 10). Berlin: Springer. https://doi.org/10.1007/978-3-319-32137-0

178. Marquardt, D. W. (1963). An algorithm for least-squares estimation of nonlinear parameters. Journal of the society for Industrial and Applied Mathematics, 11(2), 431-441. https://doi.org/10.1137/0111030

179. Mas-Pla, J., Jim Yeh, T. C., Williams, T. M., & McCarthy, J. F. (1997). Analyses of slug tests and hydraulic conductivity variations in the near field of a two-well tracer experiment site. Groundwater, 35(3), 492-501. https://doi.org/10.1111/j.1745-6584.1997.tb00110.x

180. Mastrocicco, M., Prommer, H., Pasti, L., Palpacelli, S., & Colombani, N. (2011). Evaluation of saline tracer performance during electrical conductivity groundwater monitoring. Journal of contaminant hydrology, 123(3-4), 157-166. https://doi.org/10.1016/j.jconhyd.2011.01.001

181. Maxwell, R. M., Welty, C., & Tompson, A. F. (2003). Streamline-based simulation of virus transport resulting from long term artificial recharge in a

heterogeneous aquifer. Advances in Water Resources, 26(10), 1075-1096. https://doi.org/10.1016/S0309-1708(03)00074-5

182. McCance, W., Jones, O. A. H., Edwards, M., Surapaneni, A., Chadalavada, S., & Currell, M. (2018). Contaminants of emerging concern as novel groundwater tracers for delineating wastewater impacts in urban and peri-urban areas. Water research, 146, 118-133. https://doi.org/10.1016/j.watres.2018.09.013

183. McCarthy, J. F. (2018). Sampling and characterization of colloids and particles in groundwater for studying their role in contaminant transport. In Environmental particles (pp. 247-315). CRC Press. ISBN:1351270788, 9781351270786

184. Meng, X., & Yang, D. (2019). Pore-network modeling of particle dispersion in porous media. Colloids and Surfaces A: Physicochemical and Engineering Aspects, 580, 123768. https://doi.org/10.1016/j.colsurfa.2019.123768

185. Mesticou, Z., Kacem, M., & Dubujet, P. H. (2013). Influence of the ionic strength on the deposit phenomenon and transport dynamic of microparticles through saturated porous medium. In COUPLED V: proceedings of the V International Conference on Computational Methods for Coupled Problems in Science and Engineering: (pp. 1168-1178). CIMNE. http://hdl.handle.net/2117/192762

186. Mikutis, G., Deuber, C. A., Schmid, L., Kittilä, A., Lobsiger, N., Puddu, M., ... & Stark, W. J. (2018). Silica-encapsulated DNA-based tracers for aquifer characterization. Environmental science & technology, 52(21), 12142-12152. https://doi.org/10.1021/acs.est.8b03285

187. Mikutis, G., Schmid, L., Stark, W. J., & Grass, R. N. (2019). Length-dependent DNA degradation kinetic model: Decay compensation in DNA tracer concentration measurements. AIChE Journal, 65(1), 40-48. https://doi.org/10.1002/aic.16433

188. Mobbs, T. L., Peters, R. T., Davenport, J. R., Evans, M. A., & Wu, J. Q. (2012). Effects of four soil surfactants on four soil-water properties in sand and silt loam. Journal of soil and water conservation, 67(4), 275-283. https://doi.org/10.2489/jswc.67.4.275

189. Moeck, C., Radny, D., Popp, A., Brennwald, M., Stoll, S., Auckenthaler, A., ... & Schirmer, M. (2017). Characterization of a managed aquifer recharge system using multiple tracers. Science of the Total Environment, 609, 701-714. https://doi.org/10.1016/j.scitotenv.2017.07.211

190. Mohammadi, Z., Illman, W. A., & Field, M. (2021). Review of laboratory scale models of karst aquifers: approaches, similitude, and requirements. Groundwater, 59(2), 163-174. https://doi.org/10.1111%2Fgwat.13052

191. Molnar, I. L., Pensini, E., Asad, M. A., Mitchell, C. A., Nitsche, L. C., Pyrak-Nolte, L. J., ... & Krol, M. M. (2019). Colloid transport in porous media: a review of classical mechanisms and emerging topics. Transport in Porous Media, 130, 129-156. https://doi.org/10.1007/s11242-019-01270-6

192. Molz, F. J., Güven, O., Melville, J. G., Nohrstedt, J. S., & Overholtzer, J. K. (1988). Forced-gradient tracer tests and inferred hydraulic conductivity distributions at the Mobile site. Groundwater, 26(5), 570-579. https://doi.org/10.1111/j.1745-6584.1988.tb00790.x

193. Mondal, P. K., Furbacher, P. D., Cui, Z., Krol, M. M., & Sleep, B. E. (2018). Transport of polymer stabilized nano-scale zero-valent iron in porous media. Journal

of contaminant hydrology, 212, 65-77. https://doi.org/10.1016/j.jconhyd.2017.11.004

194. Mora, C. A., Paunescu, D., Grass, R. N., & Stark, W. J. (2015). Silica particles with encapsulated DNA as trophic tracers. Molecular ecology resources, 15(2), 231-241. https://doi.org/10.1111/1755-0998.12299

195. Morley, L. M., Hornberger, G. M., Mills, A. L., & Herman, J. S. (1998). Effects of transverse mixing on transport of bacteria through heterogeneous porous media. Water resources research, 34(8), 1901-1908. https://doi.org/10.1029/98WR01210

196. Müller, K., Vanderborght, J., Englert, A., Kemna, A., Huisman, J. A., Rings, J., & Vereecken, H. (2010). Imaging and characterization of solute transport during two tracer tests in a shallow aquifer using electrical resistivity tomography and multilevel groundwater samplers. Water Resources Research, 46(3). https://doi.org/10.1029/2008WR007595

197. Nelson, K. E., & Ginn, T. R. (2005). Colloid filtration theory and the Happel sphere-in-cell model revisited with direct numerical simulation of colloids. Langmuir, 21(6), 2173-2184. https://doi.org/10.1021/la048404i

198. Neshat, A., Pradhan, B., & Javadi, S. (2015). Risk assessment of groundwater pollution using Monte Carlo approach in an agricultural region: an example from Kerman Plain, Iran. Computers, Environment and Urban Systems, 50, 66-73. https://doi.org/10.1016/j.compenvurbsys.2014.11.004

199. Niemann, W. L., & Rovey, C. W. (2000). Comparison of hydraulic conductivity values obtained from aquifer pumping tests and conservative tracer tests. Groundwater Monitoring & Remediation, 20(3), 122-128. https://doi.org/10.1111/j.1745-6592.2000.tb00278.x

200. Nocito-Gobel, J., & Tobiason, J. E. (1996). Effects of ionic strength on colloid deposition and release. Colloids and Surfaces A: Physicochemical and Engineering Aspects, 107, 223-231. https://doi.org/10.1016/0927-7757(95)03340-8

201. Ochi, J., & Vernoux, J. F. (1999). A two-dimensional network model to simulate permeability decrease under hydrodynamic effect of particle release and capture. Transport in porous media, 37(3), 303-325. https://doi.org/10.1023/A:1006690700000

202. Otz, M. H., Otz, H. K., Otz, I., & Siegel, D. I. (2003). Surface water/groundwater interaction in the Piora aquifer, Switzerland: evidence from dye tracing tests. Hydrogeology Journal, 11, 228-239. https://doi.org/10.1007/s10040-002-0237-1

203. Oudega, T. J., Lindner, G., Derx, J., Farnleitner, A. H., Sommer, R., Blaschke, A. P., & Stevenson, M. E. (2021). Upscaling transport of bacillus subtilis endospores and coliphage phiX174 in heterogeneous porous media from the column to the field scale. Environmental Science & Technology, 55(16), 11060-11069. https://doi.org/10.1021/acs.est.1c01892

204. Pang, L., Abeysekera, G., Hanning, K., Premaratne, A., Robson, B., Abraham, P., ... & Billington, C. (2020). Water tracking in surface water, groundwater and soils using free and alginate-chitosan encapsulated synthetic DNA tracers. Water Research, 184, 116192. https://doi.org/10.1016/j.watres.2020.116192

205. Pang, L., Lin, S., Hewitt, J., Premaratne, A., & Close, M. (2021). Attenuation and transport of human enteric viruses and bacteriophage MS2 in alluvial sand and gravel aquifer media—laboratory studies. Water research, 196, 117051. https://doi.org/10.1016/j.watres.2021.117051

206. Pang, L., Robson, B., Farkas, K., McGill, E., Varsani, A., Gillot, L., . . . Abraham, P. (2017). Tracking effluent discharges in undisturbed stony soil and alluvial gravel aquifer using synthetic DNA tracers. Science of the Total Environment, 592, 144-152. https://doi.org/10.1016/j.scitotenv.2017.03.072

207. Patel, V. R., & Agrawal, Y. (2011). Nanosuspension: An approach to enhance solubility of drugs. Journal of advanced pharmaceutical technology & research, 2(2), 81. https://doi.org/10.4103%2F2231-4040.82950

208. Paunescu, D., Fuhrer, R., & Grass, R. N. (2013). Protection and Deprotection of DNA—high-temperature stability of nucleic acid barcodes for polymer labeling. Angewandte Chemie International Edition, 52(15), 4269-4272. http://dx.doi.org/10.1002%2Fanie.201208135

209. Pelley, A. J., & Tufenkji, N. (2008). Effect of particle size and natural organic matter on the migration of nano-and microscale latex particles in saturated porous media. Journal of colloid and interface science, 321(1), 74-83. https://doi.org/10.1016/j.jcis.2008.01.046

210. Phenrat, T., Cihan, A., Kim, H. J., Mital, M., Illangasekare, T., & Lowry, G. V. (2010). Transport and deposition of polymer-modified Fe0 nanoparticles in 2-D heterogeneous porous media: effects of particle concentration, Fe0 content, and coatings. Environmental science & technology, 44(23), 9086-9093. https://doi.org/10.1021/es102398e

211. Phenrat, T., Kim, H. J., Fagerlund, F., Illangasekare, T., & Lowry, G. V. (2010). Empirical correlations to estimate agglomerate size and deposition during injection of a polyelectrolyte-modified Fe0 nanoparticle at high particle concentration in

saturated sand. Journal of contaminant hydrology, 118(3-4), 152-164. https://doi.org/10.1016/j.jconhyd.2010.09.002

212. Pitt, R. E., Clark, S., Parmer, K., & Field, R. (2023). Groundwater contamination from stormwater infiltration. Taylor & Francis.

213. Pollock, D., & Cirpka, O. A. (2010). Fully coupled hydrogeophysical inversion of synthetic salt tracer experiments. Water Resources Research, 46(7). https://doi.org/10.1029/2009WR008575

214. Pool, M., Carrera, J., Alcolea, A., & Bocanegra, E. M. (2015). A comparison of deterministic and stochastic approaches for regional scale inverse modeling on the Mar del Plata aquifer. Journal of Hydrology, 531, 214-229. https://doi.org/10.1016/j.jhydrol.2015.09.064

215. Porubcan, A. A., & Xu, S. (2011). Colloid straining within saturated heterogeneous porous media. Water research, 45(4), 1796-1806. https://doi.org/10.1016/j.watres.2010.11.037

216. Pradhan, B., Chand, S., Chand, S., Rout, P. R., & Naik, S. K. (2023). Emerging groundwater contaminants: A comprehensive review on their health hazards and remediation technologies. Groundwater for Sustainable Development, 20, 100868. https://doi.org/10.1016/j.gsd.2022.100868

217. Ptak, T., Piepenbrink, M., & Martac, E. (2004). Tracer tests for the investigation of heterogeneous porous media and stochastic modelling of flow and transport—a review of some recent developments. Journal of hydrology, 294(1-3), 122-163. https://doi.org/10.1016/j.jhydrol.2004.01.020

218. Puddu, M., Paunescu, D., Stark, W. J., & Grass, R. N. (2014). Magnetically recoverable, thermostable, hydrophobic DNA/silica encapsulates and their

application as invisible oil tags. ACS nano, 8(3), 2677-2685. https://doi.org/10.1021/nn4063853

219. Puls, R. W., & Powell, R. M. (1992). Transport of inorganic colloids through natural aquifer material: Implications for contaminant transport. Environmental Science & Technology, 26(3), 614-621. https://doi.org/10.1021/es00027a027

220. Qi, Z., Zhang, L., & Chen, W. (2014). Transport of graphene oxide nanoparticles in saturated sandy soil. Environmental Science: Processes & Impacts, 16(10), 2268-2277. https://doi.org/10.1039/C4EM00063C

221. Qin, X., Hua, Y., Sun, H., Xie, J., & Zhao, Y. (2020). Visualization study on aniline-degrading bacteria AN-1 transport in the aquifer with the low-permeability lens. Water Research, 186, 116329. https://doi.org/10.1016/j.watres.2020.116329

222. Rahman, T., George, J., & Shipley, H. J. (2013). Transport of aluminum oxide nanoparticles in saturated sand: Effects of ionic strength, flow rate, and nanoparticle concentration. Science of the total environment, 463, 565-571. https://doi.org/10.1016/j.scitotenv.2013.06.049

223. Rajagopalan, R., & Tien, C. (1976). Trajectory analysis of deep-bed filtration with the sphere-in-cell porous media model. AIChE Journal, 22(3), 523-533. https://doi.org/10.1002/aic.690220316

224. Raychoudhury, T., Tufenkji, N., & Ghoshal, S. (2012). Aggregation and deposition kinetics of carboxymethyl cellulose-modified zero-valent iron nanoparticles in porous media. Water research, 46(6), 1735-1744. https://doi.org/10.1016/j.watres.2011.12.045

225. Reginatto, C., Cecchin, I., Heineck, K. S., Thomé, A., & Reddy, K. R. (2020). Use of nanoscale zero-valent iron for remediation of clayey soil contaminated with

hexavalent chromium: batch and column tests. International Journal of Environmental Research and Public Health, 17(3), 1001. https://doi.org/10.3390/ijerph17031001

226. Ren, J., Packman, A. I., & Welty, C. (2000). Correlation of colloid collision efficiency with hydraulic conductivity of silica sands. Water Resources Research, 36(9), 2493-2500. https://doi.org/10.1029/2000WR900163

227. Ren, X. W., & Santamarina, J. C. (2018). The hydraulic conductivity of sediments: A pore size perspective. Engineering Geology, 233, 48-54. https://doi.org/10.1016/j.enggeo.2017.11.022

228. Ren, Z., Gui, X., Xu, X., Zhao, L., Qiu, H., & Cao, X. (2021). Microplastics in the soil-groundwater environment: aging, migration, and co-transport of contaminants–a critical review. Journal of Hazardous Materials, 419, 126455.

229. Renard, P. (2007). Stochastic hydrogeology: what professionals really need?. Groundwater, 45(5), 531-541. https://doi.org/10.1111/j.1745-6584.2007.00340.x

230. Renard, P., Alcolea, A., & Ginsbourger, D. (2013). Stochastic versus deterministic approaches. Environmental modelling: Finding simplicity in complexity, 133-149. https://doi.org/10.1002/9781118351475.ch8

231. Robin, V., Sardini, P., Mazurier, A., Regnault, O., & Descostes, M. (2016). Effective porosity measurements of poorly consolidated materials using non-destructive methods. Engineering Geology, 205, 24-29. https://doi.org/10.1016/j.enggeo.2016.02.007

232. Rojas, R., Feyen, L., & Dassargues, A. (2008). Conceptual model uncertainty in groundwater modeling: Combining generalized likelihood uncertainty estimation and

Bayesian model averaging. Water Resources Research, 44(12). https://doi.org/10.1029/2008WR006908

233. Ronayne, M. J., Gorelick, S. M., & Zheng, C. (2010). Geological modeling of submeter scale heterogeneity and its influence on tracer transport in a fluvial aquifer. Water Resources Research, 46(10). https://doi.org/10.1029/2010WR009348

234. Rosas, J., Lopez, O., Missimer, T. M., Coulibaly, K. M., Dehwah, A. H., Sesler, K., ... & Mantilla, D. (2014). Determination of hydraulic conductivity from grain-size distribution for different depositional environments. Groundwater, 52(3), 399-413. https://doi.org/10.1111/gwat.12078

235. Roychowdhury, A., Pati, S. P., Kumar, S., & Das, D. (2014). Effects of magnetite nanoparticles on optical properties of zinc sulfide in fluorescent-magnetic Fe3O4/ZnS nanocomposites. Powder technology, 254, 583-590. https://doi.org/10.1016/j.powtec.2014.01.076

236. Saar, M. O. (2011). Geothermal heat as a tracer of large-scale groundwater flow and as a means to determine permeability fields. Hydrogeology Journal, 19(1), 31. DOI:10.1007/s10040-010-0657-2

237. Sabatini, D. A. (2000). Sorption and intraparticle diffusion of fluorescent dyes with consolidated aquifer media. Groundwater, 38(5), 651-656. https://doi.org/10.1111/j.1745-6584.2000.tb02700.x

238. Sabir, I. H., Torgersen, J., Haldorsen, S., & Aleström, P. (1999). DNA tracers with information capacity and high detection sensitivity tested in groundwater studies. Hydrogeology Journal, 7(3), 264-272. https://doi.org/10.1007/s100400050200

239. Salamon, P., Fernàndez-Garcia, D., & Gómez-Hernández, J. J. (2007). Modeling tracer transport at the MADE site: The importance of heterogeneity. Water Resources Research, 43(8). https://doi.org/10.1029/2006WR005522

240. Salerno, M. B., Flamm, M., Logan, B. E., & Velegol, D. (2006). Transport of rodlike colloids through packed beds. Environmental science & technology, 40(20), 6336-6340. https://doi.org/10.1021/es0614565

241. Saley, A. D., Jardani, A., Ahmed, A. S., Antoine, R., & Dupont, J. P. (2016). Hamiltonian Monte Carlo algorithm for the characterization of hydraulic conductivity from the heat tracing data. Advances in water resources, 97, 120-129. https://doi.org/10.1016/j.advwatres.2016.09.004

242. Samari-Kermani, M., Jafari, S., Rahnama, M., & Raoof, A. (2021). Ionic strength and zeta potential effects on colloid transport and retention processes. Colloid and Interface Science Communications, 42, 100389. https://doi.org/10.1016/j.colcom.2021.100389

243. Sarris, T. S., Close, M., & Abraham, P. (2018). Using solute and heat tracers for aquifer characterization in a strongly heterogeneous alluvial aquifer. Journal of hydrology, 558, 55-71. https://doi.org/10.1016/j.jhydrol.2018.01.032

244. Sarris, T. S., Close, M., & Abraham, P. (2018). Using solute and heat tracers for aquifer characterization in a strongly heterogeneous alluvial aquifer. Journal of hydrology, 558, 55-71. https://doi.org/10.1016/j.jhydrol.2018.01.032

245. Sasidharan, S., Torkzaban, S., Bradford, S. A., Cook, P. G., & Gupta, V. V. (2017). Temperature dependency of virus and nanoparticle transport and retention in saturated porous media. Journal of contaminant hydrology, 196, 10-20. https://doi.org/10.1016/j.jconhyd.2016.11.004

246. Sattar, G. S., Keramat, M., & Shahid, S. (2016). Deciphering transmissivity and hydraulic conductivity of the aquifer by vertical electrical sounding (VES) experiments in Northwest Bangladesh. Applied Water Science, 6, 35-45. https://doi.org/10.1007/s13201-014-0203-9

247. Schijven, J. F., & Šimůnek, J. (2002). Kinetic modeling of virus transport at the field scale. Journal of Contaminant Hydrology, 55(1-2), 113-135. https://doi.org/10.1016/S0169-7722(01)00188-7

248. Schijven, J. F., Hassanizadeh, S. M., & de Bruin, R. H. (2002). Two-site kinetic modeling of bacteriophages transport through columns of saturated dune sand. Journal of Contaminant Hydrology, 57(3-4), 259-279. https://doi.org/10.1016/S0169-7722(01)00215-7

249. Schijven, J. F., Hassanizadeh, S. M., Dowd, S. E., & Pillai, S. D. (2000). Modeling virus adsorption in batch and column experiments. Quantitative Microbiology, 2(1), 5-20. https://doi.org/10.1023/A:1010062728286

250. Schijven, J. F., van den Berg, H. H., Colin, M., Dullemont, Y., Hijnen, W. A., Magic-Knezev, A., ... & Wubbels, G. (2013). A mathematical model for removal of human pathogenic viruses and bacteria by slow sand filtration under variable operational conditions. Water research, 47(7), 2592-2602. https://doi.org/10.1016/j.watres.2013.02.027

251. Shang, J., Liu, C., & Wang, Z. (2013). Transport and retention of engineered nanoporous particles in porous media: effects of concentration and flow dynamics. Colloids and Surfaces A: Physicochemical and Engineering Aspects, 417, 89-98. https://doi.org/10.1016/j.colsurfa.2012.10.030

252. Sharma, A. N., Luo, D., & Walter, M. T. (2012). Hydrological tracers using nanobiotechnology: proof of concept. Environmental science & technology, 46(16), 8928-8936. https://doi.org/10.1021/es301561q

253. Sharma, A., Foppen, J. W., Banerjee, A., Sawssen, S., Bachhar, N., Peddis, D., & Bandyopadhyay, S. (2021). Magnetic nanoparticles to unique DNA tracers: effect of functionalization on Physico-chemical properties. Nanoscale research letters, 16(1), 1-16. https://doi.org/10.1186/s11671-021-03483-5

254. Shen, C., Huang, Y., Li, B., & Jin, Y. (2008). Effects of solution chemistry on straining of colloids in porous media under unfavorable conditions. Water resources research, 44(5). https://doi.org/10.1029/2007WR006580

255. Sheng-Hua, X., Yin-Mei, L., Li-Ren, L., & Zhi-Wei, S. (2005). Computer simulation of the collision frequency of two particles in optical tweezers. Chinese Physics, 14(2), 382. 10.1088/1009-1963/14/2/028

256. Shuhua, J. I., Xiaowen, L. I. U., Xiu, M. E. N. G., Shaohui, X. U., & Qing, L. I. N. (2023). Coupled effects of pH and kaolinite colloids on antibiotic transport in porous media. Pedosphere, 33(5), 788-799. https://doi.org/10.1016/j.pedsph.2023.01.003

257. Silori, R., Shrivastava, V., Singh, A., Sharma, P., Aouad, M., Mahlknecht, J., & Kumar, M. (2022). Global groundwater vulnerability for Pharmaceutical and Personal care products (PPCPs): The scenario of second decade of 21st century. Journal of Environmental Management, 320, 115703.

258. Simunek, J., Sejna, M., Van Genuchten, M. T., Šimůnek, J., Šejna, M., Jacques, D., ... & Sakai, M. (1998). HYDRUS-1D. Simulating the one-dimensional movement of water, heat, and multiple solutes in variably-saturated media, version, 2.

259. Sirivithayapakorn, S., & Keller, A. (2003). Transport of colloids in saturated porous media: A pore-scale observation of the size exclusion effect and colloid acceleration. Water Resources Research, 39(4). https://doi.org/10.1029/2002WR001583

260. Slater, L. (2007). Near surface electrical characterization of hydraulic conductivity: From petrophysical properties to aquifer geometries—A review. Surveys in Geophysics, 28, 169-197. https://doi.org/10.1007/s10712-007-9022-y

261. Solovitch, N., Labille, J., Rose, J., Chaurand, P., Borschneck, D., Wiesner, M. R., & Bottero, J. Y. (2010). Concurrent aggregation and deposition of TiO2 nanoparticles in a sandy porous media. Environmental science & technology, 44(13), 4897-4902. https://doi.org/10.1021/es1000819

262. Soma, J., & Papadopoulos, K. D. (1995). Flow of dilute, sub-micron emulsions in granular porous media: effects of pH and ionic strength. Colloids and Surfaces A: Physicochemical and Engineering Aspects, 101(1), 51-61. https://doi.org/10.1016/0927-7757(95)03200-W

263. Song, Y., Hu, R., Liu, Q., Qiu, H., Hou, X., Qi, J., & Konadu-Amoah, B. (2023). Comparison of Hydraulic Travel Time and Attenuation Inversions, Thermal Tracer Tomography and Geostatistical Inversion for Aquifer Characterization: A Numerical Study. *Water*, *15*(13), 2401. https://doi.org/10.3390/w15132401

264. Sosa, J. I. M., Gutiérrez Anguamea, G. A., Monreal, R., Grijalva Noriega, F. J., & Tapia-Villaseñor, E. M. (2022). Hydrogeomorphologic mapping of the Transboundary San Pedro Aquifer: A tool for groundwater characterization. Water, 14(6), 906. https://doi.org/10.3390/w14060906

265. Stauffer, R. E. (1985). Use of solute tracers released by weathering to estimate groundwater inflow to seepage lakes. Environmental Science & Technology, 19(5), 405-411. https://doi.org/10.1021/es00135a003

266. Sugimoto, T., Hamamoto, S., & Nishimura, T. (2021). Inhibited nanobubble transport in a saturated porous medium: Effects of deposited colloidal particles. Journal of Contaminant Hydrology, 242, 103854. https://doi.org/10.1016/j.jconhyd.2021.103854

267. Sun, H., Jiao, R., Xu, H., An, G., & Wang, D. (2019). The influence of particle size and concentration combined with pH on coagulation mechanisms. Journal of Environmental Sciences, 82, 39-46. https://doi.org/10.1016/j.jes.2019.02.021

268. Sun, N., Elimelech, M., Sun, N. Z., & Ryan, J. N. (2001). A novel two-dimensional model for colloid transport in physically and geochemically heterogeneous porous media. Journal of contaminant hydrology, 49(3-4), 173-199. https://doi.org/10.1016/S0169-7722(00)00193-5

269. Sun, P., Shijirbaatar, A., Fang, J., Owens, G., Lin, D., & Zhang, K. (2015). Distinguishable transport behavior of zinc oxide nanoparticles in silica sand and soil columns. Science of the Total Environment, 505, 189-198. https://doi.org/10.1016/j.scitotenv.2014.09.095

270. Sun, Y., Gao, B., Bradford, S. A., Wu, L., Chen, H., Shi, X., & Wu, J. (2015). Transport, retention, and size perturbation of graphene oxide in saturated porous media: effects of input concentration and grain size. Water research, 68, 24-33. https://doi.org/10.1016/j.watres.2014.09.025

271. Sutton, D. J., Kabala, Z. J., Francisco, A., & Vasudevan, D. (2001). Limitations and potential of commercially available rhodamine WT as a groundwater tracer.

Water Resources Research, 37(6), 1641-1656. https://doi.org/10.1029/2000WR900295

272. Sutton, D. J., Kabala, Z. J., Schaad, D. E., & Ruud, N. C. (2000). The dipole-flow test with a tracer: a new single-borehole tracer test for aquifer characterization. Journal of Contaminant Hydrology, 44(1), 71-101. https://doi.org/10.1016/S0169-7722(00)00083-8

273. Syngouna, V. I., & Chrysikopoulos, C. V. (2011). Transport of biocolloids in water saturated columns packed with sand: Effect of grain size and pore water velocity. Journal of Contaminant Hydrology, 126(3-4), 301-314. https://doi.org/10.1016/j.jconhyd.2011.09.007

274. Tang, Y. (2023). Hydrodynamic behaviour of silica-DNA microparticles in surface water: A systematic laboratory-based understanding of SiDNA (Fe) tracers. https://doi.org/10.4233/uuid:7c8e98e0-21ab-4f6c-9de3-8acf8d899e88

275. Tang, Y., Foppen, J. W., & Bogaard, T. A. (2021). Transport of silica encapsulated DNA microparticles in controlled instantaneous injection open channel experiments. *Journal of Contaminant Hydrology*, *242*, 103880. https://doi.org/10.1016/j.jconhyd.2021.103880

276. Tatti, F., Papini, M. P., Raboni, M., & Viotti, P. (2016). Image analysis procedure for studying Back-Diffusion phenomena from low-permeability layers in laboratory tests. Scientific reports, 6(1), 30400. https://doi.org/10.1038/srep30400

277. Taylor, R., Cronin, A., Pedley, S., Barker, J., & Atkinson, T. (2004). The implications of groundwater velocity variations on microbial transport and wellhead protection–review of field evidence. FEMS Microbiology Ecology, 49(1), 17-26. https://doi.org/10.1016/j.femsec.2004.02.018

278. Thomas, J. M., & Chrysikopoulos, C. V. (2007). Experimental investigation of acoustically enhanced colloid transport in water-saturated packed columns. Journal of colloid and interface science, 308(1), 200-207. https://doi.org/10.1016/j.jcis.2006.12.062

279. Tian, Y., Gao, B., Silvera-Batista, C., & Ziegler, K. J. (2010). Transport of engineered nanoparticles in saturated porous media. Journal of Nanoparticle Research, 12, 2371-2380. https://doi.org/10.1007/s11051-010-9912-7

280. Tiraferri, A., Tosco, T., & Sethi, R. (2011). Transport and retention of microparticles in packed sand columns at low and intermediate ionic strengths: experiments and mathematical modeling. Environmental Earth Sciences, 63, 847-859. https://doi.org/10.1007/s12665-010-0755-4

281. Torkzaban, S., & Bradford, S. A. (2016). Critical role of surface roughness on colloid retention and release in porous media. Water research, 88, 274-284. https://doi.org/10.1016/j.watres.2015.10.022

282. Torkzaban, S., Bradford, S. A., Vanderzalm, J. L., Patterson, B. M., Harris, B., & Prommer, H. (2015). Colloid release and clogging in porous media: Effects of solution ionic strength and flow velocity. Journal of contaminant hydrology, 181, 161-171. https://doi.org/10.1016/j.jconhyd.2015.06.005

283. Torkzaban, S., Hassanizadeh, S. M., Schijven, J. F., De Bruin, H. A. M., & de Roda Husman, A. M. (2006). Virus transport in saturated and unsaturated sand columns. Vadose Zone Journal, 5(3), 877-885. https://doi.org/10.2136/vzj2005.0086

284. Torkzaban, S., Hocking, M., Bradford, S. A., Tazehkand, S. S., Sasidharan, S., & Šimůnek, J. (2019). Modeling virus transport and removal during storage and

recovery in heterogeneous aquifers. Journal of Hydrology, 578, 124082. https://doi.org/10.1016/j.jhydrol.2019.124082

285. Torkzaban, S., Kim, H. N., Simunek, J., & Bradford, S. A. (2010). Hysteresis of colloid retention and release in saturated porous media during transients in solution chemistry. Environmental science & technology, 44(5), 1662-1669. https://doi.org/10.1021/es903277p

286. Torkzaban, S., Tazehkand, S. S., Walker, S. L., & Bradford, S. A. (2008). Transport and fate of bacteria in porous media: Coupled effects of chemical conditions and pore space geometry. Water Resources Research, 44(4). https://doi.org/10.1029/2007WR006541

287. Torkzaban, S., Tazehkand, S. S., Walker, S. L., & Bradford, S. A. (2008). Transport and fate of bacteria in porous media: Coupled effects of chemical conditions and pore space geometry. Water Resources Research, 44(4). https://doi.org/10.1029/2007WR006541

288. Torrentó, C., Prasuhn, V., Spiess, E., Ponsin, V., Melsbach, A., Lihl, C., ... & Hunkeler, D. (2018). Adsorbing vs. nonadsorbing tracers for assessing pesticide transport in arable soils. Vadose Zone Journal, 17(1), 1-18. https://doi.org/10.2136/vzj2017.01.0033

289. Tosco, T., Bosch, J., Meckenstock, R. U., & Sethi, R. (2012). Transport of ferrihydrite nanoparticles in saturated porous media: role of ionic strength and flow rate. Environmental science & technology, 46(7), 4008-4015. https://doi.org/10.1021/es202643c

290. Tosco, T., Tiraferri, A., & Sethi, R. (2009). Ionic strength dependent transport of microparticles in saturated porous media: Modeling mobilization and

immobilization phenomena under transient chemical conditions. Environmental Science & Technology, 43(12), 4425-4431. https://doi.org/10.1021/es900245d

291. Tourbin, M., & Frances, C. (2009). Monitoring of the aggregation process of dense colloidal silica suspensions in a stirred tank by acoustic spectroscopy. Powder technology, 190(1-2), 25-30. https://doi.org/10.1016/j.powtec.2008.04.067

292. Treumann, S., Torkzaban, S., Bradford, S. A., Visalakshan, R. M., & Page, D. (2014). An explanation for differences in the process of colloid adsorption in batch and column studies. Journal of contaminant hydrology, 164, 219-229. https://doi.org/10.1016/j.jconhyd.2014.06.007

293. Tufenkji, N., & Elimelech, M. (2004). Correlation equation for predicting single-collector efficiency in physicochemical filtration in saturated porous media. Environmental science & technology, 38(2), 529-536. https://doi.org/10.1021/es034049r

294. Tufenkji, N., & Elimelech, M. (2005). Breakdown of colloid filtration theory: Role of the secondary energy minimum and surface charge heterogeneities. Langmuir, 21(3), 841-852. https://doi.org/10.1021/la048102g

295. Urumović, K., & Urumović Sr, K. (2014). The effective porosity and grain size relations in permeability functions. Hydrology and Earth System Sciences Discussions, 11(6), 6675-6714. https://doi.org/10.5194/hessd-11-6675-2014

296. Vandenbohede, A., & Lebbe, L. (2003). Combined interpretation of pumping and tracer tests: theoretical considerations and illustration with a field test. Journal of Hydrology, 277(1-2), 134-149. https://doi.org/10.1016/S0022-1694(03)00090-8

297. Varouchakis, E. A., & Hristopulos, D. T. (2013). Comparison of stochastic and deterministic methods for mapping groundwater level spatial variability in sparsely

monitored basins. Environmental monitoring and assessment, 185, 1-19. https://doi.org/10.1007/s10661-012-2527-y

298. Vasiliadou, I. A., & Chrysikopoulos, C. V. (2011). Cotransport of Pseudomonas putida and kaolinite particles through water-saturated columns packed with glass beads. Water Resources Research, 47(2). https://doi.org/10.1029/2010WR009560

299. Vereecken, H., Döring, U., Hardelauf, H., Jaekel, U., Hashagen, U., Neuendorf, O., ... & Seidemann, R. (2000). Analysis of solute transport in a heterogeneous aquifer: the Krauthausen field experiment. Journal of Contaminant Hydrology, 45(3-4), 329-358. https://doi.org/10.1016/S0169-7722(00)00107-8

300. Vincent Henri, C., & Harter, T. (2019). Stochastic assessment of nonpoint source contamination: joint impact of aquifer heterogeneity and well characteristics on management metrics. Water Resources Research, 55(8), 6773-6794. https://doi.org/10.1029/2018WR024230

301. Vitorge, E., Szenknect, S., Martins, J. M., & Gaudet, J.-P. (2013). Size-and concentration-dependent deposition of fluorescent silica colloids in saturated sand columns: transport experiments and modeling. Environmental Science: Processes & Impacts, 15(8), 1590-1600. https://doi.org/10.1039/C3EM30860J

302. Vouillamoz, J. M., Sokheng, S., Bruyere, O., Caron, D., & Arnout, L. (2012). Towards a better estimate of storage properties of aquifer with magnetic resonance sounding. Journal of Hydrology, 458, 51-58. https://doi.org/10.1016/j.jhydrol.2012.06.044

303. Voyiadjis, G. Z., & Song, C. R. (2003). Determination of hydraulic conductivity using piezocone penetration test. International Journal of Geomechanics, 3(2), 217-224. https://doi.org/10.1061/(ASCE)1532-3641(2003)3:2(217)

304. Walton, W. C. (2019). Groundwater pumping tests. CRC Press. https://doi.org/10.1201/9780367811198

305. Wang, C., Bobba, A. D., Attinti, R., Shen, C., Lazouskaya, V., Wang, L. P., & Jin, Y. (2012). Retention and transport of silica nanoparticles in saturated porous media: effect of concentration and particle size. Environmental science & technology, 46(13), 7151-7158. https://doi.org/10.1021/es300314n

306. Wang, D., Paradelo, M., Bradford, S. A., Peijnenburg, W. J., Chu, L., & Zhou, D. (2011). Facilitated transport of Cu with hydroxyapatite nanoparticles in saturated sand: effects of solution ionic strength and composition. water research, 45(18), 5905-5915. https://doi.org/10.1016/j.watres.2011.08.041

307. Wang, L., Xu, S., & Li, J. (2011). Effects of phosphate on the transport of Escherichia coli O157: H7 in saturated quartz sand. Environmental science & technology, 45(22), 9566-9573. https://doi.org/10.1021/es201132s

308. Wang, S., Li, D., Zhang, M., Chen, M., Xu, N., Yang, L., & Chen, J. (2020). Competition between fulvic acid and phosphate-mediated surface properties and transport of titanium dioxide nanoparticles in sand porous media. Journal of Soils and Sediments, 20, 3681-3687. https://doi.org/10.1007/s11368-020-02699-9

309. Wang, Y., Bradford, S. A., & Šimůnek, J. (2013). Transport and fate of microorganisms in soils with preferential flow under different solution chemistry conditions. Water resources research, 49(5), 2424-2436. https://doi.org/10.1002/wrcr.20174

310. Wang, Z., Shen, C., Du, Y., Zhang, Y., & Li, B. (2019). Influence of phosphate on deposition and detachment of TiO_2 nanoparticles in soil. Frontiers of

Environmental Science & Engineering, 13, 1-11. https://doi.org/10.1007/s11783-019-1163-y

311. Ward, A. S., Kelleher, C. A., Mason, S. J., Wagener, T., McIntyre, N., McGlynn, B., ... & Payn, R. A. (2017). A software tool to assess uncertainty in transient-storage model parameters using Monte Carlo simulations. Freshwater Science, 36(1), 195-217. https://doi.org/10.1086/690444

312. Widory, D., Kloppmann, W., Chery, L., Bonnin, J., Rochdi, H., & Guinamant, J. L. (2004). Nitrate in groundwater: an isotopic multi-tracer approach. Journal of contaminant hydrology, 72(1-4), 165-188. https://doi.org/10.1016/j.jconhyd.2003.10.010

313. Won, J., & Burns, S. E. (2017). Influence of ionic strength on clay particle deposition and hydraulic conductivity of a sand medium. Journal of Geotechnical and Geoenvironmental Engineering, 143(10), 04017081. https://doi.org/10.1061/(ASCE)GT.1943-5606.0001780

314. Won, J., Choo, H., & Burns, S. E. (2020). Impact of solution chemistry on deposition and breakthrough behaviors of kaolinite in silica sand. Journal of Geotechnical and Geoenvironmental Engineering, 146(1), 04019123. https://doi.org/10.1061/(ASCE)GT.1943-5606.0002199

315. Won, J., Wirth, X., & Burns, S. E. (2019). An experimental study of cotransport of heavy metals with kaolinite colloids. Journal of hazardous materials, 373, 476-482. https://doi.org/10.1016/j.jhazmat.2019.03.110

316. Worthington, S. R. (2022). Estimating effective porosity in bedrock aquifers. Groundwater, 60(2), 169-179. https://doi.org/10.1111/gwat.13171

317. Wu, T., Yang, Z., Hu, R., & Chen, Y. F. (2023). Three-dimensional visualization reveals pore-scale mechanisms of colloid transport and retention in two-phase flow. Environmental Science & Technology, 57(5), 1997-2005. https://doi.org/10.1021/acs.est.2c08757

318. Wu, X., Lyu, X., Li, Z., Gao, B., Zeng, X., Wu, J., & Sun, Y. (2020). Transport of polystyrene nanoplastics in natural soils: Effect of soil properties, ionic strength and cation type. Science of the Total Environment, 707, 136065. https://doi.org/10.1016/j.scitotenv.2019.136065

319. Xinqiang, D., Yalin, S., Xueyan, Y., & Ran, L. (2019). Colloid clogging of saturated porous media under varying ionic strength and roughness during managed aquifer recharge. Journal of Water Reuse and Desalination, 9(3), 225-231. https://doi.org/10.2166/wrd.2019.041

320. Xu, L., Liang, Y., Liao, C., Xie, T., Zhang, H., Liu, X., ... & Wang, D. (2022). Cotransport of micro-and nano-plastics with chlortetracycline hydrochloride in saturated porous media: Effects of physicochemical heterogeneities and ionic strength. Water Research, 209, 117886. https://doi.org/10.1016/j.watres.2021.117886

321. Xu, S., Gao, B., & Saiers, J. E. (2006). Straining of colloidal particles in saturated porous media. Water Resources Research, 42(12). https://doi.org/10.1029/2006WR004948

322. Xu, S., Liao, Q., & Saiers, J. E. (2008). Straining of nonspherical colloids in saturated porous media. Environmental science & technology, 42(3), 771-778. https://doi.org/10.1021/es071328w

323. Yan, C. H. E. N., & Ji-chun, W. U. (2005). Effect of the spatial variability of hydraulic conductivity in aquifer on the numerical simulation of groundwater. Advances in Water Science, 16(4), 482-487.

324. Yang, H., Tong, M., & Kim, H. (2013). Effect of carbon nanotubes on the transport and retention of bacteria in saturated porous media. Environmental science & technology, 47(20), 11537-11544. https://doi.org/10.1021/es4022415

325. Yang, S., Zhou, H., Zhang, S., & Wang, L. (2019). Analytical solutions of advective–dispersive transport in porous media involving conformable derivative. Applied Mathematics Letters, 92, 85-92. https://doi.org/10.1016/j.aml.2019.01.004

326. Yao, K. M., Habibian, M. T., & O'Melia, C. R. (1971). Water and waste water filtration. Concepts and applications. Environmental science & technology, 5(11), 1105-1112. https://doi.org/10.1021/es60058a005

327. Ye, X., Cui, R., Du, X., Ma, S., Zhao, J., Lu, Y., & Wan, Y. (2019). Mechanism of suspended kaolinite particle clogging in porous media during managed aquifer recharge. Groundwater, 57(5), 764-771. https://doi.org/10.1111/gwat.12872

328. Yin, M., Ma, R., Zhang, Y., Chen, K., Guo, Z., & Zheng, C. (2022). A Dual Heterogeneous Domain Model for Upscaling Anomalous Transport with Multi-Peaks in Heterogeneous Aquifers. Water Resources Research, 58(4), e2021WR031128. https://doi.org/10.1029/2021WR031128

329. Yuan, H., & Shapiro, A. (2012). Colloid transport and retention: recent advances in colloids filtration theory. Colloids: Classification, properties and applications, 201-242. ISBN (Print) 978-1-62081-143-6

330. Yuan, R., Zhang, W., Tao, X., Wang, S., & Zhang, L. (2020). Coupled effects of high pH and chemical heterogeneity on colloid retention and release in saturated

porous media. Colloids and Surfaces A: Physicochemical and Engineering Aspects, 586, 124285. https://doi.org/10.1016/j.colsurfa.2019.124285

331. Zech, A., Attinger, S., Bellin, A., Cvetkovic, V., Dietrich, P., Fiori, A., ... & Dagan, G. (2019). A critical analysis of transverse dispersivity field data. Groundwater, 57(4), 632-639. https://doi.org/10.1111/gwat.12838

332. Zevi, Y., Dathe, A., Gao, B., Zhang, W., Richards, B. K., & Steenhuis, T. S. (2009). Transport and retention of colloidal particles in partially saturated porous media: Effect of ionic strength. Water Resources Research, 45(12). https://doi.org/10.1029/2008WR007322

333. Zha, Y., Yeh, T. C. J., Illman, W. A., Mok, C. M. W., Tso, C. H. M., Carrera, B. A., & Wang, Y. L. (2019). Exploitation of pump-and-treat remediation systems for characterization of hydraulic heterogeneity. Journal of Hydrology, 573, 324-340. https://doi.org/10.1016/j.jhydrol.2019.03.089

334. Zhang, Q., Raoof, A., & Hassanizadeh, S. M. (2015). Pore-scale study of flow rate on colloid attachment and remobilization in a saturated micromodel. Journal of Environmental Quality, 44(5), 1376-1383. https://doi.org/10.2134/jeq2015.01.0058

335. Zhang, W., Li, S., Wang, S., Lei, L., Yu, X., & Ma, T. (2018). Transport of Escherichia coli phage through saturated porous media considering managed aquifer recharge. Environmental Science and Pollution Research, 25, 6497-6513. https://doi.org/10.1007/s11356-017-0876-3

336. Zhang, Y., Hartung, M. B., Hawkins, A. J., Dekas, A. E., Li, K., & Horne, R. N. (2021). DNA tracer transport through porous media—The effect of DNA length and adsorption. Water Resources Research, 57(2), 2020WR028382. https://doi.org/10.1029/2020WR028382

337. Zhao, C., Zhang, X., Fang, X., Zhang, N., Xu, X., Li, L., ... & Xia, Y. (2022). Characterization of drinking groundwater quality in rural areas of Inner Mongolia and assessment of human health risks. Ecotoxicology and Environmental Safety, 234, 113360. https://doi.org/10.1016/j.ecoenv.2022.113360

338. Zheng, C., & Wang, P. P. (1999). MT3DMS: a modular three-dimensional multispecies transport model for simulation of advection, dispersion, and chemical reactions of contaminants in groundwater systems; documentation and user's guide. http://hdl.handle.net/11681/4734

339. Zhuang, J., & Jin, Y. (2003). Virus retention and transport through Al-oxide coated sand columns: effects of ionic strength and composition. Journal of Contaminant Hydrology, 60(3-4), 193-209. https://doi.org/10.1016/S0169-7722(02)00087-6

340. Żychowski, J., & Bryndal, T. (2015). Impact of cemeteries on groundwater contamination by bacteria and viruses–a review. Journal of Water and Health, 13(2), 285-301.

CV

Swagatam Chakraborty

Postdoctoral researcher, Department of Earth Sciences, Göteborg University, Sweden

Academics	
Master of Science Water Science and Engineering specialization in Groundwater and Global Change – Impacts of AdaptationIST-Lisbon, Portugal UNESCO-IHE, Delft, the Netherlands Technical University of Dresden, Germany	Sept'2016 – Sept'2018
Master of Science Biotechnology PESIT, Bangalore University, India	Sept'2011 – Sept'2013
Bachelor of Science Biotechnology, Biochemistry, Genetics Garden City College, Bangalore University, India	Sept'2008 – Aug'2011

Research experience	
Post-doctoral researcher Göteborg University, Göteborg, Sweden	Apr'2024 - Present
Doctoral researcher, Geosciences Utrecht University, the Netherlands	Oct'2018 – June'2024
Research Intern, Geosciences TU Delft, the Netherlands	Aug'2017 – Sept'2017
Research scholar, Environmental sciences PESIT, Bangalore University, India	Dec'2013 – Dec'2015
Research intern, Environmental sciences Indian Institute of Management, Bangalore, India	May'2013 – Sept'2013

Academic awards	
Distinction award in Master of Science Biotechnology PESIT, Bangalore University, India	Sept'2013
Distinction award in bachelor's in science biotechnology Garden City College, Bangalore University, India	Sept'2011
Cream Outgoing Student award Garden City College, Bangalore University, India	Sept'2011